Titre: Title:	Quantification of the Hydrologic Performance and Modelling in SWMM of a Bioretention Basin and Vegetated Swale with a Trapezoidal Cross-section
Auteur: Author:	Julia Bond
Date:	2020
Type:	Mémoire ou thèse / Dissertation or Thesis
Référence: Citation:	Bond, J. (2020). Quantification of the Hydrologic Performance and Modelling in SWMM of a Bioretention Basin and Vegetated Swale with a Trapezoidal Cross-section [Mémoire de maîtrise, Polytechnique Montréal]. PolyPublie. https://publications.polymtl.ca/5258/

POLYTECHNIQUE MONTRÉAL

affiliée à l'Université de Montréal

Quantification of the Hydrologic Performance and Modelling in SWMM of a Bioretention Basin and Vegetated Swale with a Trapezoidal Cross-section

JULIA BOND

Département de génies civil, géologique et des mines

Mémoire présenté en vue de l'obtention du diplôme de *Maîtrise ès sciences appliquées*

Génie Civil

Mai 2020

POLYTECHNIQUE MONTRÉAL

affiliée à l'Université de Montréal

Ce mémoire intitulé :

Quantification of the Hydrologic Performance and Modelling in SWMM of a Bioretention Basin and Vegetated Swale with a Trapezoidal Cross-section

Présenté par **Julia BOND**

en vue de l'obtention du diplôme de *Maîtrise ès sciences appliquées* a été dûment accepté par le jury d'examen constitué de :

Tew-Fik MAHDI, président

Musandji FUAMBA, membre et directeur de recherche

Sophie DUCHESNE, membre externe

DEDICATION

Rain is grace; rain is the sky descending to the earth; without rain, there would be no life.

~ John Updike

ACKNOWLEDGEMENTS

I would like to thank those that were directly involved in the project. Musandji Fuamba, the project director. Essoyeke Batchabani who met with me weekly to go over the progress of the project, it could not be completed without his generous insight and diligent attitude. Étienne Bélanger, the technician in the Hydraulics Laboratory, who was always available to discuss solutions to various technical issues that arose during data collection. Evelyne Pouliot and Mariam Sylla who worked very hard during their summer internship to advance data processing and analysis. Alexandra A.Maisonneuve who made a great teammate, managed field work scheduling and did much of the hard labor.

I would also like to thank those that funded the project; the city of Montreal. More specifically, thank you to Guy Trudel, landscape architect and David Courchesne, engineer at EXP, for your guidance and inspiration. They have worked hard for years to bring such a well-thought-out project to life.

A big thank you to Carl Gagnon-Ouellette who was my first friend at Polytechnique Montréal and met with me on weekends to discuss the project, even while he had already started working as a Junior Engineer. I would also like to thank Élodie Mellado who kept me company in our office and with whom I had some great conversations.

Eva Défranoux and Zahia Makkeb, classmates whom I will remember and cherish from this great experience I have had at Polytechnique Montréal.

Finally, thank you to my family, my partner Vijaykarthik and Marlène Gauthier who supported through the completion of this project.

RÉSUMÉ

Les débordements d'égouts unitaires peuvent causer des problèmes majeurs de pollution des cours d'eaux récepteurs. De plus, l'augmentation des surfaces imperméables, une conséquence de l'expansion des villes urbaines au cours du dernier siècle, a engendré une augmentation des volumes et débits de ruissellement des eaux pluviales. Ceci entraîne une réduction de la recharge des eaux souterraines, une augmentation de la masse de polluants rejetés et une érosion des berges des cours d'eaux récepteurs. Les pratiques de gestion optimales (PGO) favorisent les chances qu'un site retrouve ses caractéristiques hydrologiques initiales, avant développement, en gérant le ruissellement à la source. Ces nouvelles mesures de gestion des eaux pluviales, sous forme d'ouvrages à faible impact écologique, bénéficient de systèmes naturels pour augmenter l'infiltration et l'évapotranspiration. Les modèles hydrologiques permettent la conception de ces projets et peuvent être utilisés pour comprendre les avantages de la mise en œuvre des PGOs sur un territoire à l'étude. Dans le cadre d'un projet pilote à Montréal, un suivi hydrologique a été complété en 2019 sur deux types de structures. Le premier type, le bassin de biorétention, inclut un drain perforé et un potentiel de stockage des eaux de ruissellement à sa surface tandis que l'autre, la noue végétalisée, ne possède aucune de ces deux caractéristiques. Leurs performances hydrauliques ont été quantifiées à l'aide d'indices de performance tels que le volume initialement absorbé avant la mesure d'un écoulement de sortie, le pourcentage de rétention volumique pour un évènement pluvieux, le pourcentage de réduction du débit de pointe et le retard de la pointe. Le bassin de biorétention a pu absorber, en moyenne, les 23 m^3 initiaux du ruissellement généré par un évènement de pluie. Parmi tous les événements mesurés, 91% (bassin de biorétention) et 78% (noue végétalisée) ont atteint une rétention volumique supérieure à 67% (cible suggérée). La valeur cible de 67% pour la réduction du débit de pointe a été atteinte pour 98% (bassin de biorétention) et 94% (noue végétalisée) des événements. Un décalage minimal de la pointe de débit a été mesuré. La cible de 600% de l'occurrence de la pointe (sortie/entrée) a été dépassée pour seulement 25% (bassin de biorétention) et 30% (noue végétalisée) des événements. Le bassin de biorétention a montré une performance de rétention volumétrique globale supérieure comparé à deux autres : dans le premier, la couche de substrat est deux fois plus épaisse et dans le deuxième, la couche de substrat contient une zone interne avec un potentiel de stockage de l'eau (zone ″IWS″). Ceci est dû à la grandeur du rapport entre la superficie du bassin de biorétention et la superficie drainée. Cependant, le bassin de biorétention n'a pas complètement retenu le volume généré par les petites

pluies. Ce résultat démontre la nécessité de combiner l'augmentation du rapport entre la superficie du PGO et la surface tributaire avec une des quatre options suivantes : un approfondissement de la couche de substrat, l'addition d'une zone ″IWS″, une plus grande teneur en argile dans le substrat ou l'installation d'un régulateur à la sortie du drain perforé.

Le modèle SWMM (Stormwater Management Model) de l'agence américaine de protection de l'environnement utilise un objet de modélisation spécifique, appelé « LID control module », pour représenter les PGOs. Les données recueillies sur le terrain ont été utilisées pour vérifier la capacité du « LID control module » à simuler avec précision l'écoulement de l'eau au travers d'ouvrages dont la section transversale est atypique. Initialement, la surface des ouvrages a été modélisée comme étant identique à la surface construite. Une calibration initiale des paramètres a nécessité d'accroitre la conductivité hydraulique du substrat (140 mm/h) et de diminuer la pente de la conductivité hydraulique (30). L'amélioration de la calibration du modèle a nécessité l'ajustement de la conception intégrée au modèle. Les valeurs globales de l'indicateur d'efficacité de Nash-Sutcliff résultant sont alors passées de 0,206 à 0,614 pour la noue végétalisée et de -0,686 à -0,348 pour le bassin de biorétention. Ainsi, le modèle présentait de meilleures capacités prédictives pour un ouvrage avec une conception globale plus simple, soit la noue végétalisée. Une méthode générale est suggérée, à l'aide des outils déjà disponibles dans le logiciel, pour modéliser des ouvrages avec des sections transversales trapézoïdales afin d'assurer la prédiction précise de leurs performances.

ABSTRACT

Low Impact Development (LID) increases the chances for a site to have "predevelopment hydrology" by managing runoff at the source. New stormwater control measures (SCMs) in the form of structural micro-solutions (LID-Best Management Practices or LID-BMPs) have been implemented around the world as control strategies benefitting from natural systems to increase infiltration and evapotranspiration of stormwater. Hydrologic models permit the design of these projects and can be used to understand the benefits of implementing LID facilities into the landscape and predict their capabilities in handling a variety of rainfall events. Two types of LID structures were monitored in 2019 as part of a pilot project in Montreal; one with an underdrain pipe and runoff storage potential (bioretention basin) and the other without (vegetated swale). Their hydraulic performance was quantified using metrics such as bioretention abstraction volume, volume retention, peak flow reduction and peak delay. The bioretention abstraction volume was determined to be approximately 23 m^3. Of the measured events, 91% (bioretention basin) and 78% (vegetated swale), achieved volume reduction above 67% (the suggested target). The target value of 67% for peak flow reduction was attained for 98% (bioretention basin) and 94% (vegetated swale) of events. A minimal peak delay was measured with the target of 6 times (unitless) being exceeded for only 25% (bioretention basin) and 30% (vegetated swale) of events. Due to the large BMP Area to Impervious Drainage Area (BA:IDA) ratio of the bioretention basin, it showed superior global volume retention performance when compared to a structure with a larger soil layer and one with an Internal Water Storage (IWS) zone. However, the bioretention basin did not completely retain the flow from small storm events demonstrating the necessity of combining the larger BA:IDA ratio with a deepening of the soil depth, the addition of an IWS zone, an increase in the media clay content or the installation of a cap-orifice device on the underdrain exit.

The United States Environmental Protection Agency's Stormwater Management Model (USEPA's SWMM) uses a specific modelling object, termed LID control module to represent the structures. The collected field data was used to verify the ability of the bio-retention control to accurately simulate outflow from structures with an atypical cross-section. Initially, the surface area of the structures was modelled as identical to the field area. A parametric calibration required maximizing the hydraulic conductivity of the soil (140 mm/hr) and minimizing the conductivity slope (30). It was necessary to adjust the design component of the model to improve the calibration with resulting Nash-Sutcliff Efficiency values increasing from 0.206 to 0.614 for the vegetated swale and from -

0.686 to -0.348 for the bioretention basin. Thus, the module presented better predictive capabilities for a basin with a simpler overall design. A general method is suggested to model structures with trapezoidal cross-sectional areas ensuring the accurate prediction of their performance using the tools already available in the software.

TABLE OF CONTENTS

LIST OF TABLES

LIST OF FIGURES

LIST OF SYMBOLS AND ABBREVIATIONS

ADD	Antecedent Dry Days
BA:IDA	BMP Area to Impervious Drainage Area
BAV	Bioretention Abstraction Volume
BB	Bioretention Basin
BMP	Best Management Practice
CI	Confidence Interval
FC	Field Capacity
HCO	Conductivity Slope
IAW	Instrumentation Access Wells
IETD	Inter-Event Time Definition
IWS	Internal Water Storage
LID	Low Impact Development
LMS	Lower Media Zone
NSE	Nash-Sutcliff Efficiency
PCSWMM	Personal Computer Storm Water Management Model
RZMS	Root Zone Management System
SAT	Saturation
SCM	Stormwater Control Measure
SM	Silty Sand
STD	Standard Monitoring Site
SWMM	Storm Water Management Model
USCS	Unified Soil Classification System
USEPA	United States Environmental Protection Agency

VDR	Volume Discharge Ratio
VS	Vegetated Swale
WP	Wilting Point

LIST OF APPENDICES

CHAPTER 1 INTRODUCTION

1.1 Problem statement

Conventionally, stormwater management focused primarily on preventing flooding (Chapman & Horner, 2010). Urban runoff was typically drained as quickly and efficiently as possible from impervious surfaces to downstream water bodies from street gutters connected to an underground conveyance system of pipes (MDDEFP, 2014). However, concerns emerged about the influence of continual pollutant and runoff loading of downstream lakes and rivers. An initial focus was put on point source pollution with the implementation of water treatment centers for centralized downstream treatment (end-of-pipe treatment) of wastewater. Nevertheless, there remained a lack of research on the effects of non-point source pollution on downstream water bodies. This lack of concrete data made it almost impossible to implement any regulations to control the rejection of stormwater downstream. In order to understand the effects of stormwater on the environment, the USEPA conducted a largescale nationwide study which was used to understand the pollutant loadings from stormwater (USEPA, 1983). It was established that in fact one of the largest contributors to non-point source pollution of estuaries and lakes is the urban runoff generated by regularly occurring storm events which make up 90% of storms in a year (USEPA, 1983). The expansion of urban development, involving the increase of impervious surfaces and soil compaction due to the vast construction of roads, sidewalks, drive ways, roofs, commercial lots, condos and other city structures, exasperates the issues of reduced infiltration, river baseflow and groundwater recharge and increased runoff volume, peak flow and stream bank erosion (Harbor, 1994; Moscrip & Montgomery, 1997; USGS, 1999).

Therefore, rainfall runoff management cannot solely concentrate on reducing damages from rarely occurring large storms but must also consider the cumulative consequences of frequent events (MDDEFP, 2014). In the 1990’s, a new thinking around stormwater management called Low Impact Development (LID) evolved as a method that ensured that a site is designed to have “predevelopment hydrology” ("Energy Independence and Security Act (EISA),") by managing runoff at the source. A variety of structural micro-solutions (termed LID-Best Management Practices or LID-BMPs) have been developed as mitigation strategies to encourage the infiltration of rainwater into the ground. Examples include, roof gardens, rain gardens, bioswales, bioretention

cells, pervious pavement, etc. These types of solutions can be expensive and, if widespread integration were to occur, would mean an extensive redevelopment of the urban territory. Another important aspect is that they function optimally when they are properly maintained. Therefore, a clear and adoptable plan must be put in place to ensure their continual functioning.

As with many sectors of engineering, the rules, laws and regulations of a certain construction method are slow to catch up with the development of technology. This is often the case when a new technology/method is developed that is unfamiliar and presents a certain risk if adopted. Since LID structural solutions are relatively new, their implementation has not yet been standardized. Their actual performance and cost/benefit ratio is still unclear. Therefore, studies like the one presented in this memoire are not only important but necessary. They provide a way to evaluate the actual post-construction performance of the structure. Another difficulty with these types of solutions is that they are often site specific. They also require a certain overhead and time for maintenance. The cost of this must be included in the budget and a detailed maintenance plan must be laid out. Therefore, although it might be possible to standardize them to a certain degree, it will always be necessary to do an in-depth analysis of the site in question to carefully consider which solutions fit best and will be the most effective.

Finally, it is important to note that LID structures are not meant as stand-alone solutions. There are already solutions available to manage rare rainfall events (>10 years recurrence). An example is underground concrete detention structures. The main difference between these solutions remains the fact that LID structures encourage sustainable development. They are part of the modern category of multidisciplinary solutions. Bioretention basins are part of these solutions which, if implemented correctly, treat both runoff quantity and quality problems and contribute to the overall well-being of society.

This study aims to understand the hydraulic performance of bioretention and vegetated basins post-construction through a monitoring programme which took place from April 2019 to November 2019. The data collected will also be used to calibrate a hydrologic Stormwater Management Model (SWMM) of the site and understand the model's ability to predict the performance of a bioretention cell. Water quality data was also collected however the focus of this memoire is on the quantitative reduction of runoff performance of the basins.

1.2 Main research objective

The broad objective of the project is to evaluate the ability of the vegetated swale and bioretention basin to meet the proposed LID efficacy targets. Furthermore, in order to predict the future performance of the structures, it is economical to build a model of the system. It is necessary to calibrate and validate the model with the collected field data to ensure it provides an accurate forecast of hydraulic performance. The target accuracies are a Nash-Sutcliffe Efficiency (NSE) coefficient > 0.5 and an error between simulated and measured outflow volume and peak flow less than 25%.

1.2.1 Specific objectives

1. Evaluate the effect of a large BMP Area to Impervious Drainage Area (BA:IDA) ratio and a large bowl depth on the hydraulic performance of the structures in terms of volume retention, peak flow reduction and peak delay efficiency;
2. Compare the hydraulic performance of the vegetated swale and bioretention basin;
3. Build an accurate representation of the site in the PCSWMM model, determine the appropriate initial input parameter values, perform a sensitivity analysis and calibrate and validate the model.

1.2.2 Hypotheses

H1: Due to the large BA:IDA ratio and bowl volume of the bioretention basin, the structure will be able to handle not only small rainfall events but also large ones.

Originality: Bioretention basins are assumed to be most useful in the case of small events therefore less focus is placed on their ability to handle the largest events.

Refutability: The hypothesis will be rejected if the performance targets are not met for events with a return period over 2 years.

H2: A bioretention basin designed with an elevated overflow drain and a conventional underdrain system will result in a superior hydrologic performance than a vegetated basin where the runoff is not forced into the soil media.

Originality: There are few studies which compare directly these two types of structures to understand the additional performance benefits of an elevated overflow drain and conventional drainage system.

Refutability: The hypothesis will be rejected if the monitoring of the vegetated swale presents an acceptable hydrologic performance.

H3: The fact that SWMM assumes a rectangular cross-section in the LID control module and does allow for a user defined cross-section and side slopes of the layers will have an impact on the predicted outflow.

Originality: No studies have been found that discuss methods which ensure that a LID structure with an atypical cross-section can be accurately represented using the tools SWMM currently offers.

Refutability: The hypothesis will be rejected if it is possible to model and calibrate the structures using typical methods with a resulting NSE > 0.5 and an error between simulated and measured outflow volume and peak flow less than 25%.

1.3 Structure of the memoire

The thesis has been structured by first presenting the field data collection procedures and results, which were necessary to proceed with model calibration, and subsequently the modelling procedures and results. The following chapters present a review of the literature (chapter 2), monitoring methods (chapter 3), overview of the site (chapter 4), journal article focused on the basin performance results (chapter 5), complete journal article on the modelling of the basins (chapter 6), global discussion (chapter 7) and conclusions/recommendations (chapter 8).

CHAPTER 2 REVIEW OF LITERATURE

2.1 Bioretention basins

Bioretention basins (also called rain gardens) emulate natural watersheds by infiltrating and treating stormwater runoff (DeBusk et al., 2010; PGCo, 2007; USEPA, 1999). Their standard design includes a depression in the ground containing an engineered soil material, a downstream elevated drain or overflow and appropriate vegetative species, which together function as a flow regulator permitting runoff storage, infiltration and evapotranspiration (Figure 2.1).

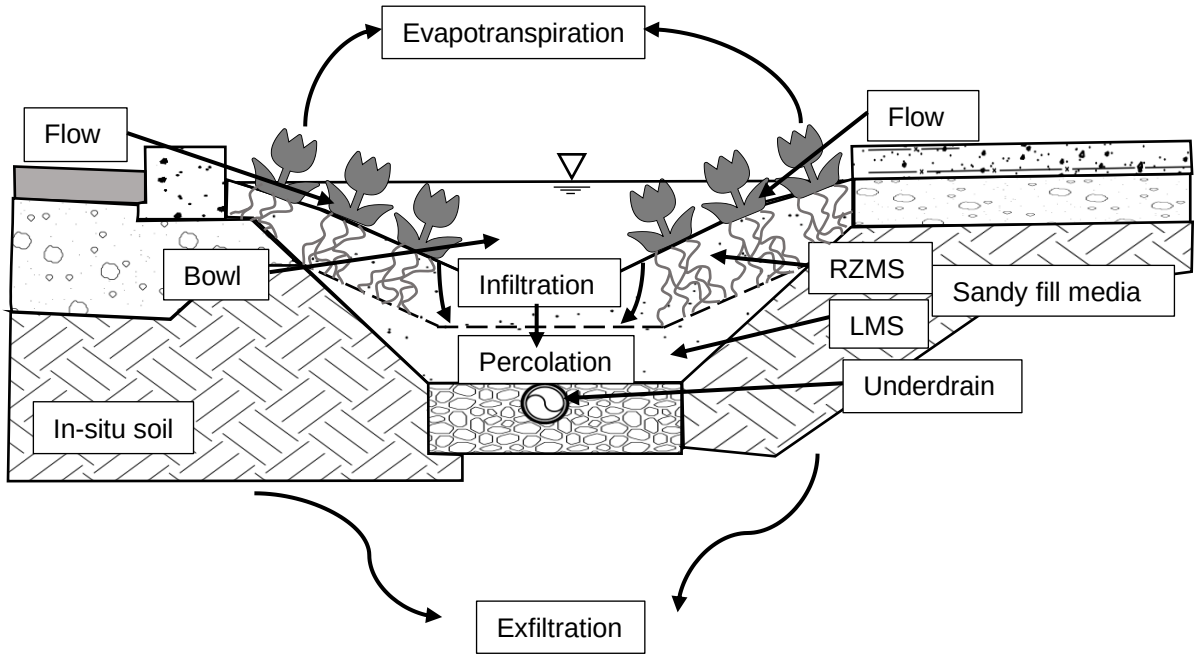

Figure 2.1 Typical cross section of a bioretention basin (Les Services EXP inc. 2018 on behalf of the City of Montreal)

The soil layer is commonly between 0.6 and 1.2 m deep, and can be subdivided into two sections, the root zone, or Root Zone Management System (RZMS), and the Lower Media Storage (LMS). The RZMS represents the top layer which contains the roots of the plants and is assumed to be approximately 30 cm deep (Davis et al., 2012). The LMS is the remaining soil below the RZMS. A layer of bark mulch is placed on top to prevent soil erosion.

An optional perforated underdrain pipe draining to the local waterways can be included depending on site-specific conditions. As a LID solution, bioretention provides a multitude of benefits, namely, peak flow attenuation, runoff volume and pollutant loading reduction/elimination, increase in evapotranspiration and biological activity, reduction in stream erosion and replenishment of groundwater aquifers (Davis, 2008; Davis et al., 2009; Dietz, 2007; Dietz & Clausen, 2005).

2.2 Performance of bioretention basins

The decision to implement any LID structure on a site must consider the local soil characteristics, particularities of the site (e.g. topography), utilization of the surrounding land and scale of impervious surfaces (Aceves & Fuamba, 2016). Landscape characteristics represent only one of many elements influencing the performance of LID solutions (Passeport et al., 2013; Zahmatkesh et al., 2014). Regional rainfall patterns also direct their effectiveness (Gallo et al., 2012; Jennings et al., 2012; Qin et al., 2013). A direct consequence of the large influence of local site conditions on LID-BMP performance is the resistance of professionals towards implementation without direct physical proof of their benefits. Therefore, local pilot projects are a necessity to encourage overall adoption (Eckart et al., 2017; Ewing et al., 2000). Furthermore, in order to advance the fundamental understanding and quantification of the benefits of these solutions, it is instrumental to establish field monitoring research studies focused on providing science-based performance evaluations (Davis et al., 2012).

In general, studies show that the ability of a bioretention structure to reduce both runoff volume and peak flow can vary largely, from 40-97% (Ahiablame et al., 2012). Géhéniau et al. (2014) evaluated the ability of a rain garden to reduce runoff from a parking lot by up to 81.4% (warm period) and 74.7% (cold period). This was compared to a study by Khan et al. (2012) evaluating a bioretention basin which had a volume reduction capacity of 93.5% (warm period). A bioretention cell retrofitted into a parking lot attenuated 97% of runoff volume and 99% of the peak flow (DeBusk & Wynn, 2011). Bioretention basins subjected to a series of rainfall events in Maryland and North Carolina showed a median peak flow attenuation of 52% and 99.6%, respectively (Davis, 2008; Hunt et al., 2008).

Precipitation events can be defined based on their rainfall depth, duration and time-to-peak ratio all of which have been proven to influence LID solution performances. Therefore, it is also

necessary to consider regional rainfall patterns during the design process (Eckart et al., 2017). Davis et al. (2012) presented the common ability of bioretention basins to completely assimilate small rainfall events. This was also confirmed in a study by Mahmoud et al. (2019) presenting a bioretention structure which eliminated runoff from small rainfall events (< 8.1 mm in this case). However, Géhéniau et al. (2014) found that there were cases where small events did generate outflow and thus no clear trend of hydraulic retention efficiency as a function of rainfall depth was established. Considering a large-sized rain event (38.3 mm in over 10h), Mahmoud et al. (2019) found that the measured runoff in the impervious section reached peak flow values of 1.12 $L/m^2/min$ in the 1^{st} hour whereas the section treated through bioretention did not surpass 0.076 $L/m^2/min$ in the following 9 hours. Showing that not only can bioretention be used to reduce runoff volume (92% in this case) but also delay the start time of runoff and reduce the peak flow (Mahmoud et al., 2019). Generally, these types of structures are unable to handle very large precipitation events (Eckart et al., 2017; Holman-Dodds et al., 2003; Williams & Wise, 2006).

2.3 Bioretention basin design

A variety of underdrain configurations can be utilized and can affect the retention capacities of a bioretention basin (Brown & Hunt, 2011). Designing the underdrain such that an Internal Water Storage (IWS) zone is formed, has been shown to positively influence volume retention performance (Brown & Hunt, 2011; Dietz & Clausen, 2006; Li et al., 2009). The end point of the underdrain is elevated to create an upturned elbow resulting in a saturated zone at the bottom of the bioretention basin (typically 0.3-0.75-m deep) (Hunt et al., 2006; Passeport et al., 2009).

Winston et al. (2016) present the hydrologic results for 3 bioretention basins build in poorly drained soils which include an IWS zone in their design. Nevertheless, there is a lack of available field data on the performance of bioretention basins constructed in low permeability natural soils. It would be beneficial to study the hydrologic performance of LID structures built in low permeability soils in the absence of an IWS zone.

2.4 Modelling of bioretention basins

Hydrologic models permit the design of these pilot projects and can be used to understand the benefits of implementing LIDs into the landscape and predict their capabilities in handling a variety of rainfall events. Modelling LID structures accurately requires the representation of a multitude

of processes from surface runoff to infiltration and soil percolation. The strength of the model depends on the detail of representation of these processes and the methods which connect them (Elliott & Trowsdale, 2007).

One popular and complex model used for a range of applications is PCSWMM (Personal Computer Storm Water Management System), a modelling software available through Computational Hydraulics Inc. which uses the U.S. Environmental protection agency's (USEPA's) SWMM engine. In 2010, the SWMM5 engine (version 5.0.021) was upgraded to allow the modelling of a variety of LIDs such as bio-retention cells, infiltration trench, permeable pavement, rain barrel, vegetative swale, rain garden, green roof and rooftop disconnection.

A review of SWMM's performance for a multitude of applications inspired by over 150 peer-reviewed journal articles concluded that a major focus of model development should be improving and validating the incorporation of LID solutions. Considering the continually growing interest in implementing these stormwater management practices, research is needed, which would aid in understanding SWMM's ability to predict their behavior and performance (Niazi et al., 2017).

McCutcheon and Wride (2013) compared measured outflow data with outflow simulated by the bio-retention cell module in SWMM. The structures modelled were two small rain gardens which collected water from a rooftop and had a typical rectangular cross-section. The tributary area to rain garden area ratio was 5:1. The performance was assessed based on the volume of water which had overflowed from the rain gardens. Results depicted a good alignment between observed and simulated results for both long-term and single-event analysis (McCutcheon & Wride, 2013). A previous study completed in 2012 by the same author which also involved modeling bio-retention basins in SWMM but was not calibrated against field data was used as comparison. It was established that calibrating the model with field data ensured a much better prediction of outflow.

There are a few other studies that cover the validation of the green-roof module which is comparable to the bio-retention cell control. Burszta-Adamiak and Mrowiec (2013) stipulated that the SWMM5 engine was insufficient in its capability to simulate the runoff from 3 green-roofs whose performance was measured experimentally. In this specific case, the main issue was finding a compromise between proper estimation of the volume and proper estimation of the peak flow. Possible reasons for this quandary include a lack of parameterization of certain phenomena and the simplification of complex processes behind the drying of the soil layer (Burszta-Adamiak &

Mrowiec, 2013). In fact, SWMM calculates evapotranspiration using daily averages based on entered user values or climate files (temperature, wind speed and direction) thus not considering other elements of influence (Herrera et al., 2017). Other notable limitations in the model include: no explicit calculation of the evaporation in a bare soil and the inability to fully encapsulate the water dynamics in a soil layer. In order to justly simulate the performance of LID structures for which infiltration is the main component, appropriate representation of surface/subsurface flow interaction and the continuous influence of evapotranspiration on soil water content is primordial (Herrera et al., 2017).

One aspect of modelling LID structures in SWMM which is not discussed in the literature is the influence a change in the cross-sectional area could have on the water balance analysis. The LID control module does not require a user input value for the slope of the sides of the layers. Instead, it assumes a rectangular cross-section. No other studies were identified which discuss the impact of this assumption nor provide solutions to properly model this type of situation.

In order to assess the capacity of the SWMM bio-retention control module to simulate the transformation from rainfall to runoff/outflow through LID structures with trapezoidal cross-sections, it is beneficial to begin with a structure which has less parameters and represents a simpler design. Thus, a LID-BMP which does not include an underdrain (vegetated swale) will first be modelled in SWMM followed by the bioretention basin. A method which utilizes the tools already implemented in PCSWMM will be developed to improve the accuracy of the simulations.

The steps required to complete the modelling of the LID structures in PCSWMM are:

1. Building an accurate representation of the site in the model.
2. Determining appropriate initial input parameter values.
3. Performing a Sensitivity Analysis.
4. Determining the optimal values of the influential parameters (calibration).
5. Validating the calibration with an independent dataset.
6. If necessary, re-calibrating and re-validating until the prescribed performance criteria are met.

CHAPTER 3 GENERAL LID-BMP MONITORING METHODOLOGY

A detailed methodology for monitoring LID-BMP performance is presented in the Urban Stormwater BMP Performance Monitoring Manual (2009). Only two important elements are focused on in this chapter:

1. The analytical approach and acceptance criteria used to assess the performance of a LID structure.
2. The methods used to obtain the required data.

Any process included in the water balance across a LID structure must be measured to calculate its ability to capture and retain stormwater runoff. It is crucial that the design and implementation of the monitoring components be accurate and complete. This means an accurate quantification of the volume entering the unit and the volume of stormwater exiting the unit. Two main phenomena must be monitored to do so: rainfall and runoff. Both require different types of equipment of which there are multiple options dependent on the constraints of the project (structural drainage configuration, budgetary, precision required, local rules and regulations, etc). Another major component of LID-BMP monitoring is the measurement of water quality data. However, since this study is focused on the hydraulic performance of LID solutions, the methods to measure water quality will not be further discussed.

3.1 Acceptance criteria and analytical approach used to assess the performance of the LID structures

3.1.1 General assessment of LID-BMP performance

There are multiple ways to assess the performance of LID structures. The goal of implementing these solutions is to encourage infiltration into the ground. Therefore, one major criterion is the retention efficiency of the structure, which assesses how much of the inflow volume has been infiltrated into the constructed soil. However, the volume retained will not only be transformed into infiltration but also evapotranspiration. This division was not considered in the analysis and therefore only one value is computed for the volume retained.

Another issue that these solutions can improve is the erosion of downstream riverbanks due to frequent surges in runoff. Many regions use combined sewer networks to collected rainwater and wastewater. These have an overflow section that diverts the combination of rainwater and sewage to downstream water bodies should the passing volume be too large. Therefore, in order to reduce the amount of runoff being redirected downstream, it is necessary to reduce the peak of the flow passing through the system and increase the duration of the runoff (Figure 3.1). These performance metrics describe the detention performance of the structure and include the time to start, duration, peak flow and peak delay of the hydrograph (Peng & Stovin, 2017).

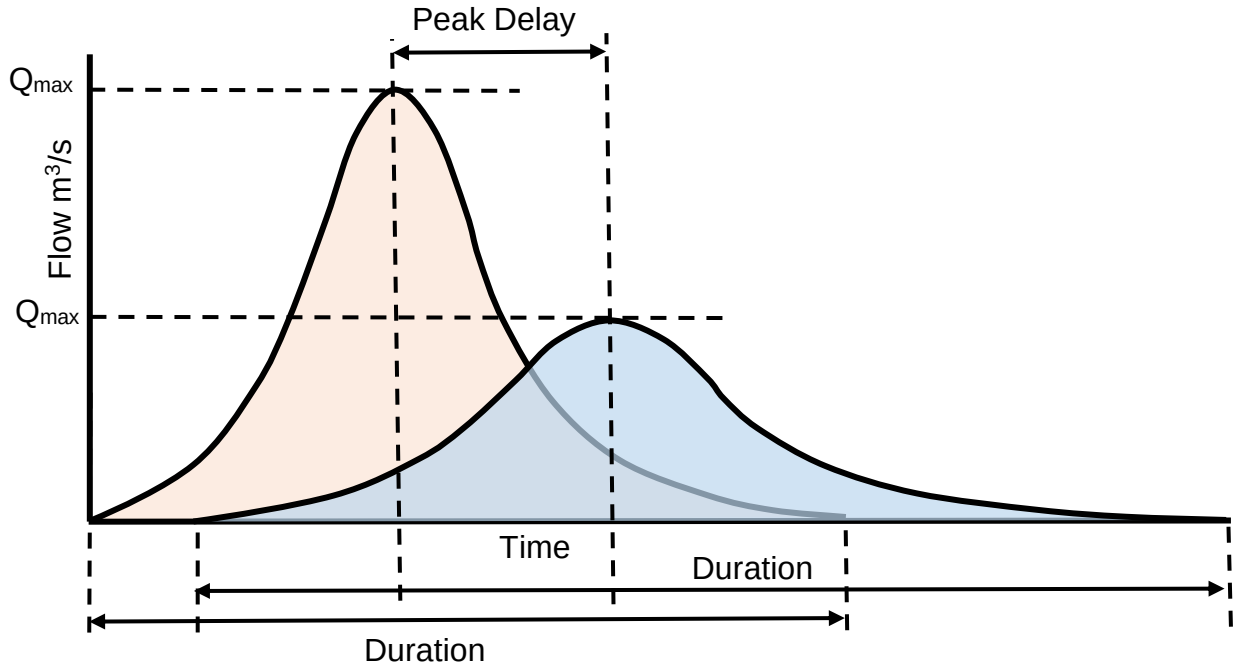

Figure 3.1 Performance assessment using retention and detention metrics: runoff volume, peak flow magnitude and timing, time to start of runoff and duration

3.1.2 Bioretention abstraction volume

Davis et al. (2012) used the Bioretention Abstraction Volume (BAV), which is the volume of inflow completely withheld by the structure, as an initial evaluation metric. The BAV is dependent

on the LID-BMP design and can change over time as a function of rainfall characteristics and the nature of a soil's initial moisture content.

In the case of a bioretention basin with an underdrain system, it is necessary for the infiltration rate to surpass the drain outflow rate and soil percolation rate before the bowl is utilized for storage. A suggestion was made by Davis et al. (2012) to calculate the average BAV theoretically which considers the underdrain's ability to quickly drain the deeper soil layer. The soil layer is divided into two layers. The top layer is called the Room Zone Management System (RZMS) and the deeper layer is termed the Lower Media Storage (LMS). The minimum water content in the RZMS is dictated by Wilting Point (WP) which is the lowest moisture content necessary for plant survival. The LMS is dictated by the Field Capacity (FC) which is the residual moisture content of an initially saturated soil which has drained freely by gravity. The theoretical average BAV is a function of the storage capacity of the two layers given by Eq. (3.1):

$$Ave\ BAV = RZMS * (SAT - WP) + LMS * (SAT - FC) \tag{3.1}$$

where SAT = moisture content of the Soil at Saturation (the maximum).

It is necessary to add the bowl volume to Eq. (3.1) to obtain the theoretical maximum BAV. The minimum BAV (*low BAV*) can be calculated with Eq. (3.2):

$$Low\ BAV = RZMS * (SAT - WP) \tag{3.2}$$

3.1.3 Volume retention and peak flow reduction and delay

Three additional criteria can be used to asses the influence of the LID-BMPs on the entrance hydrographs (Davis, 2008; Li et al., 2009; Winston et al., 2016): the volume discharge ratio (VDR or f_{V24}) [Eq. (3.3)], the peak flow rate ratio R_{peak} [Eq. (3.4)], and the peak discharge time span ratio R_{delay} [Eq. (3.5)], which are expressed as:

$$f_{v24} = \frac{V_{out-24}}{V_{in}} \tag{3.3}$$

$$R_{peak} = \frac{q_{peak-out}}{q_{peak-in}} \tag{3.4}$$

$$R_{delay} = \frac{t_{q-peak-out}}{t_{q-peak-in}} \tag{3.5}$$

where V_{out-24} and V_{in} denote the total volume of outflow (within 24 hours of the rainfall event) and inflow (m^3) to enter and exit the structure; $q_{peak-out}$ and $q_{peak-in}$ are the peak discharges of the outflow and inflow hydrographs (L/s); and $t_{q-peak-out}$ and $t_{q-peak-in}$ are the timespans from the beginning of the outflow and inflow to the peak discharges (hh:mm). Target values were suggested by Davis (2008), namely, f_{v24} < 0.33, R_{peak} < 0.33, and R_{delay} > 6.

3.1.4 Methods to calculate runoff volume

3.1.4.1 Hypotheses

- The intensity of the rain at a given moment is identical throughout the project site for the duration of the event.

3.1.4.2 The Reimann approximation

In the case of measured runoff, the Reimann approximation (Figure 3.2) method can be used to estimate the volume under a hydrograph (flow through time).

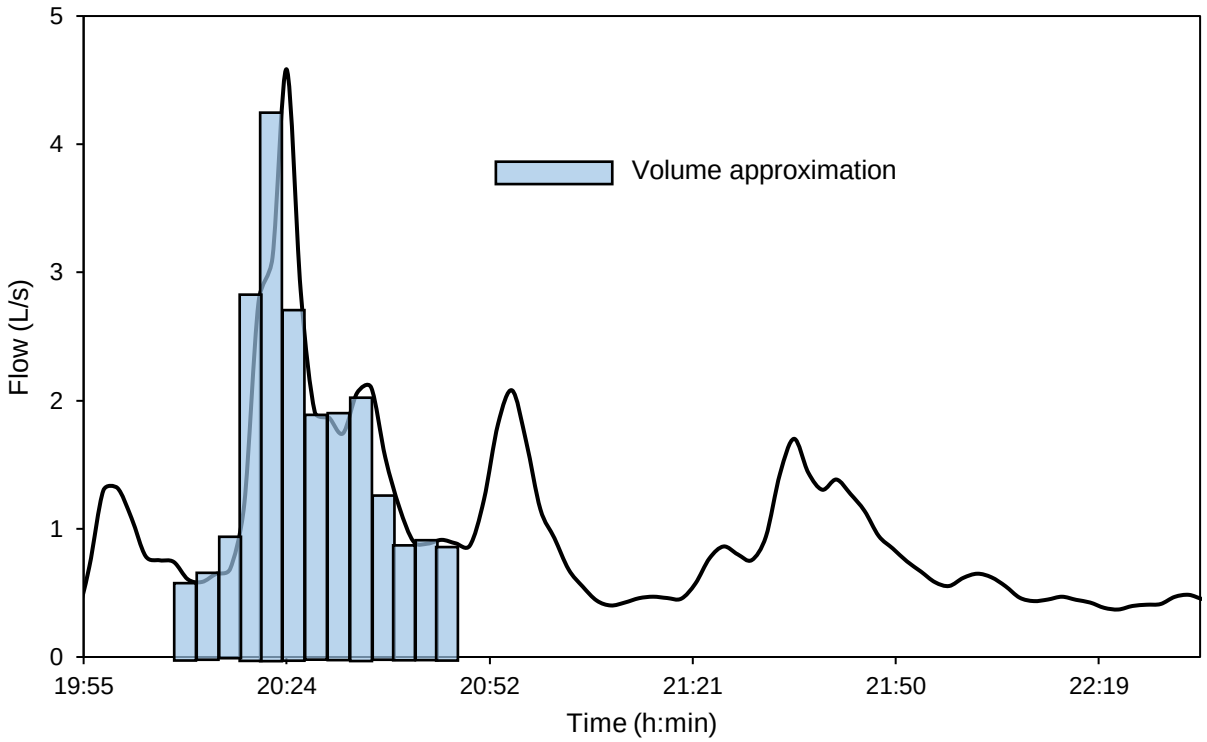

Figure 3.2 The Reimann approximation used to calculate the volume under a hydrograph

The total volume was obtained by taking the sum of all incremental volumes obtained by multiplying each momentary flow by the previous time-step, as in Eq. (3.6):

$$V_{\mathrm{r\_m}} = \sum_{i=1}^{n} Q_i \, (t_i - t_{i-1}) \tag{3.6}$$

where $V_{\mathrm{r\_m}}$ = measured runoff volume (m^3); Q_i = instantaneous flow (m^3/s) and t = time (s).

3.1.4.3 The rational method

When lacking measured data, the rational method calculates V_r theoretically by Eq. (3.7) using the drainage area, the height of the rain and a coefficient describing the nature of the surface. The drainage areas can be determined from site construction plans (profile drawings and elevation data) and confirmed by going on the site during a rain event and observing the direction of flow:

$$\mathrm{V_{r\_t}} = \mathrm{c} * \mathrm{A_d} * \mathrm{H_p} \tag{3.7}$$

where $V_{\mathrm{r\_t}}$ = theoretical runoff volume (m^3); c = rational method runoff coefficient; A_d = area contributing to the runoff (m^2) and H_p = depth of the precipitation event (m).

This method can also be used to calculate the volume of rain (using the surface area of the structure and assuming a coefficient of 1.0) which fell into the LID structure directly and must be included in the total inflow volume.

3.1.4.4 Indirect measurement using a control point

Runoff volume produced by impervious drainage surfaces connected to the LID structure can be measured indirectly using control sites (termed standard or STD sites) where the flow from the street is measured directly without passing through a LID structure. The inflow volume per unit area of impervious surface was calculated by dividing the measured inflow volume (calculated using the Reimann approximation) by the impervious drainage area of the control site according to Eq. (3.8):

$$V_{\mathrm{r\_u}} = {V_{\mathrm{r\_m}}}\Big/{A_{\mathrm{d\_imperv}}} \tag{3.8}$$

where V_{r_u} = the entrance volume per unit area of drainage surface (m^3/m^2); $V_{\mathrm{r\_m}}$ = measured runoff volume (m^3); $A_{\mathrm{d\_imperv}}$= impervious drainage area (m^2).

By multiplying the result by the impervious drainage area connected to the LID structure, the hypothetical runoff volume ($V_{\mathrm{r\_h}}$) is obtained according to Eq. (3.9):

$$V_{\text{r\_h}} = V_{\text{r\_u}} * A_{\text{d\_imperv}} \quad (3.9)$$

Pervious surfaces are not considered because it is necessary to use areas of the same nature as that of the control site to justify this calculation. Therefore, one major hypothesis that must be considered is that the impervious drainage areas of the control site have characteristics like those of the impervious drainage areas connected to the LID structure.

3.2 Data measurement and processing methods

General aspects to consider when choosing any type of device include the proximity of the site to those responsible for data collection, the budgetary constraints, the precision required and the local climate.

Sources of error associated with the collection of meteorological and flow data are presented in section 3.2.3.1.

3.2.1 Meteorological data

The effective measurement of precipitation data will permit an understanding of the volume of water being collected by the LID structure and permit an analysis of the performance of the structure under a variety of rainfall conditions. A tipping bucket rain gauge is frequently used since it is easy to install and not very costly. Weaknesses include that it cannot be used in freezing weather and the rocker mechanism can fail during intense storm events. Therefore, it is important to validate the rainfall data with another rain gauge located near the site. A weather station can be used to measure not only precipitation but also temperature, humidity, wind speed and direction, barometric pressure and UV radiation. Evapotranspiration may be measured with an atmometer.

3.2.2 Flow data

It is important to use a system which can accurately measure both low and high flows since rainfall event intensities vary greatly. Details to consider when choosing the method include:

- Range of flow rates
- Accuracy requirements
- Construction, installation, operating and maintenance requirements (including cost)

- Headloss and flow characteristics
- Vandalism potential and environmental impact
- Sediment and debris

3.2.2.1 Depth-based methods

Depth-based devices, such as weirs and flumes, are commonly used to measure flow and act as a control section in the channel. An empirical equation, which must be either developed in laboratory, provided by the manufacturer or available as a standard curve, correlates the depth of flow (at a specific point before the device) to a flow rate.

A weir is a vertical obstruction placed inside the channel forcing the flow to pass through a critical depth. The weir opening is called a notch and the top edge is called the crest. Typical shapes include rectangular, trapezoidal or triangular. A flume is also an obstruction however it controls the flow in the horizontal direction (reduces the width of the channel instead of the height). Weirs are generally less expensive, more accurate and easier to install than flumes (Grant & Dawson, 1997; Spitzer, 1996). A disadvantage is that in order to maintain open-channel flow above the weir crest, a relatively large head must be available in the channel. Additionally, contracting the diameter of the channel opening also reduces its capacity to pass flow increasing the likelihood of backflow and upstream flooding. Therefore, when installing weirs, one of the most important aspects to consider is if the system can handle this reduction in conveyance capacity and ensure that installing weirs is permitted in the area of study. Large headloss is not an issue when it comes to flumes, which can also provide acceptable results without requiring much maintenance. Thin-plate weirs are the best option for small to moderate flows with the triangular notch shape being most suitable (ASTM, 1995). Although potentially less accurate, small Palmer-Bowlus flumes are also used to measure low flow. For large flows, flumes and broad-crested weirs are the better options (BMP Database, 2009).

The instrument used to measure the water depth behind the weir or flume is called the secondary flow measurement device. Examples include float gage, bubbler tube, ultrasonic depth sensor, pressure probe, ultrasonic “uplooking” and radar/microwave. Most instruments have a minimum measurable water depth value. Therefore, when choosing the device, it is necessary to ensure it will not always be operating near its threshold value (Spitzer, 1996).

Accuracy of the discharge measurements is optimized when the required flow conditions are maintained. If the nature of the flow deviates from the prescribed conditions, the measurements may be completely erroneous (USBR, 2001). For example, if the weir installed does not control the flow along the entire cross-section of the pipe then its ability to accurately measure pipe-full flows is limited potentially increasing measurement errors for large storms. Essentially, it is necessary to know the range of flows for which the weir provides an accurate measurement. The weir and secondary measurement device must also be properly installed, the head measured at the appropriate location based on the standard method, the weir maintained in good functioning form and the turbulence in the channel must be minimized.

3.2.3 Measurement uncertainty

There are two terms that must be defined to properly establish the quality and reliability of collected data.

Uncertainty is defined as: "parameter, associated with the result of a measurement, that characterizes the dispersion of the values that could reasonably be attributed to the measurand" and absolute error of measurement is the "result of a measurement minus a true value of the measurand" (JCGM, 2008).

When measuring physical quantities, there will be imperfections in the measuring method and procedure which will give rise to either systematic or random errors. Care must be taken to understand what the important sources of error are and how they can be minimized. Random error, which occurs due to unpredictable variations of influence quantities, can be reduce by increasing the number of measurements taken. In order to reduce systematic errors, the source of the latter must be identified, the error quantified, and a correction can be applied to counteract it. The accuracy of a measurement considers how close the value of the measurement is to its true value and the repeatability considers the closeness of the resulting values of the same measurement performed multiple times under the same conditions. With any measurement, there will always be an associated uncertainty that must be reported when stating the value of the measurement (JCGM, 2008).

It is therefore necessary to understand the possible sources of both random and systemic error in a LID-BMP monitoring study, establish methods to eliminate them as much as possible and quantify the uncertainty that will exist in the reported results.

3.2.3.1 Sources of error

Precipitation Data

- Temporal and spatial non-homogeneity of rainfall:
    - ensure the device is installed as close as possible to the site (< 1.6 km) and at a similar elevation
    - ensure multiple rain gauges are available to validate the precipitation data collected at the main gauge. An acceptable error must be established
- Installation: carefully follow manufacturer's guidelines
- Calibration: Do so twice a year

Flow Data

- Maintenance: for weirs, it is necessary to remove any debris that has amassed behind the weir, so the water depth measured remains accurate
- Unsteady and low flows: ensure that the second measuring device is not frequently operating near its threshold value
- Calibration: verify the calibration frequently and re-calibrate multiple times during the monitoring campaign
- Fabrication and installation: ensure the weir is designed and installed based on the standard for flow measurement using a weir (ASTM, 2013)
- Operation: proper user operation with sufficiently frequent inspection and maintenance procedures (USBR, 2001)

3.2.3.2 Uncertainty quantification

3.2.3.2.1 Error propagation

To calculate the propagation of the error associated with the height measurement, the typical error propagation equations are used (WCI Physics).

Multiplication by a constant

For a value multiplied by a constant, the propagated uncertainty, Δz, is calculated using Eq. (3.10):

$$\Delta z = \sqrt{C_1(\Delta x)^2 + C_2(\Delta y)^2 + \cdots} \tag{3.10}$$

where $Z = C_1 * x + C_2 * y + \ldots$.

Note that Δ represents the absolute uncertainty of the value.

Value to a power

For a value to a power, the propagated uncertainty, Δz, is calculated using Eq. (3.11):

$$\Delta z = |n| \frac{\Delta x}{|x|} \, |Z| \tag{3.11}$$

where $Z = x^n$.

Value for a summation

For a summation, the propagated uncertainty, Δz, is calculated using Eq. (3.12):

$$\Delta z = \sqrt{(\Delta x)^2 + (\Delta y)^2 + \cdots} \tag{3.12}$$

where $Z = x + y + \ldots$.

3.2.3.2.2 Standard error from LINEST

The LINEST function is built into Microsoft Excel and utilizes the least squares method to determine the statistics associated with a trendline, outputting an array describing the line. Information obtained includes the standard error of the y value and of the associated constants a and b.

3.2.3.2.3 Total system error

Eq. (3.13) combines each individual error contribution and can be used to estimate the total percentage error of a flow measurement (ASTM, 2013):

$$e_t = \sqrt{(e_1)^2 + (e_2)^2 + \cdots} \tag{3.13}$$

3.2.4 Separation, validation and categorization of rainfall events

The criterion used to differentiate independent rain events from continuous rain events is the Inter-Event Time Definition (IETD). This criterion therefore represents the time interval between the end of the rain and the end of the run-off exiting the LID structure. Therefore, when the onset of runoff is not superimposed with the end of runoff from previous rainfall, both rains are considered two independent events. Conversely, both rains are considered as one event (Joo et al., 2014). Constant values can also be used to define the minimum period required with no rainfall between individual events (e.g. 3 hours).

Precipitation events can be characterized using various attributes, namely, total depth of rain, duration of event, average intensity over the entire duration, the maximum intensity of a time-step, Antecedent Dry Days (ADD) and return period.

CHAPTER 4 SITE DESCRIPTIONS AND METHODS

4.1 Description of the study area

4.1.1 Overview of the project

The site under study is a small urban sub-catchment; more specifically, a 1.5 km stretch of a large boulevard located in the city of Montreal. The total drainage area of the site is approximately 5 hectares. The redevelopment consists of 38 individual rainwater retention cells (standard size = 30 m long x 3.5 m wide). These cells are located along the East side of the street between the 10 m road span and the 4 m sidewalk (Figure 4.1).

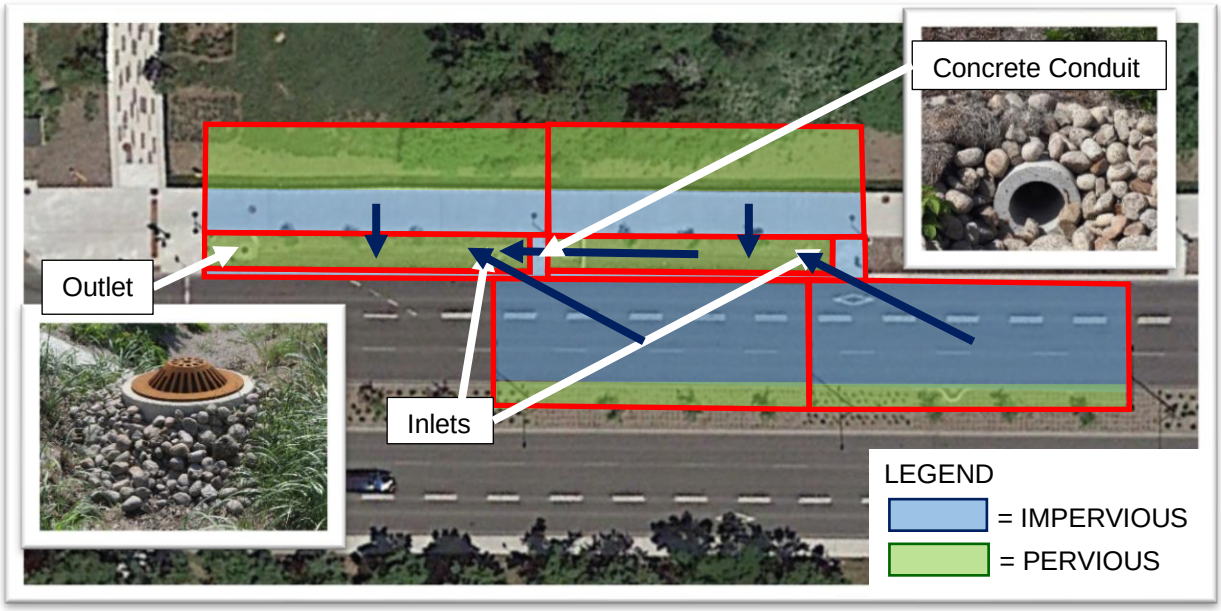

Figure 4.1 Plan view of a bioretention structure taken from Google Earth

The tributary area to LID-BMP area is approximately 4.5:1. Each individual cell has a 0.5 to 1 % slope and collects water from a section of the street through a rectangular stormwater drain and single 150 mm diameter pipe located at their upstream end (Figure 4.2) and from the adjacent sidewalk. Runoff from part of the grass land adjacent to the sidewalk and the street median (highlighted in green in Figure 4.1) is considered negligible.

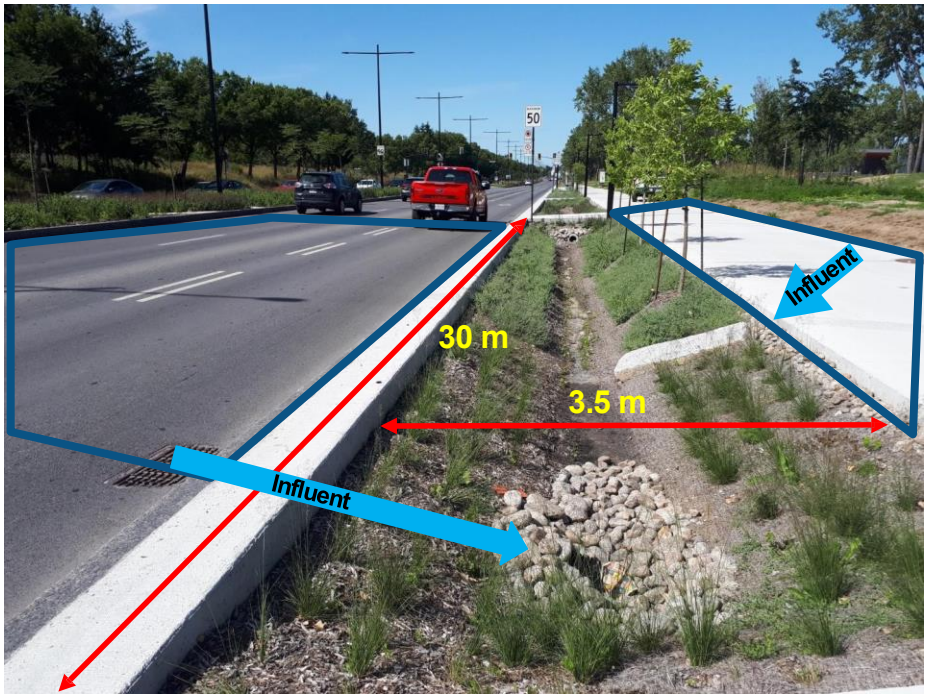

Figure 4.2 Representation of the main aspects of an individual cell

The site is composed of two different kinds of basin units: bioretention (BB) and vegetated swales (VS). A basin is composed of 1 to 3 individual cells in series, which are connected by a 200 mm diameter concrete pipe. Each basin drains to the combined sewer network (located under the sidewalk) through an overflow drain located at the downstream end of the last cell making up the basin (Figure 4.1). The difference between the two types of basins is the flow path the collected runoff will follow. In the case of the bioretention unit, the downstream overflow drain is elevated (500 mm) forcing the rainwater to be stored in the cell, percolate deeply into the soil and be collected by a perforated pipe installed underneath the soil structure (Figure 4.3).

Figure 4.3 Overflow downstream drain of a bioretention basin

The vegetated basin does not store runoff since its overflow drain is at the same elevation as the bottom of the cell and does not have an underground perforated conduit (Figure 4.4).

Figure 4.4 Lowered downstream drain of a vegetative swale

This means that once the surface layer of the soil is saturated, the excess runoff will flow towards the overflow drain and empty into the combined sewer network directly without first passing through the 600 mm soil layer. This greatly reduces the water treatment capabilities of the vegetated basins. In addition, the basins analyzed in this study include flow regulators at their exit installed on the conduit linking the overflow drain to the sewer system (Figure 4.5).

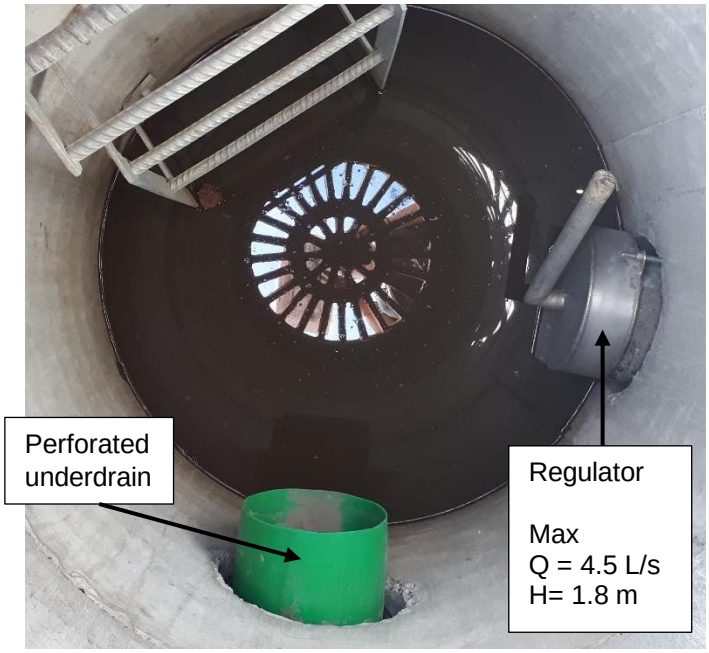

Figure 4.5 Top view inside the downstream overflow of a bioretention basin showing the regulator fitted on the conduit connecting the structure to the sewer line

Geotechnical tests completed on the natural soil of the site presented a natural soil with low hydraulic conductivity. This confirmed the requirement to install a perforated underdrain in the bio-retention basins. This is because the natural soil will greatly reduce deep percolation not permitting the water to escape when there is a large rainfall event. The average seepage rate in the natural soil obtained was 0.875 mm/hr. However, caution must be taken when using these values since the small number of boreholes present a limited survey of the site. In this project, the basins are not being used to replenish the water table.

4.1.2 Additions for monitoring

Manhole units were constructed in the sidewalk (Figure 4.6) at 3 locations to intersect runoff directly from the street and called standard (STD) monitoring points. The STD monitoring sites were added as a substitute to measuring the inflow into each cell since this was deemed impossible (the design of the basin runoff inflow points does not facilitate installation of monitoring equipment). These measurement points permit the approximation of the inflow runoff per unit area of impervious surface.

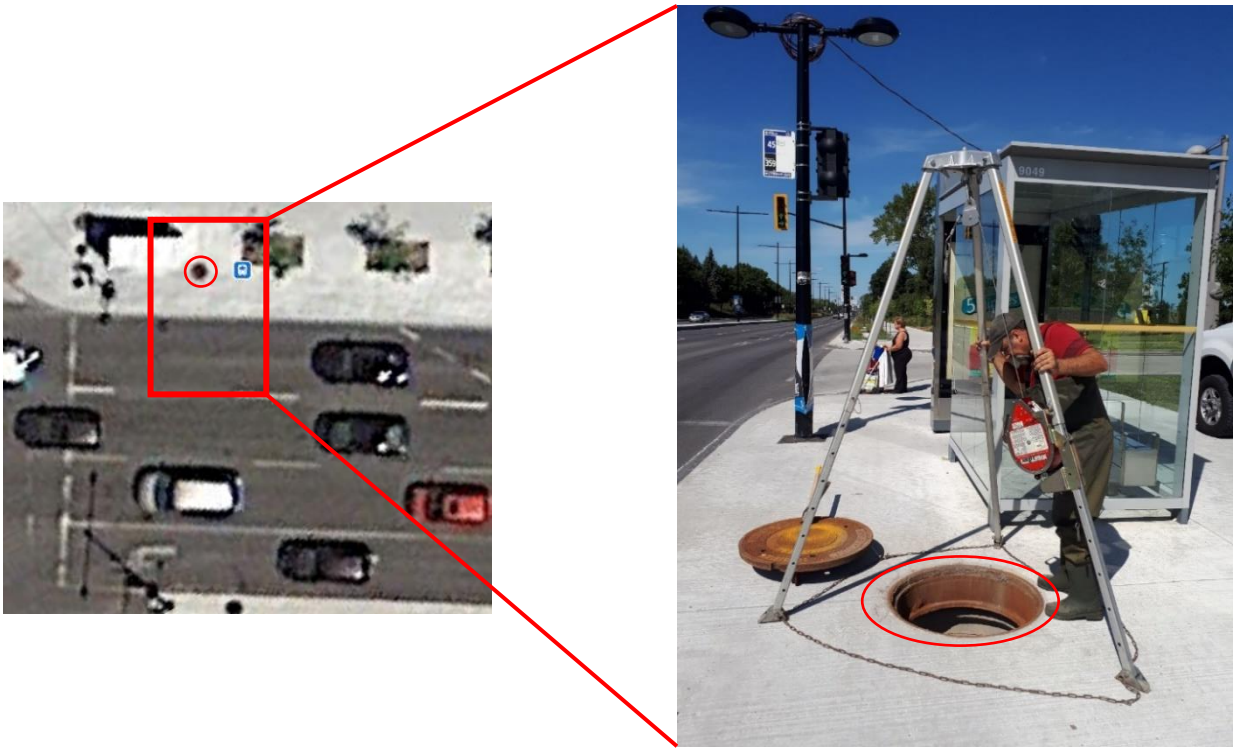

Figure 4.6 Example of an STD monitoring site

Additional manhole units were constructed to intersect the outflow from 9 basins and facilitated the installation of flow measurement equipment. This includes compound weirs which were calibrated in laboratory and installed on the conduit connecting the basin overflow drain and the manhole unit.

4.1.3 Location of the monitoring sites

The two sites of focus in this study are the vegetated swale VS-M3 and the bioretention basin BB-M10. The control site used to indirectly measure the inflow into the LID units (STD-M12) is located at the northern end of the study. The rain gauge located within the boundaries of the study area is used as the main source of rainfall data. Those located in the areas around the site were used as verification as shown in Figure 4.7.

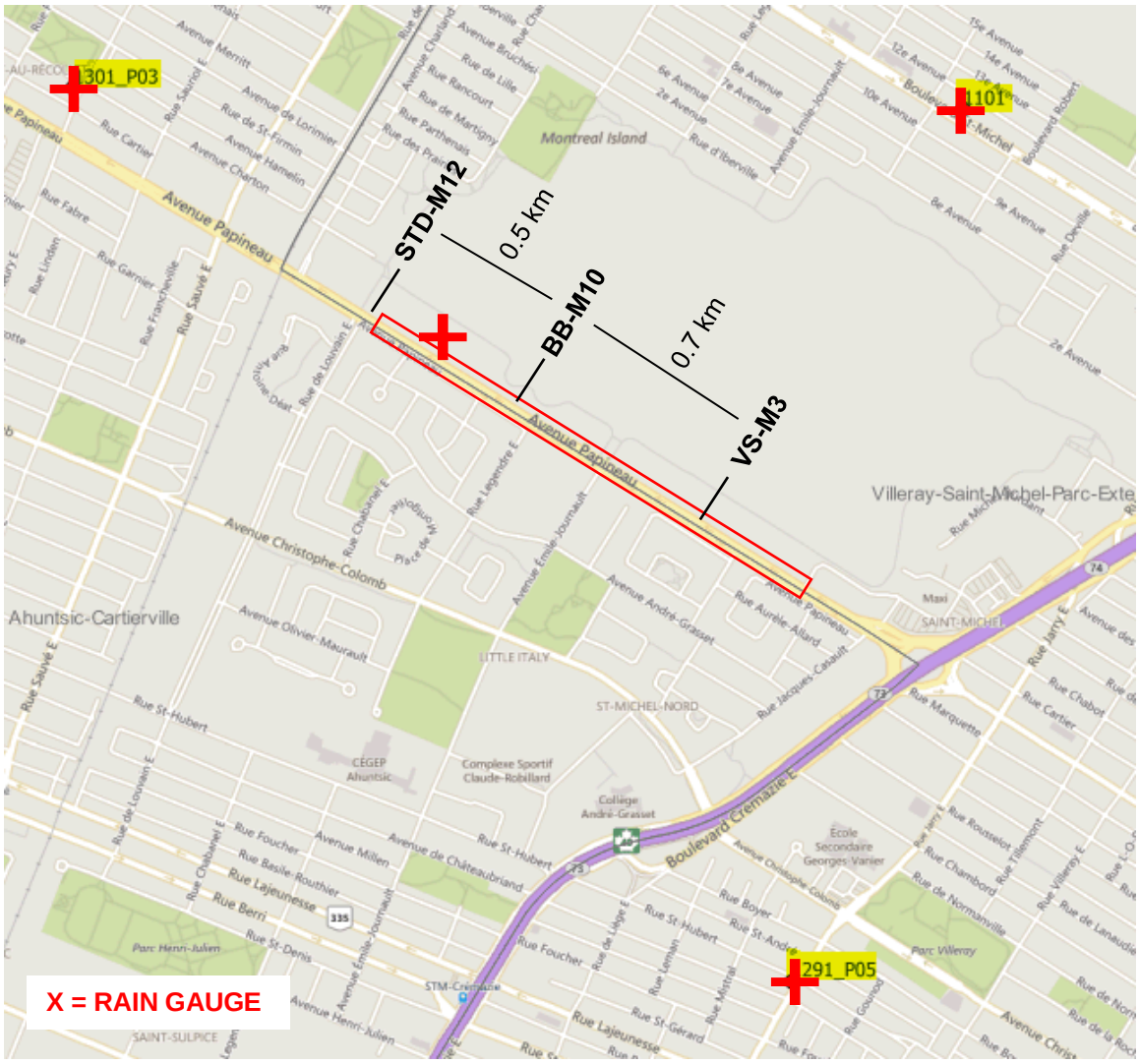

Figure 4.7 Location of each monitoring site and the rain gauge along the 1.5 km span of boulevard as well as the 3 city gauges

4.1.4 Characteristics of the monitoring sites

The depth of the bioretention cell is approximately 50 cm, after which any ponded water will exit through the elevated overflow drain. The potential bowl storage is 54 m^3 which is equivalent to 6.3 cm of runoff over the drainage area. The vegetated swale surface area represents 20% of the 855 m^2 impervious catchment and the bowl volume is 45 m^3 which is equivalent to 5.2 cm of runoff over the drainage area. However, this storage would only be utilised if the capacity of the draining conduit is breached and backflow occurred in the cells. A summary of all relevant design characteristics for both structures is presented in Table 4.1 and additional details are noted in Appendix A.

Table 4.1 Descriptive characteristics of LID structures and drainage areas

Characteristics	**VS-M3 (Vegetated Swale)**	**BB-M10 (Bioretention Basin)**
Catchment area[a] (m^2)	855	859
Catchment composition	Street section + sidewalk	Street section + sidewalk
Catchment percent imperviousness (%)	100	100
LID-BMP surface area (m^2)	167	204
BA:IDA ratio (%)	20	24
Cross-section shape	Trapezoid	Trapezoid
Surface storage volume (m^3)	45	54
Average bowl storage depth (cm)	NA	50
Fill media depth (cm)	60	60
Gravel layer thickness (cm)	NA	40
Underdrain diameter[b] (mm)	NA	200
Media characteristics	82% sand, 18% fines	74% sand, 26% fines
Media textural classification[c]	Silty Sand	Silty Sand
Porosity	0.467	0.54
Media saturated hydraulic conductivity[d] (mm/hr)	91	91

[a]It is possible that for very large events the street catch basin capacity was breached and therefore not all runoff from the surfaces entered the cells.
[b]Perforated PVC.
[c]Sieve analysis tests were performed in the Polytechnique Montreal University geotechnical laboratory and classification was determined through the Unified Soil Classification System (USCS).
[d]Literature value obtained from Rossman and Huber (January 2016)

4.2 Equipment used to obtain the required data

4.2.1 Flow measured in 2018

Runoff measurements were initially collected only with Teledyne ISCO 2150-Area-Velocity flow modules which measure the height of the water using a pressure transducer, the velocity using the Doppler Effect and calculate the flow using the Manning equation. The data was collected at 15-minute intervals. The flowmeters were used to measure outflow and therefore installed inside the conduits which connect the outlet overflow drains of the LID structures to the sewer system (inside sidewalk manholes). In the case of the street connexions, the flowmeters were installed in the conduit which directly connects the street catch basin to the sewer system. The instrument set up inside each monitoring manhole can be seen in Figure 4.8.

Figure 4.8 Set-up of a Teledyne ISCO 2150-Area-Velocity flowmeter inside a monitoring manhole

When the runoff depth inside the conduit was small, three velocity reading scenarios were noted:

- The value measured by the flowmeter is correct;
- The value measured by the flowmeter is zero;
- The value measured by the flowmeter is over-estimated.

This resulted in very few correct velocity readings during the 2018 monitoring period and therefore few flow values. Additionally, the minimum height value which can be accurately measured by the probe is 10 mm. The outflow measured was frequently close to this value. Therefore, although it was possible to use the Manning equation to calculate the flows from the height readings, the values were not considered correct. The data collected in 2018 was thus not used for analysis.

4.2.2 Flow measured in 2019

4.2.2.1 Equipment installed

An important conclusion established after the first data collection campaign is the Teledyne ISCO 2150-Area-Velocity flowmeters are not well suited for low flow measurements (0-2 L/s). The nature of the project involves frequent low flow measurements since a large portion of the rainfall runoff is retained by the basins. In the second year of data collection it was necessary to install compound weirs on the downstream end of the conduits (Figure 4.9) which permit an accurate measurement of both low and high flow (see section 3.2.2.1 for general theory).

Figure 4.9 Compound weir and Teledyne ISCO 2150 probe installed on the downstream end of an outflow conduit in 2019

The rating curves of these weirs were generated in the laboratory setting using a controlled flow and were subsequently verified in-situ. These curves determine the relationship between the height in the conduit and the flow that is passing. In this way, the necessity of using the flowmeters to measure velocity was eliminated. The detailed calibration steps, the curves determined for each site and photos of the set up can be found in Appendix B.

The Teledyne ISCO flow modules were still used as secondary measurement devices to monitor the head above the weir crest. The time-step used when there was no flow was 15 minutes and once the flow reached a certain height it changed to 2 minutes (possible to program this into the flowmeter).

4.2.2.2 Comparison with Doppler velocity data

It was possible to obtain flow data directly from the flowmeter velocity readings (measured using the doppler effect) since the weirs block approximately 3 cm of flow from passing and there is always a depth of water in the conduit. In Figure 4.10, a hydrograph obtained directly from the flowmeter was compared to one obtained via the weir calibration curve equation for the monitoring site STD-M-12 during the rainfall event of April 19th.

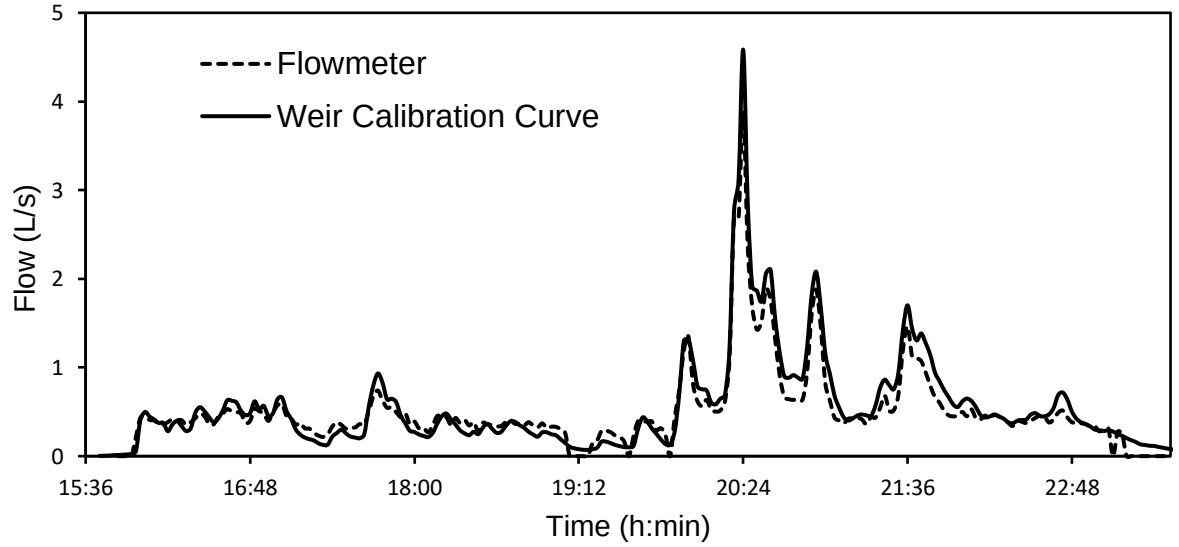

Figure 4.10 Comparison between hydrographs obtained using the flowmeter directly vs the weir calibration curve at the control point STD-M12 (event of April 19th, 2019)

The general shape of the two curves is similar. For flow rates greater than 0.5 L/s, the differences between the two curves are minimal. Moreover, peak flows seem to match. However, when the flow rate is smaller than 0.5 L/s, the two curves show a greater difference. Between 18:43 and 19:07, the probe seems to overestimate the flow compared to that calculated by the rating curve. In addition, zero values are measured by the probe when the flow rate is smaller than 0.2 L/s. Therefore, the use of the rating curve is prioritized to calculate the flow rate so as not to overestimate or underestimate the small flows and volumes measured during smaller rainfall events. This confirms the correctness of the calibration curve established in the laboratory.

4.2.3 Rain and weather

The rain was measured on the site using a tilting rain gauge (674 ISCO rain gauge) installed on the roof of a nearby sports center. The rain was collected every 5 minutes by the gauge and validated using three other city gauges located around the site (Figure 4.7). A Davis instruments Vantage Pro2 weather station was also used to collect meteorological data every 10 minutes: wind direction and speed, rainfall, the temperature and UV radiation as well as the humidity index.

4.2.4 Media type, moisture content and surface ponding

Tests on the soil in the basins were completed in October 2019. Particle size analysis and analysis by sedimentation were completed to characterize the nature of the soil using the Unified Soil Classification System (García-Gaines & Frankenstein, 2015). HOBO data logger probes measuring moisture content of the soil were installed in one cell of each basin monitored in 2019 (Soil Moisture Smart Sensor S-SMx-M005). These permit an understanding of the drying rate of the soil during period without precipitation. Piezometer wells (80 cm long and 5 cm in diameter) were installed in the top section of the soil layer. The water level in the LID-BMP bowls was measured using HOBO data loggers (U20L-04 water level data logger) to identify outflow through the elevated overflow drains.

4.3 Rainfall categorization

Appendix C contains the list of all rainfall events measured in 2019 characterized using 5 attributes: duration, height of precipitation, average intensity (I_{avg}), maximum intensity (I_{max}) and Antecedent Dry Days (ADD). Rainy events were then categorized by ranking from 1 to 5 the strength of each of their attributes as presented in Appendix D. The intervals for each category for each characteristic are presented in Table 4.2.

Table 4.2 Values for each attribute category division

# of the category	Duration (h)	I_{avg} (mm/h)	I_{max}[a] (mm/h)	Total Height (mm)	# ADD
1	0 to 2	0 to 1	0 to 5	0 to 5	0 to 2
2	2 to 4	1 to 2	5 to 10	5 to 10	2 to 3
3	4 to 7	2 to 3	10 to 20	10 to 15	3 to 4
4	7 to 14	3 to 7	20 to 40	15 to 25	4 to 6
5	14 to 40	7 to 30	40 to 100	25 to 75	6 to 20

[a]Data collected on a time step of 10 minutes.

4.4 Examples of error and uncertainty

4.4.1 Error from weir set up

4.4.1.1 The calibration curves

As presented in Appendix B, a separate calibration curve was plotted for the v-notch section and the rectangular section of each weir. In the case of the STD-M12 (Figure 4.11), a third curve (power trendline) was used for the lowest values in the v-notch section. This was necessary since the vertex of the polynomial curve is 8.94 mm producing an undesired increase in flow as the height tends to zero. In order to avoid this, the power equation was used for $H < 8.94$ mm. A more straightforward method to avoid this would be to force the polynomial curve to pass through zero (an option when plotting trendlines in Microsoft Excel).

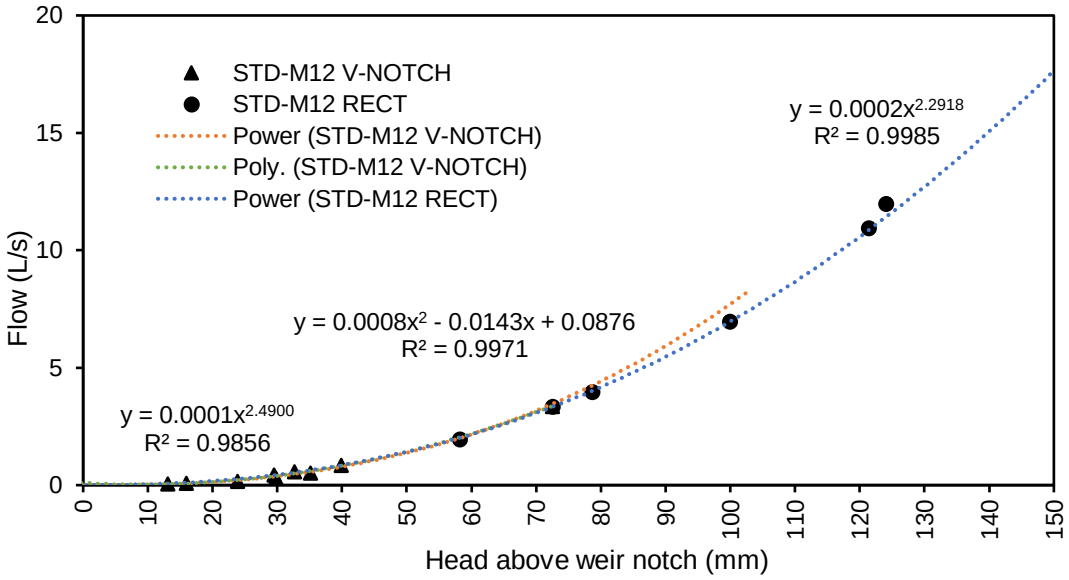

Figure 4.11 Rating curves developed in the laboratory for STD-M12 defining the relationship between the flow and the head measured above the notch of the weir

When calculating the flow associated with a single height measurement, only one equation is involved. Errors in this calculation included the propagation of the uncertainty of the height measurement and of the trendline used to relate the two variables. The rating curve is also affected by the slope however this was considered during the calibration process by setting the open channel to the same slope as the conduit in the field.

4.4.1.2 Threshold value

The threshold value is defined as the height from the bottom of the conduit to the v-notch and must be subtracted from the total height measured by the probe. This is because a weir rating curve is developed by plotting the flows as a function of the heights measured above the weir crest. Theoretically, the threshold represents the height the runoff must attain before flowing over the weir crest and should remain constant since it is dependent on the physical dimension of the conduit and of the weir. Thresholds were determined by pouring water in the conduits on the field and noting at what exact height the water started flowing over the crest.

4.4.2 Field data collection issues

There were a variety of issues which arose during the data collection campaign depending on the type of measurement equipment:

Flowmeters

- Dead batteries
- De-calibration of the probes
- General malfunction of the module which required a replacement and re-installation on the field

Rain-gauge

- Erroneous setting of the collection time-step
- Inability to capture the precipitation data for very large events (the instrument would cease data collection during the most intense periods of the storm and eventually restart)

Weather station

- Improper set up of the weather station in the program which did not initiate the measurement properly therefore 2 weeks of data was not collected

Moisture Content

- Water got into the collection case since it was not properly sealed

These monitoring issues affected the amount of data which was successfully collected. Additionally, there is always the issue of data capacity with most instruments. It is important to know this value and ensure that the period of data collection is frequent enough, so the device does not reach this capacity and begins to erase previously collected data.

A more in-depth description of the main challenges addressed during the research project is presented in Appendix E.

4.4.3 Conduit surcharge

Another important point to note is the constraint of the flowmeters which are supposed to be used for open-channel flow. The diameter of all conduits in which the probe is place is 200 mm. However, during a large storm event on July 30th, 2019, there were measured water heights which exceeded this at STD-M-12 (Table 4.3).

Table 4.3 Heights measured and flows calculated for the peak intensity at site STD-M-12

Date	Time (h:min)	Height (mm)	Flow (L/s)
7/30/2019	19:28	125.70	12.95
7/30/2019	19:30	226.62	49.99
7/30/2019	19:32	154.64	20.82

During the calibration of STD-M-12 in the laboratory, the maximum flow that could pass through the conduit was measured to be approximately 21 L/s. Looking at the third row in the table, the height is almost equal to the diameter of the pipe and the flow is close to 21 L/s. Therefore, it is possible to conclude that right before this, the conduit became surcharged. At this moment, the value read by the probe can no longer be considered realistic. On top of that, the height value measured is outside the range of the calibration curve. The trendline used to obtain the calibration curve (Figure 4.11) of the weir was a power curve. This means that the curve will grow quickly as it continues along the x-axis. This results in the incredibly large flow of 50 L/s being assigned to a height of 226 mm.

Therefore, the methods and instruments used to obtain the observed hydrographs have a limit to their accuracy in the face of very large rainfall events.

4.5 Modelling process

Chapter 6 of this document provides a detailed overview of the entire modelling procedure as well as a quantification of the findings. A summary of the steps involved in both the parametric and redesign calibrations of the modelled LID-BMPs is presented in Appendix E.

CHAPTER 5 ARTICLE 1: HYDROLOGIC PERFORMANCE OF A BIORETENTION BASIN AND VEGETATED SWALE CONSTRUCTED IN LOW PERMEABILITY NATURAL SOILS IN MONTREAL, CANADA.

Julia Bond, M.ScA Candidate; Essoyeke Batchabani, P. Eng, Ph.D.; Musandji Fuamba, P. Eng., Ph.D., M.ASCE, David Courchesne, P. Eng., and Guy Trudel, Arch.

Journal Science of the Total Environment

Abstract

Low Impact Development (LID) encompasses design concepts to reduce degradation of a site's natural runoff index. New Stormwater Control Measures (SCMs) in the form of structural micro-solutions (termed LID-Best Management Practices or LID-BMPs) have been implemented around the world as control strategies benefitting from natural systems to increase infiltration and evapotranspiration. It is important to quantify the performance of these solutions to assess the value of their implementation and continuously improve their design. In this paper, two types of best management practices were monitored, a bioretention basin and a vegetated swale. Their hydraulic performance was quantified using metrics such as bioretention abstraction volume, volume retention, peak flow reduction and peak delay. The bioretention abstraction volume was determined to be approximately 23 m^3. Of the measured events, 91% (bioretention basin) and 78% (vegetated swale), achieved volume reduction above 67% (the suggested target). The target value of 67% for peak flow reduction was attained for 98% (bioretention basin) and 94% (vegetated swale) of events. A minimal peak delay was measured with the target of 6 times (unitless) being exceeded for only 25% (bioretention basin) and 30% (vegetated swale) of events. The vegetated swale is an example of a less costly design which provides acceptable hydraulic control. Due to the large BMP Area to Impervious Drainage Area (BA:IDA) ratio of the bioretention basin, it showed superior global volume retention performance when compared to a structure with a larger soil layer and one with an Internal Water Storage (IWS) zone. However, the bioretention basin did not completely retain the flow from small storm events demonstrating the necessity of combining the larger BA:IDA ratio with one of the following: a larger soil depth, IWS zone, larger media clay content or installation of a controllable cap-orifice device on the underdrain exit.

5.1 Introduction

Traditional stormwater management methods have the objective to drain runoff as quickly and efficiently as possible to downstream water bodies (MDDEFP, 2014). However, it was established that one of the largest contributors to non-point source pollution of estuaries and lakes is the urban runoff generated by regularly occurring storm events which make up 90% of storms in a year (Booth & Jackson, 1997; Konrad et al., 2005; Marsalek et al., 1999; USEPA, 1983). Furthermore, with the rise in urban development and subsequent expansion of impervious areas, stormwater runoff volume has increased leading to more frequent combine sewer overflows (CSO) and conveyance system surcharge (Stovin et al., 2013). In order to address these issues, termed the so-called “Urban Stream Syndrome” (Walsh et al., 2005), a new thinking around stormwater management evolved. Low Impact Development (LID) increases the chances for a site to have “predevelopment hydrology” ("Energy Independence and Security Act (EISA),") by managing runoff at the source. New stormwater control measures (SCMs) in the form of structural micro-solutions (termed best management practices or LID-BMPs) have been implemented around the world as mitigation strategies which benefit from natural systems by utilizing soils and vegetation to encourage infiltration and evapotranspiration of rainwater (National Research Council, 2008).

The decision to implement any LID-BMP must consider the particularities of the site. Landscape characteristics represent only one of many elements influencing the performance of LID solutions (Passeport et al., 2013; Zahmatkesh et al., 2014). Regional rainfall patterns also direct their effectiveness (Gallo et al., 2012; Jennings et al., 2012; Qin et al., 2013). A consequence of the large influence of local site conditions on LID-BMP performance is the resistance of professionals towards implementation without direct physical proof of their benefits. Therefore, local pilot projects are a necessity to encourage overall adoption (Eckart et al., 2017; Ewing et al., 2000). Furthermore, in order to advance the fundamental understanding and quantification of the benefits of these SCMs, it is instrumental to establish field monitoring research studies focused on providing data-based performance evaluations (Davis et al., 2012).

An example of an SCM being increasingly used in developed areas is bioretention (also called rain garden). Their standard design includes a depression in the ground containing an engineered soil material and appropriate vegetative species and a layer of bark mulch to prevent soil erosion. An optional perforated underdrain pipe draining to the sewer system can be included depending on

site-specific conditions. As a LID solution, bioretention provides a multitude of benefits, namely, peak flow attenuation, runoff volume and pollutant loading reduction/elimination, increase in evapotranspiration and biological activity, reduction in stream erosion and replenishment of groundwater aquifers (Davis, 2008; Davis et al., 2009; Dietz, 2007; Dietz & Clausen, 2005).

Davis et al. (2012) presented the common ability of bioretention basins to completely assimilate small rainfall events. This was also confirmed in studies by Mahmoud et al. (2019) and Li et al. (2009) who showed that not only can bioretention be used to assimilate small events but also reduce and delay the peak flow for larger events. Generally, these types of structures are unable to handle extremely large precipitation events (Eckart et al., 2017; Holman-Dodds et al., 2003; Williams & Wise, 2006). Altogether, studies show that the quantitative hydrologic performance of a bioretention structure cannot be normalized since it can vary largely depending on the rainfall event and differences in site characteristics (Davis et al., 2012).

A variety of underdrain configurations can be utilized and affect the retention capacities of a bioretention basin (Brown & Hunt, 2011). Designing the underdrain such that an Internal Water Storage (IWS) zone is formed has been shown to positively influence volume retention performance (Brown & Hunt, 2011; Dietz & Clausen, 2006; Li et al., 2009). The end point of the underdrain is elevated to create an upturned elbow resulting in a saturated zone at the bottom of the bioretention basin (typically 0.3-0.75-m deep) (Hunt et al., 2006; Passeport et al., 2009).

Winston et al. (2016) presented the hydrologic results for 3 bioretention basins built in poorly drained soils which included an IWS zone in their design. Nevertheless, there is a lack of available field data on the performance of bioretention basins constructed in low permeability natural soils.

The objective of this study is therefore to quantify the hydrologic performance of a bioretention basin constructed in low permeability natural soils without the addition of an Internal Water Storage (IWS) zone. This will be compared to another LID-BMP (called a vegetated swale in this paper) designed without an underdrain and with a downstream drain at the bottom of the cell. The regulations in the region do not permit the implementation of an elevated overflow in a structure without underdrain if the natural soils have low permeability. Furthermore, a unique design aspect of both structures is that each is made up of 2-3 individual cells connected in series by a 250 mm concrete conduit. This contrasts with other studies which often present just one cell.

Other design parameters evaluated include, soil layer characteristics, bowl storage volume and BMP Area to Impervious Drainage Area (BA:IDA) ratio. Hydraulic performance is quantified using the bioretention abstraction volume, retention capacity/volume discharge ratio, peak flow mitigation and delay in peak timing.

5.2 Performance assessment

The components of the elemental water balance across a bioretention cell can be analyzed by considering a typical cross-section (Figure 5.1). Runoff from adjacent surfaces first enters the depression (bowl), which has a typical depth ranging from 15 to 52 cm. It then infiltrates and is stored in the substrate layer, commonly between 0.6 and 1.2 m deep, which can be subdivided into two sections, the root zone, or Root Zone Management System (RZMS), and the Lower Media Storage (LMS). The RZMS represents the top layer which contains the roots of the plants and is assumed to be approximately 30 cm deep (Davis et al., 2012). The LMS is the remaining soil below the RZMS.

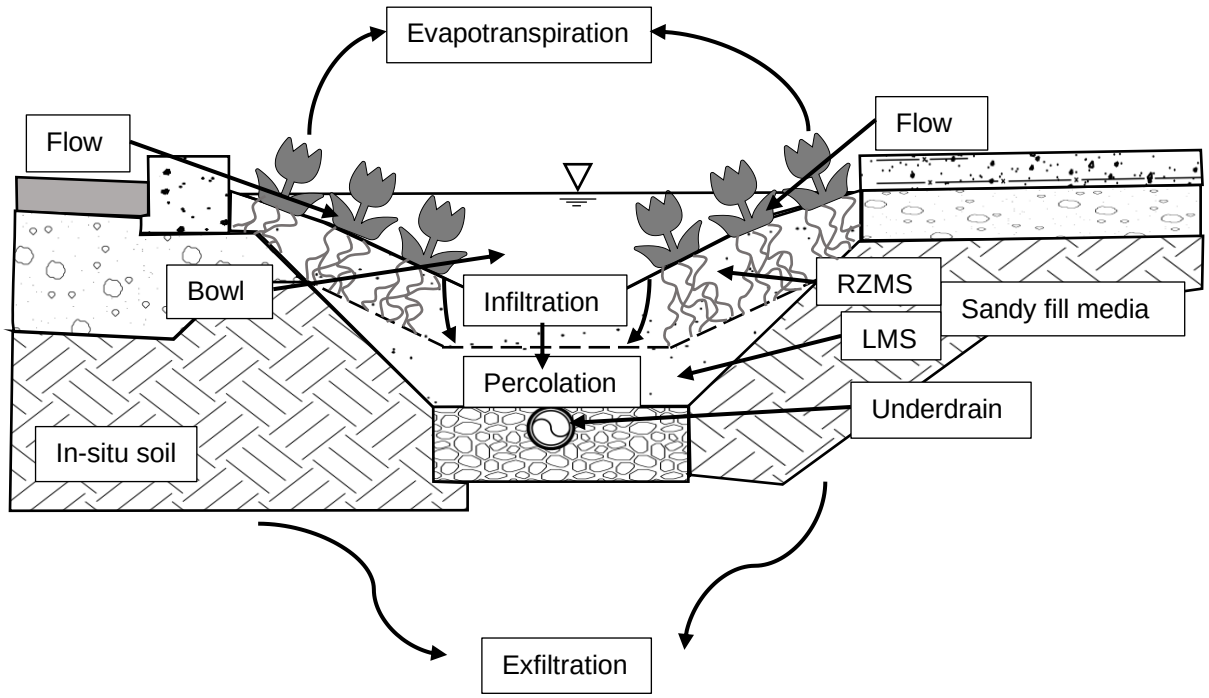

Figure 5.1 Cross section of a bioretention SCM (Les Services EXP inc. 2018 on behalf of the City of Montreal).

The field capacity (FC) of a soil is the residual moisture fraction of a previously saturated soil which has drained freely by gravity (Schwab et al., 1993). Once the FC is surpassed, the water will start percolating from the RZMS to the LMS and exit by either the underdrain or exfiltration to the adjacent natural soils. The initial soil moisture content affects both the amount of available pore space for storage and the speed at which FC occurs. The wilting point (WP) is the minimum moisture fraction required for plant survival. The water will begin filling the bowl of the structure once the inflow rate surpasses the percolation and exfiltration rates. Essentially, the bowl of structure stores runoff which undergoes evapotranspiration and the soil layer collects runoff of which a portion is exfiltrated to the in-situ soils thus restraining overall transfer to downstream waterways.

5.2.1 Description of LID-BMP performance and acceptance criteria

The performance of the LID-BMPs was evaluated based on retention efficiency which represents the proportion of the inflow which did not drain from the structure and was transformed into a combination of exfiltration and evapotranspiration. Performance metrics used to quantify this include Bioretention Abstraction Volume (BAV) and the Volume Discharge Ratio (VDR). Additionally, in order to reduce the amount of runoff being redirected directly to downstream waterbodies (combined sewer overflows), it is beneficial to reduce and delay the peak flow passing through the system. This capacity was quantified using the peak flow rate ratio and the peak discharge time span ratio.

Davis et al. (2012) used the BAV, which is the volume of inflow completely withheld by the structure, as an initial evaluation metric. The BAV is dependent on the LID-BMP design and is a function of rainfall characteristics and the nature of a soil's initial moisture content.

In the case of a bioretention basin with an underdrain system, it is necessary for the infiltration rate to surpass the drain outflow rate and soil percolation rate before the bowl is utilized for storage. A suggestion was made by Davis et al. (2012) to calculate the average BAV (*ave BAV*) theoretically which considers the underdrain's ability to quickly drain the deeper soil layer. The LMS is therefore assumed to have attained FC in Eq. (5.1):

$$Ave\ BAV = RZMS * (SAT - WP) + LMS * (SAT - FC) \tag{5.1}$$

where SAT and WP = moisture content of the Soil at Saturation and Wilting Point.

It is necessary to add the bowl volume to Eq. (5.1) to obtain the theoretical maximum BAV. The minimum BAV (*low BAV*) can be calculated with Eq. (5.2):

$$Low\ BAV = RZMS * (SAT - WP) \tag{5.2}$$

Three additional criteria can be used to assess the influence of the LID-BMPs on the entrance hydrographs (Davis, 2008; Li et al., 2009; Winston et al., 2016): the volume discharge ratio (VDR or f_{V24}) [Eq. (5.3)], the peak flow rate ratio R_{peak} [Eq. (5.4)], and the peak discharge time span ratio R_{delay} [Eq. (5.5)], which are expressed as:

$$f_{v24} = \frac{V_{out-24}}{V_{in}} \tag{5.3}$$

$$R_{peak} = \frac{q_{peak-out}}{q_{peak-in}} \tag{5.4}$$

$$R_{delay} = \frac{t_{q-peak-out}}{t_{q-peak-in}} \tag{5.5}$$

where V_{out-24} and V_{in} denote the total volume of outflow (within 24 hours of the rainfall event) and inflow (m^3) to enter and exit the structure; $q_{peak-out}$ and $q_{peak-in}$ are the peak discharges of the outflow and inflow hydrographs (L/s); and $t_{q-peak-out}$ and $t_{q-peak-in}$ are the timespans from the beginning of the outflow and inflow to the peak discharges (h:min). Suggested target values are f_{v24} < 0.33, R_{peak} < 0.33, and R_{delay} > 6 (Davis, 2008).

The retention capacity of a structure can be calculated using Eq. (5.6):

$$Retention\ capacity = 1 - f_{v24} \tag{5.6}$$

5.2.2 Calculating inflow and outflow volumes and peak flows

At certain locations called standard (STD) control points, additional manhole units were implemented to directly intersect impervious surface runoff. The STD monitoring sites act as a substitute to measuring the inflow into each LID structure since the design of the inflow points does not facilitate installation of monitoring equipment. Therefore, instead of calculating the inflow using a theoretical method, the runoff per unit area of impervious surface was approximated from the measured data according to Eq. (5.7):

$$V_{\text{r\_u}} = {}^{V_{\text{r\_m}}}\Big/_{A_{\text{d\_imperv\_STD}}} \tag{5.7}$$

where V_{r_u} = the runoff volume per unit area of drainage surface (m^3/m^2); V_{r_m} = the total runoff volume measured directly at the STD site (m^3); and $A_{\mathrm{d\_imperv\_STD}}$ = the impervious drainage area of the control site (m^2).

By multiplying the result by the impervious area draining into the LID structure, the hypothetical inflow runoff ($V_{\mathrm{r\_h}}$) is obtained according to Eq. (5.8):

$$V_{\mathrm{r\_h}} = V_{\mathrm{r\_u}} * A_{\mathrm{d\_imperv\_LID-BMP}} \tag{5.8}$$

where $A_{\mathrm{d\_imperv\_LID-BMP}}$ = the impervious drainage area of the LID-BMP structure (m^2).

It is assumed that the drainage area of the control site, which is impervious, is characteristically like the impervious drainage area of the LID structure. The same method was used to obtain the peak inflow rates. The values obtained were compared to those calculated using the Rational Method (Kuichling, 1889) with a coefficient of 0.9, commonly used for impervious areas, and found to be similar.

The volume of rain which falls directly onto the LID-BMP cells must be included in the total inflow volume and is calculated by simply multiplying the LID-BMP surface area by the rainfall depth as in Eq. (5.9):

$$\mathrm{V_{r\_t}} = \mathrm{A_d} * \mathrm{H_p} \tag{5.9}$$

where $\mathrm{V_{r\_t}}$ = theoretical runoff volume (m^3); A_d = surface area of the LID-BMP cell (m^2); and H_p = height of the precipitation event (m).

The intensity of the rain at a given moment was assumed to be identical throughout the project site for the duration of the event. Any amount of runoff from pervious surfaces adjacent to the sidewalk or from the pervious street median was considered negligible. As for the measured outflow volume ($\mathrm{V_{out\text{-}24}}$), it was calculated by numerical integration of the measured flow (Q) over increments of time (dt) for the entire duration, t_d, of the hydrograph as in Eq. (5.10):

$$V_{out-24} = \int_0^{t_d} Q(t)dt = \sum_{t=0}^{t_d} Q(t)\Delta t \tag{5.10}$$

The weirs used to measure flow were a combination of v-notch and rectangular. Equations for each section [(Eq. (5.11), (5.12), (5.13), (5.14)] were established to relate the height measured above the crest and the flow passing through:

$$Q_{VS\_R} = 9 * 10^{-4}H^2 - 0.017H + 0.112 \quad (5.11)$$

where Q_{VS_R} = the flow passing through the rectangular section of the vegetated swale weir (m^3/s); H = the height measured above the weir crest (m).

$$Q_{VS\_V} = 6 * 10^{-5}H^2 + 0.014H + 0.097 \quad (5.12)$$

where Q_{VS_V} = the flow passing through the v-notch section of the vegetated swale weir (m^3/s).

$$Q_{BB\_R} = 2.3 * 10^{-3}H^{1.63} \quad (5.13)$$

where Q_{BB_R} = the flow passing through the rectangular section of the bioretention basin weir (m^3/s).

$$Q_{BB\_V} = 1.3 * 10^{-3}H^{1.92} \quad (5.14)$$

where Q_{BB_V} = the flow passing through the v-notch section of the bioretention basin weir (m^3/s).

5.3 Site descriptions and methods

Construction of a series of vegetated swales (VS) and bioretention basins (BB) between a 10 m road span and 4 m sidewalk located along the East side of a large boulevard in Montreal, as seen in Figure 5.2, was completed in 2017.

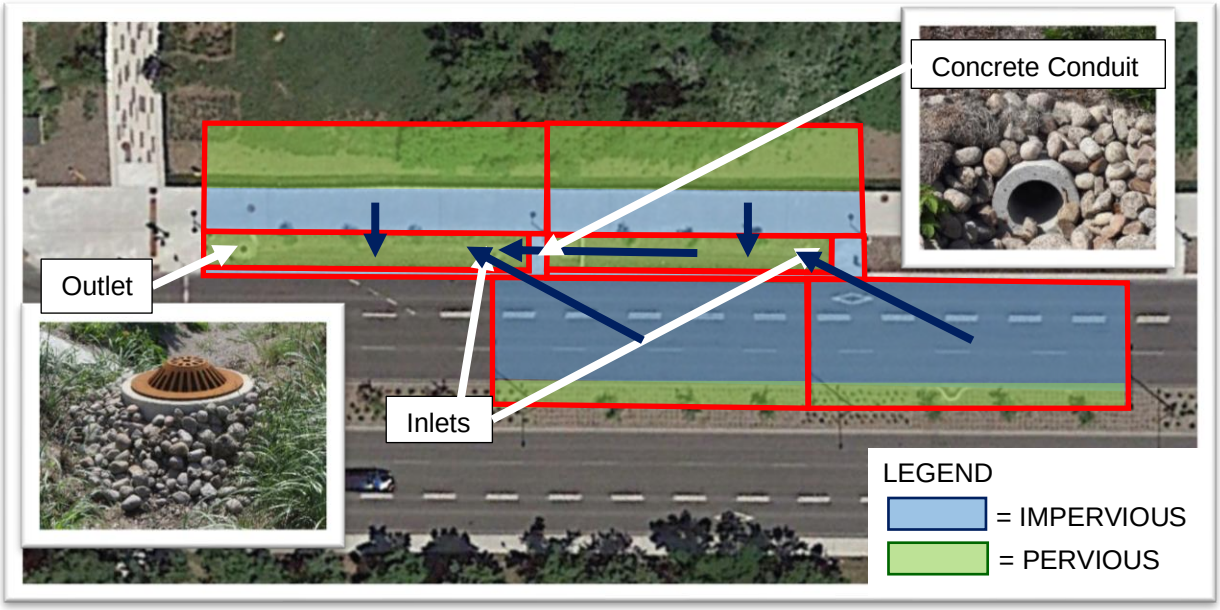

Figure 5.2 Plan view of a bioretention basin obtained from Google Earth

A basin is composed of 2 to 3 individual cells in series, which are connected by a 250 mm diameter concrete pipe. Each structure drains to the combined sewer network (located under the sidewalk) through a drain located at the downstream end of the last cell making up the basin. In the case of the bioretention unit, the downstream drain is elevated (termed overflow) forcing the rainwater to be stored in the cell and percolate into the soil. The vegetated swale does not store runoff since its drain is at the bottom of the cell. This means that once the surface layer of the soil is saturated, the excess runoff will flow towards the drain and empty into the combined sewer network directly without first passing through the soil layer. This greatly reduces the water treatment capabilities of the vegetated swales. In addition, the basins analyzed in this study include flow regulators (maximum design flow of 4.5 L/s) at their exit installed on the conduit linking the drain to the sewer system (Figure 5.3).

Design guidance in Quebec stipulates that bioretention basins must treat the volume from a 25-mm rainfall event. However, no regulations exist that require a certain amount to be completely captured. Therefore, the structures were not designed to capture any specific event volume. The bioretention basin monitored in this study was designed to treat 859 m^2 of impervious catchment consisting of a section of the adjacent sidewalk and street (Figure 5.3). The LID-BMP surface area represents 24% of the impervious catchment, which is larger than the 5-10% recommended by the MDDEFP (2014).

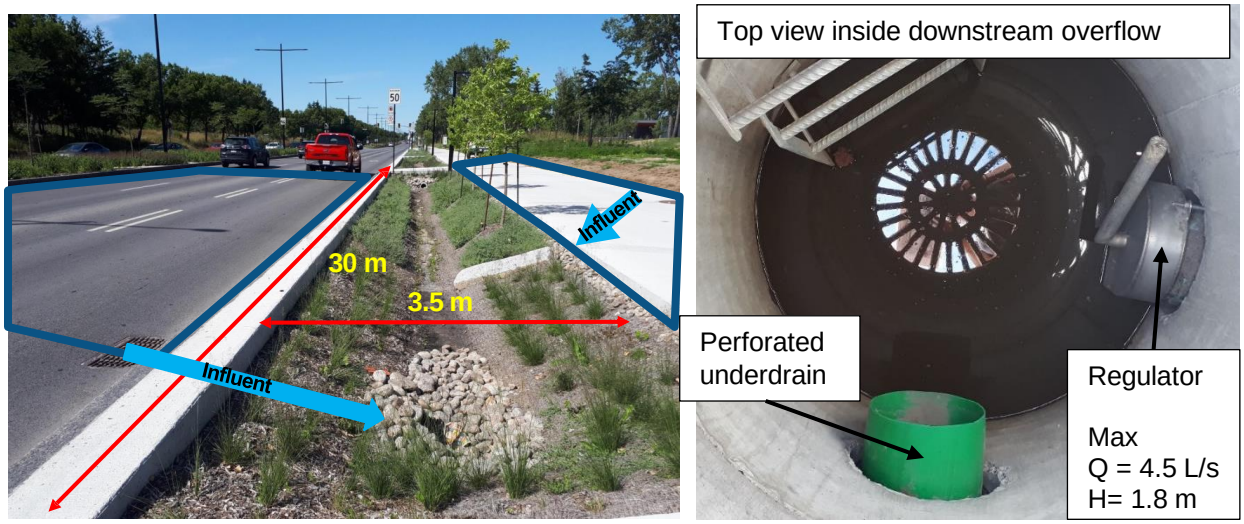

Figure 5.3 Main dimensions and drainage areas of an individual cell and view of vortex regulator

The depth of a bioretention cell is approximately 50 cm, after which any ponded water will exit through the elevated overflow drain. The potential bowl storage is 54 m^3 which is equivalent to 6.3 cm of runoff over the drainage area. The vegetated swale surface area represents 20% of the 855 m^2 impervious catchment and the bowl volume is 45 m^3 which is equivalent to 5.2 cm of runoff over the drainage area. However, this storage would only be utilised if the capacity of the exit conduit is breached and backflow occurred in the cells. A summary of all relevant design characteristics for both structures is presented in Table 5.1.

Table 5.1 Descriptive characteristics of LID structures and drainage areas

Characteristics	**VS-M3 (Vegetated Swale)**	**BB-M10 (Bioretention Basin)**
Year built	2017	2017
Catchment area[a] (m^2)	855	859
Catchment composition	Street section + sidewalk	Street section + sidewalk
Catchment percent imperviousness (%)	100	100
LID-BMP surface area (m^2)	167	204
BA:IDA ratio (%)	20	24
Cross-section shape	Trapezoid	Trapezoid
Surface storage volume (m^3)	45	54
Average bowl depth (cm)	NA	50
Fill media depth (cm)	60	60
Gravel layer thickness (cm)	NA	40
Underdrain diameter[a] (mm)	NA	200
Media characteristics	82% sand, 13% silt, 5% clay	74% sand, 22% silt, 4% clay
Media textural classification[b]	Silty Sand (SM)	Silty Sand (SM)
Porosity	0.467	0.54
Media saturated hydraulic conductivity[c] (mm/hr)	91	91

[a]Perforated PVC.
[b]Sieve analysis tests were performed in the Polytechnique Montreal University geotechnical laboratory and classification was determined through the Unified Soil Classification System (USCS).
[c]Literature value obtained from Rossman and Huber (January 2016).

Geotechnical tests completed on the natural soil of the site resulted in low values of hydraulic conductivity (estimated at 0.875 mm/hr) and a classification of silt loam. Consequentially, a single 20-cm diameter conventional perforated underdrain (no forced saturation or IWS zone) was

installed in the bio-retention basin. In this project, the basins are not being used to replenish the water table. An impermeable membrane was installed (only on the West side of the cells) in order to prevent seepage under the adjacent street structure.

The vegetated swale media was 82% sand, and 12% fines resulting in a silty sand classification. As for the bioretention basin, the classification was the same with 74% sand, and 26% fines. The soil thickness for both was 0.6 m and for the bioretention basin, was underlain by 0.4 m of gravel (the invert of the underdrain was in the center of the gravel layer).

Instrumentation access wells (manholes) were constructed in the sidewalk to intersect the outflow from the basins and the control sites facilitating the installation of flow measurement equipment.

5.3.1 Data collection

A Vantage Pro Weather Station installed on the top of a building (free of obstructions) 500 m away from the LID-BMPs measured precipitation data at a time-step of 10 minutes (0.254-mm resolution tipping bucket rain gauge). All relevant details of data measurement equipment are presented in Table 5.2. The rainfall data was validated using two city gauges located in the general area around the site.

Table 5.2 Descriptive characteristics of each instrument used to collect necessary data

Data measured	**Characteristic**
Duration	April 18th-November 5th 2019
Rainfall	Vantage Pro Weather Station (0.254-mm resolution)
Outflow (at LID-BMP exits and STD control points)	Primary measurement device: Compound weirs (90° v-notch and rectangular)
	Secondary measurement device: Teledyne ISCO 2150 Area Velocity Flow Module and Sensor (differential pressure transducer)
Soil Moisture Content	HOBO data loggers: Soil Moisture Smart Sensor (S-SMx-M005)
Surface Ponding	HOBO U20L-04 water level data logger

Outflow from both structures and the runoff at the STD control point was measured using compound weirs (90° v-notch and rectangular) which were fabricated in-house (Figure 5.4). The calibration curves were established through a laboratory set up which had similar conditions to the

field. The secondary measurement device, a differential pressure transducer sensor placed $4H_{max}$ upstream of the weir (ASTM, 2013), measured height values at a 2-min time step.

Figure 5.4 Compound weir and flowmeter installed on the downstream end of the conduit connecting a monitored point to the sewer (inside an IAW)

The inflow into the LID-BMPs was established indirectly from the flow measured at the STD control point. HOBO data loggers soil moisture smart sensors were installed in each basin to measure the variation in the soil moisture content. Piezometer wells (80 cm long and 5 cm in diameter) were installed in the top section of the soil layer. The water level in the LID-BMP bowls was measured using HOBO data loggers to identify bypass through the elevated overflow drains (Figure 5.5).

Figure 5.5 Piezometric well measuring the ponded depth of runoff stored in a bioretention cell

5.3.2 Data handling and statistical analyses

The measurement error of the Teledyne ISCO probe height reading as per the manufacturer`s datasheet is 0.008 m/m (Teledyne ISCO, 2016). The resulting flow error is obtained by applying the error propagation equations (WCI Physics). When combined with the standard error on the y value of the calibration curves, obtained using the LINEST function in Microsoft Excel, the total outflow volume error is obtained. For example, an event occurring May 23rd yielded 584 L of outflow (for bioretention basin) with an error of only 0.96 L, which seems very low (0.1%). Realistically, there are several other sources of errors which are difficult to quantify which would result in a larger error.

The error management actions taken during this project include removing debris from behind the weirs, verifying the calibration of the probe, validating the rainfall data using other rain gauges (located close to the site) and a verification of the laboratory-derived calibration curves in the field.

An issue which occurred during data processing involved the choice of the threshold value to be subtracted from the total height measured by the probe. Theoretically, the threshold should stay constant since it is the physical distance between the bottom of the conduit and the bottom of the

v-notch section of the weir. However, at certain locations the water level did not stabilize between events even after the weir was verified for leaks. Additionally, using the physical threshold value resulted in an unrealistic total volume. For these cases the inflow was calculated using the rational method and a value of 0.9 for the runoff coefficient. The reason the choice of the threshold value is important is since a small variation (as low as 1 millimeter) can result in a large variation in the calculated volume (for example 5 m^3), depending on the event. This is due to the cumulative nature of the calculation (integral over hours of outflow).

There were cases where the measured heights were larger than the diameter of the conduit indicating conduit surcharge. This only occurred at the STD control point. In these cases, the Rational Method was used (coefficient of 0.9 for impervious surfaces).

Discrete storm events were identified by a minimum of 3 h without rainfall and depth of at least 1 mm.

The probability plots presented in the results section were established by ranking the performance metrics (with 1 being the largest value) and calculating their exceedance probability, p, Eq. (5.15):

$$p = \frac{i-\alpha}{(n+1-2\alpha)} \tag{5.15}$$

where i = the rank of the number; and n = the sample size. A value of α=3/8 is used for a normal distribution (Cunnane, 1978; Flint & Davis, 2007; Leon Harter, 1984).

5.4 Results and discussion

5.4.1 Rainfall statistics

Data was measured from April 18th to November 5th, 2019, during which 47 individual rainfall events occurred. The measured characteristics are presented in Table 5.3. Median values for the relevant attributes were 10.41 mm of rainfall, 4.5 hours in duration, 10.68 mm/hr maximum intensity (10-min time step) and 3.15 Antecedent Dry Days (ADD).

Table 5.3 Rainfall statistics for each relevant attribute

Statistics	Height (mm)	Duration (h:min)	Average Intensity (mm/hr)	Max Intensity[a] (mm/hr)	Antecedent Dry Days[b] (ADD)
Minimum	1.01	00:20	0.58	3.00	0.13
Median	10.41	04:30	2.15	10.68	3.15
Mean	16.40	07:37	3.56	17.49	4.52
90^{th} percentile	45.67	17:42	8.39	43.22	9.48
Maximum	74.55	39:20	29.12	100.56	18.49

[a]Max intensity to occur over a 10-min timestep.
[b]Number of days with no rainfall prior to the event.

The total depth of rain measured was 80.3 cm, which was high compared to the average total precipitation height of 57.8 cm measured at the Montreal/Pierre Elliott Trudeau airport rain gauge station from 1981 to 2010. This value was calculated by summing the monthly precipitation data obtained from Environment Canada (2018). The values for the months of April and November were fractioned based on the proportion of the month during which data was collected.

5.4.2 Performance of the bioretention basin

5.4.2.1 Comparing global retention capacity to the literature

The outflow volume from the bioretention basin was measured successfully for 40 of the 47 precipitation events monitored. The total inflow volume was calculated as 733 m^3 and the total outflow volume was measured as 120 m^3. The overall retention capacity was 84%. Individual event retention capacities ranged between 52% and 100%. The bioretention basin completely withheld the runoff for only 5% of the overall precipitation events. The results of this study and other similar studies are presented in Table 5.4.

Table 5.4 Global retention efficiency results

Study	Site Name	Bowl volume (m^3)	Fill media depth (m)	Total inflow[a] (m^3/m^2)	Total outflow as overflow (m^3/m^2)	Total outflow as drainage (m^3/m^2)	Retention capacity (%)	#events completely captured (%)
This Study	BB-M10	54.0	0.6	0.853	0.0	0.140	84	2/40 (5%)
Winston et al. (2016)	HA North	48.0	0.9	0.525	0.036	0.300	36	28/90 (31%)
	HA South	35.0	0.84	0.511	0.035	0.261	42	44/90 (49%)
	UC	60.0	0.6	0.570	0.043	0.189	59	34/50 (68%)
Li et al. (2009)[b]	CP	23.4	0.5-0.8	NA	NA	NA	NA	6/22 (27%)
	SS	40.5	0.9	NA	NA	NA	NA	32/60 (53%)
	G1	45.0	1.2	NA	NA	NA	NA	40/63 (63%)
	G2	43.2	1.2	NA	NA	NA	NA	22/63 (35%)
	L1	32.4	0.5-0.6	0.581	0.135	0.290	27	3/27 (11%)
	L2	19.8	0.5-0.6	0.499	0.056	0.350	19	1/27 (0.04%)
Davis et al. (2012)[c]	Pennsylvania	36.0	1.2	3.80	1.84		52	258/372 (69%)
	Maryland	31.0	0.9	0.91	0.20		78	
	North Carolina	23.6	1.1	1.33	0.18		86	
DeBusk and Wynn (2011)[d]	BRC	3.5	0.8	0.068	0.0018		97	23/28 (82%)

NA = non-available

[a]The volume of inflow (m^3) per m^2 of impermeable surface area.

[b]No overflow occurred at sites CP and SS due to smaller storms and a larger bowl depth, respectively.

[c]It was mentioned in the paper that overflow occurred for both the Pennsylvania and North Carolina sites with no quantification. It was not explicitly mentioned for the Maryland site.

[d]Overflow occurred for one event out of 5 which produced runoff from the LID-BMP.

Li et al. (2009) demonstrated that a larger media depth improves bioretention hydraulic performance. The site SS with a BA:IDA ratio of 2% and higher hydraulic loading was compared to CP with a BA:IDA ratio of 6%. The site SS presented superior hydraulic performance, which was attributed to the larger media depth (0.9 m vs 0.5-0.8 m). The general trend noted in Table 5.4

shows that sites with a small media depth are less likely to completely retain runoff; this includes BB-M10 with a depth of 0.6 m.

The largest water levels measured in the bowl of BB-M10 (50 cm depth) ranged from 14 to 17.5 cm for an event which took place October 1st (event characteristics in Table 5.5). The max depth of 17.5 cm represents only 35% of the total depth.

Table 5.5 Event which caused the highest ponding depth in BB-M10 during 2019

Event Date	Depth (mm)	Duration (h)	I_{max} (mm/h)	ADD (days)
October 1st	50.13	7.6	58.11	0.5

The maximum rainfall intensity of the event occurred at 4:30 pm and by 4:50 pm the intensity was zero. The water level inside the bowl went from 17.5 to 13.6 cm between 4:40 pm and 5 pm. This means the infiltration rate was around 120 mm/h. This rate is high considering the fact that bioretention basins are typically designed assuming an infiltration rate which has been reduced by clogging on the order of 25.4 mm/h (Guo & Luu, 2015). The same event ended around 8:10 pm, and by 9 pm the depth in the bowl was zero. Therefore, although the bowl depth is large, it is not being fully utilized.

5.4.2.2 Bioretention Abstraction Volume (BAV)

Davis et al. (2012) suggested determining an empirical average BAV by plotting the outflow volume for each rainfall event as a function of the inflow volume. Theoretically, once the inflow volume surpasses the BAV, there exists a linear relationship between the inflow and outflow. The relation can be characterized by a linear regression analysis of the events which produced outflow as seen in Figure 5.6.

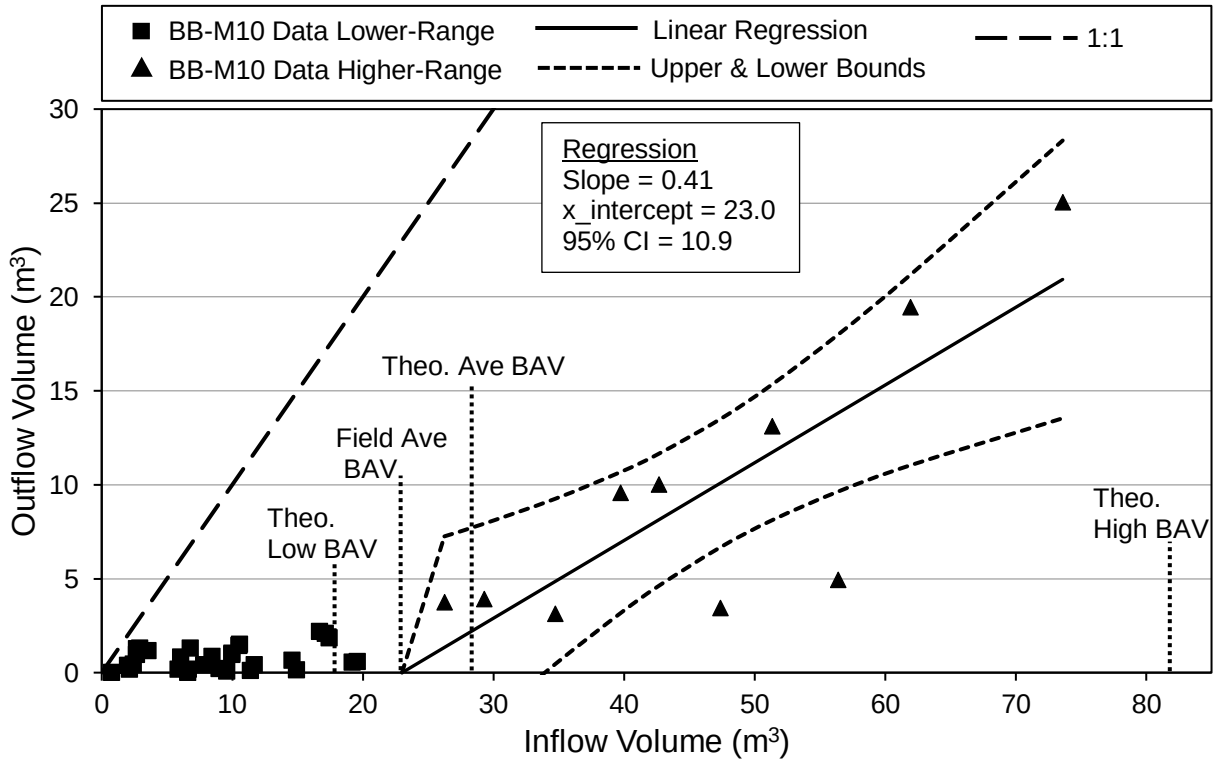

Figure 5.6 Relating outflow and inflow volumes for the bioretention basin and determination of field BAV (95% CI determined from x-intercept of lower bound curve)

Normally, it is expected that a bioretention basin retain outflow completely from small storms (Davis, 2008), which for the purposes of this study are those with a return period below the 2-year, 5-minute rainfall intensity (Mailhot & Talbot, 2012). BB-M10 was only able to entirely capture 2 small events. Nevertheless, Figure 5.6 presents a cluster of events with a very low outflow (<2.5 m^3) up until an inflow of 20 m^3 after which a clear linear relationship between outflow and inflow is established. The field derived average BAV of 23 ± 10.9 m^3 [95% confidence interval (CI)] was thus determined from the linear regression (x-intercept) of events with an inflow larger than 20 m^3.

The theoretical equations presented by Davis et al. (2012) were used to calculate a low, average and high BAV of 41.2 m^3, 59.1 m^3 and 113.1 m^3, respectively. These represent idealized cases where the initial soil moisture content has reached the wilting point in the RZMS and the field capacity in the LMS. However, moisture content data collected in the field indicated that these values were never attained during the study period. Table 5.6 presents the comparison between theoretical and the field derived BAV.

Table 5.6 Comparison between theoretical BAVs calculated using the literature WP/FC values, the theoretical BAVs calculated using measured initial moisture contents and the field derived BAV

Volumetric Initial Soil Moisture Content[a] RZMS (%)	**Volumetric Initial Soil Moisture Content[a] LMS (%)**	**Theoretical low[b] BAV (m^3)**	**Theoretical average[c] BAV (m^3) (difference between theo. and field average of 23 m^3)**	**Theoretical high[d] BAV (m^3)**
30 (Field Min.)		20.5	30.7 (34%)	84.7
32 (Field Ave.)		18.8	28.1 (22%)	82.1
34 (Field Max.)		17.1	25.6 (11%)	79.6
5.7 (WP)[e]	12.1 (FC)[e]	41.2	59.1 (157%)	113.1
13.7 (WP)[f]	25.1 (FC)[f]	34.4	46.7 (103%)	100.7

[a]Of the 10 events utilized to establish the field BAV.
[b]Calculated using Eq. (5.2).
[c]Calculated using Eq. (5.1).
[d]Calculated using Eq. (5.1) and adding the bowl volume.
[e]Values for the soil type (silty sand) in BB-M10 (Rossman & Huber, January 2016).
[f]Values for sandy loam soil taken from Maryland site characteristics (Davis et al., 2012).

Using a field derived initial moisture content for the calculation of theoretical BAV values was more accurate. The values calculated using the average field moisture content of 32% were highlighted in Figure 5.6 and although the error is 22%, the theoretical BAV of 28.1 m^3 is within the 95% CI of 10.9 m^3. This demonstrates the variation that can occur in the BAV depending on rainfall characteristics and initial soil moisture content.

An inconsistency previously mentioned is further established by the fact that most of the events which were not considered in the linear regression but still produced outflow are smaller than the low BAV of 18.8 m^3. Conversely, a basin in Maryland (Davis et al., 2012) with a similar field derived BAV (17.3 m^3) was able to completely capture small events. Table 5.7 compares the design characteristics of the two structures.

Table 5.7 Comparison between two bioretention LID-BMPs with a conventional underdrain system

Characteristic	Maryland[a]	BB-M10
Bioretention surface area (m^2)	102	204
Impermeable watershed area (m^2)	1560.6	859
BA:IDA ratio (%)	7	24
Bowl volume (m^3)	31	54
Fill media depth (m)	0.9	0.6
Sand-silt-clay (%)	54-0-20	74-22-4
Saturation (%)	44.5	54.0
Wilting point (%)	13.7	5.6
Field capacity (%)	25.1	12.1

[a]Davis et al. (2012)

Theoretical values for the low, average and high BAV of 34.4 m^3, 46.7 m^3 and 100.7 m^3 were obtained when using the Maryland soil WP and FC (Table 5.6). This shows that the theoretical storage capacity of a structure is directly proportional to sand content. The Maryland site has a smaller BA:IDA ratio, smaller bowl volume and smaller sand content than the BB-M10 site. Thus, the advantage of the Maryland site over BB-M10 is the larger soil depth which has proven to increase performance in many studies (Brown & Hunt III, 2011; Li et al., 2009). The superior performance of BB-M10 is seen when considering the largest events to occur during the study period. The slope of the linear regression in Figure 5.6 is 0.41 representing a volumetric management of 59% following the BAV. This is in contrast with the Maryland site which had a slope of 0.72 and thus only 28% of inflow retained.

5.4.3 Bioretention basin vs vegetated swale

5.4.3.1 Volume discharge ratio

The outflow volume from the vegetated swale was measured successfully for 42 of the 47 precipitation events monitored. The inflow volume was calculated as 706 m^3 and the outflow volume was measured as 195 m^3. The overall retention capacity was 72% (12% less than the bioretention basin). The vegetated swale completely withheld the runoff for 14% of the overall precipitation events.

Figure 5.7 presents the results for the retention capacity of both LID structures as ranked probability distributions [Eq. (5.15)]. For events which had no outflow, a value of 0.001 was arbitrarily used for inclusion on the log plot. Davis (2008) proposed a VDR ≤ 0.33, which represents volume retention ≥ 67%, as a goal for LID-BMP efficiency.

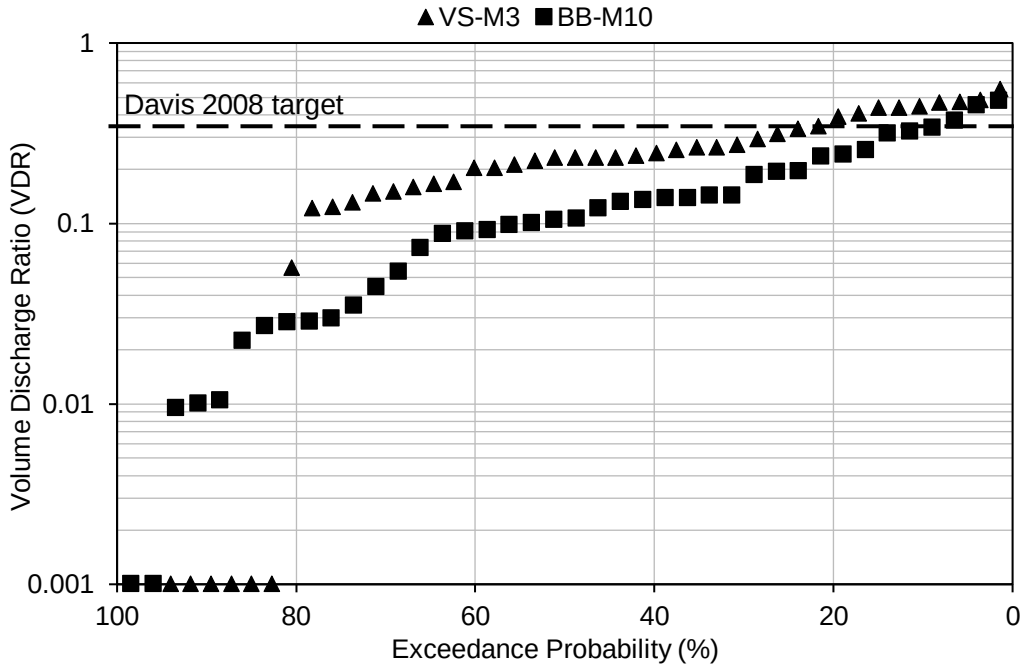

Figure 5.7 Volume discharge ratio for all monitored events for the vegetated swale and bioretention basin

For the vegetated swale and bioretention basin, respectively, 78 and 91% of the events have a VDR ≤ 0.33 (Davis, 2008), with median values of 0.23 and 0.11 (Table 5.8). This means that the retention capacity was inferior to 67% for only 22% (VS) and 9% (BB) of the events monitored.

Table 5.8 Comparing median VDR values and the probability of reaching target VDR values with similar studies

Performance Metric		**VDR ($f_{V24}= \frac{V_{out-24}}{V_{in}}$)**	
Target value		**<0.33**	
Study	**Site Name**	**Expected probability of achieving target (%)**	**Median value**
This study	VS-M3	78	0.23
	BB-M10	91	0.11
Davis (2008)	Deep cell A	55	0.23
	Shallow cell B	62	0.18
Winston et al. (2016)	HA North	51	0.3
	HA South	67	0.001
	UC	82	0.001
Li et al. (2009)	CP	40	0.60
	SS	75	<0.10
	G1	80	<0.01
	G2	82	<0.10
	L1	44	0.36
	L2	15	0.60

Although two of the sites studied by Winston et al. (2016), HA South and UC, showed the lowest median values (0.001), they did not have the largest probability of achieving the target (67%/82%). The site BB-M10 presented herein had the highest probability (91%) and a low median value (0.11). Sites G1 and G2 in Li et al. (2009) also presented promising results. It is probable that the regulator installed in VS-M3 contributed to its volume retention capacity since a flow larger than 4.5 L/s would've create backflow into the bowl of the structure ensuring a larger infiltration of runoff.

5.4.3.2 Peak flow rate ratio and peak discharge time span ratio

A summary of peak flow results is presented in Table 5.9. The maximum peak outflow was 1.93 L/s for the bioretention basin and 4.94 L/s for the vegetated swale. Both structures had a regulator (max flow = 4.5 L/s) installed on the conduit connecting the downstream drain to the sewer system. Seeing as the maximum peak outflow for the BB never surpassed 4.5 L, it was concluded the

regulator only acted on the VS outflows. Therefore, when considering the peak reduction performance for the vegetated swale, it must be acknowledged that the performance is not only due to the intrinsic characteristics of the structure but also the control of the regulator.

Table 5.9 General peak flow results for inflow to and outflow from the bioretention basin and vegetated swale

Site	Location	Median peak flow rate (L/s)	75th percentile peak flow rate (L/s)	90th percentile peak flow rate (L/s)	Range of peak flow rate (L/s)
Bioretention Basin	Inflow	2.52	7.88	20.41	0.27-24.2
	Outflow	0.08	0.19	1.23	0-1.93
Vegetated Swale	Inflow	2.28	7.41	19.21	0.41-24.1
	Outflow	0.16	0.48	3.8	0-4.94

Figures 5.8 and 5.9 present the results for the peak reduction and peak delay ratios, respectively, as ranked exceedance probabilities for each event monitored [Eq. (5.15)]. For the events in which no output flow was observed, a R_{peak} value of 0.001 was chosen to maintain the probability distribution (Davis et al., 2012). For R_{delay} a value of 100 was used (arbitrarily assigned since values ranged from 1 to 60).

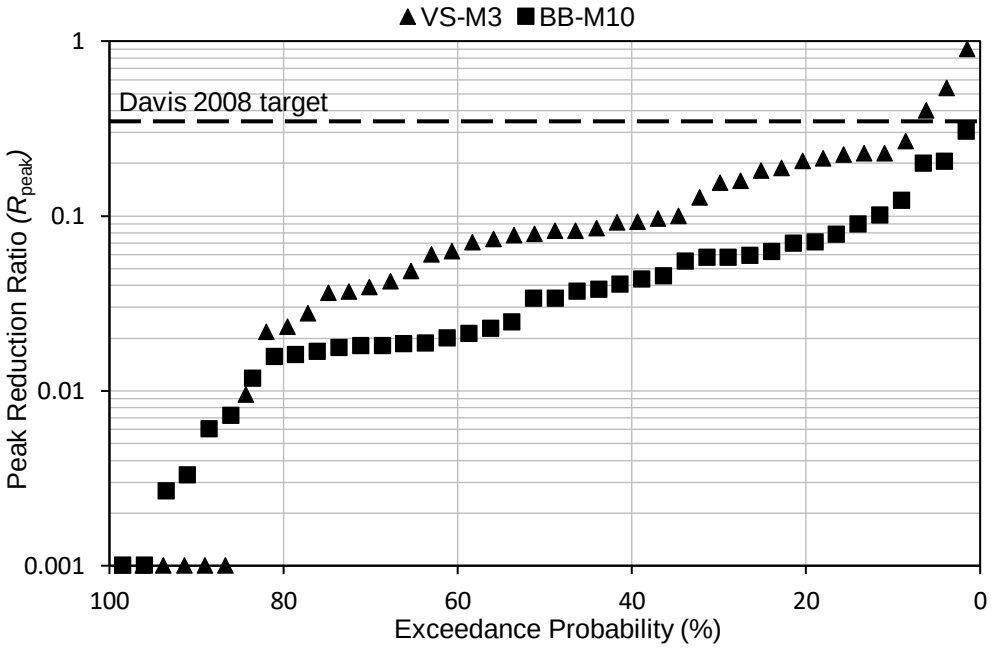

Figure 5.8 Peak reduction ratios for each event for the vegetated swale and bioretention basin

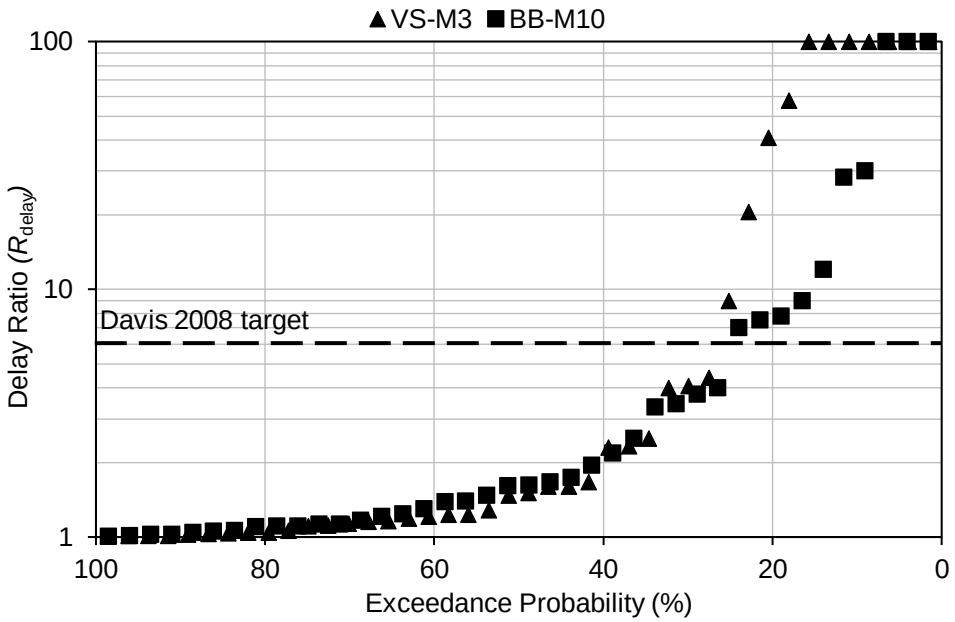

Figure 5.9 Peak delay ratio for the vegetated swale and bioretention basin

All measurable events had peak reduction (R_{peak} < 1), with median R_{peak} values of 0.08 (VS) and 0.03 (BB). The predicted probability for the cells to achieve the target R_{peak} value (<0.33), which represents a reduction of 67% (Davis, 2008), is 94% (VS) and 98% (BB). This means that the peak reduction was inferior to 67% for only 6% (VS) and 2% (BB) of the events monitored.

The median R_{delay} values were 1.49 (VS) and 1.62 (BB) as summarized in Table 5.10. For both structures, only a small portion of the events, namely, 30% (VS) and 25% (BB), saw a delay in the occurrence of the peak outflow ($t_{q-peak-out}$) of more than 6 times (target R_{delay} > 6) the delay of the inflow peak ($t_{q-peak-in}$).

Table 5.10 Comparing median R_{peak} and R_{delay} values and the probability of reaching target R_{peak} and R_{delay} values with similar studies

Metric		$\boldsymbol{R_{peak}}$ $(\frac{q_{peak-out}}{q_{peak-in}})$		$\boldsymbol{R_{delay}}$ $(\frac{t_{q-peak-out}}{t_{q-peak-in}})$	
Target value		**<0.33**		**> 6**	
Study	**Site Name**	**Expected probability of achieving target (%)**	**Median value**	**Expected probability of achieving target (%)**	**Median value**
This study	VS-M3	94	0.08	30	1.49
	BB-M10	98	0.03	25	1.62
Davis (2008)	Deep cell A	30	0.40	38	2
	Shallow cell B	42	0.48	31	2.7
Li et al. (2009)	CP	70	0.14	70	22
	SS	>90	0.02	>80	200[a]
	G1	>99	<0.01	75	200[a]
	G2	>99	<0.01	60	13
	L1	>90	0.04	45	4
	L2	>90	0.10	25	3

[a]A value of 200 was chosen for events with no outflow (since values ranged from 1-180).

Sites G1 and G2 (Li et al., 2009) presented the lowest median value (< 0.01) and highest expected probability (>99%) of achieving the target for R_{peak}. Nevertheless, both VS-M3 and BB-M10 perform relatively well in terms of peak reduction. It is believed the vortex regulator of VS-M3 contributed largely to the high peak reduction values. The highest median value and highest expected probability of achieving the target for R_{delay} are 200 (SS and G1) and >80 (SS), respectively. The sites BB-V3 and BB-M10 present low values for both. Thus, the structures did not perform well in terms of peak timing delay.

5.4.4 Hydrologic impact of LID-BMP design

5.4.4.1 Bioretention Abstraction Volume (BAV)

Of the 30 events with an inflow less than or equal to the field derived BAV of 23 m^3 (ranging from 0.76 to 19.6 m^3), only 2 were completely retained. The rest yielded outflows ranging from 0.09 to 2.19 m^3 translating to retention capacities ranging from 52% to 99%. Thus, rainfall events which

contributed relatively small inflows to the bioretention basin were not retained. The same phenomenon can be seen in a graph produced by Winston et al. (2016) which they used to determine a discharge threshold (mm). The bioretention media (Winston et al., 2016) had a high sand content (88%) comparable to the soil in BB-M10 (74% sand). Small rainfall events (< 5 mm) were found to produce discharge from all three bioretention units studied (Winston et al., 2016). This begs the question: is it accurate to attempt to identify a baseline BAV? As stated by Davis et al. (2012), the BAV is not expected to stay constant since it is a function of rainfall characteristics and antecedent moisture conditions in the soil. Therefore, these factors could contribute to outflow even for small rainfall events.

5.4.4.2 Flow control using a cap-orifice device

For smaller events, the larger BA:IDA ratio and larger bowl volume of BB-M10 did not guarantee better performance in the presence of a high sand content, an underdrain and low permeability natural soils. A compromise must be made to ensure the soil optimally regulates the runoff without constant bypass through the downstream overflow. Another solution to ensure that the BB-M10 basin captures the runoff from small events is to increase the clay content of the soil. Although this can lead to an increase in overflows, the large bowl depth can ensure frequent bypass does not occur.

A disadvantage of an increase in clay content is that the soil's lifespan will be reduced in relation to clogging. An alternative solution is to install a cap-orifice regulator at the exit of the underdrain to control the flow. When a structure is at the early stage of its lifespan, the infiltration rate of the media is higher than the design rate. Therefore, the soil will not be adequately regulating the runoff and can benefit from cap-orifice control. As time goes by and the soil clogs, the infiltration rate will decrease. The soil will control the flow adequately, no longer requiring the support of the cap-orifice (Guo & Luu, 2015). The existing regulator implemented at BB-M10 is installed on the upstream end of the conduit connecting the downstream overflow drain to the sewer system. As seen in Table 5.9, the peak outflow rates from the bioretention basin were small preventing control by the installed regulator. The question remains if the basin would be able to handle the event presented in Table 5.5 if a cap-orifice was placed on the exit of the underdrain conduit instead and was completely closed creating a hybrid of the two structures under study. This would depend on the ability of the natural soils to drain the runoff which might be higher than expected.

Nevertheless, due to the uncertainty in the permeability of the natural soils to drain runoff between events, the situation would need close monitoring and if issues arise, the cap-orifice settings would need adjustments.

5.4.4.3 Soil layer characteristics, BA:IDA ratio and bowl storage volume

Both the site G2 (Li et al., 2009) and BB-M10 have a conventional underdrain design (no IWS zone). Although it is not explicitly mentioned in the paper by Li et al. (2009), it is assumed, since the G2 site was designed with an underdrain, that the natural soils drain poorly. The sites have the same engineered soil type and similar bowl storage volumes (43.2 m^3 for G2 and 54 m^3 for BB-M10). The site G2 has a BA:IDA ratio of 5% which is much smaller compared to the 24% BA:IDA ratio of BB-M10. In contrast, the fill media depth of G2 (1.2 m) is large compared to BB-M10 (0.6 m). BB-M10 had 9% more events reach the target volume reduction than G2 (Table 5.8). However, the G2 site was able to completely capture 35% of events (compared to 5% for BB-M10). Thus, the larger soil depth for G2 will ensure it captures small events but the much larger BA:IDA ratio of BB-M10 ensures that it will perform better overall. High volume retention performance is also noted for the site UC (Winston et al., 2016) which is built in low permeability soils but with the addition of an IWS zone. In this case, the UC has a higher sand content (87%) than BB-M10 (74%) but the same soil media depth and bowl volume. The main difference is the BA:IDA ratio with 7% for UC. Although it is expected that BB-M10 would greatly outperform UC, it only has a 9% higher probability of achieving the target 67%. This demonstrates the effectiveness of the IWS zone for UC. It is important to understand the differences between the rainfall characteristics which were measured at each site. When comparing the rainfall statistics, the maximum average intensity to occur at site UC was 12.9 mm/h in comparison to the 29.2 mm/h to occur at BB-M10. It is possible BB-M10 faced larger storms than the UC site. The BB-M10 showed an overall volume retention of 84% which is 25% more than UC (59%) but was not able to completely retain events as well (68% for UC). Thus, an alternative to implementing an IWS zone is to increase the BA:IDA ratio of a bioretention basin built in low permeability soils with a conventional underdrain design.

The same tendency noted previously between G2 and BB-M10 applies to the peak flow reduction since both have very high probabilities of achieving the target (almost 100% as presented in Table 5.10). Thus, even if the BA:IDA ratio of G2 is much smaller than BB-M10, the deeper soil layer ensures it performs equally well.

This is not the case for the delay in peak timing. Both structures show reduced probabilities, with BB-M10 being the lowest of all studies with only 25%. It is hypothesized by Li et al. (2009) that a lack of peak delay is found in structures which have a combination of highly sandy media, shallow media depth and poorly drained natural soils. This leads runoff to quickly infiltrate and exit by the underdrain structure and could explain the behavior of BB-M10. Alternatively, assuming the bulk of the media layer is adequately regulating the flow since a significant volume and peak reduction were measured, the presence of preferential flow paths could permit a portion of the runoff to reach the underdrain quickly.

The highest peak delay was noted for site SS (Li et al., 2009) with >80%. The structure has a reduced bowl volume (40.5 m^3) and the media layer is deeper (0.9 m) with a much higher clay content (20%) than BB-M10 (4% clay). A major difference is the BA:IDA ratio with 2% for SS. The SS site showed a larger capacity to completely capture events with 32/60 events with no outflow. Additionally, SS does have relatively large volume retention and peak flow performance with 75% and >90% of events over target values. Due to the differences in design parameters between the structures, it is difficult to establish the influence of one. It is hypothesized that the larger clay content of the SS site and relatively large bowl volume enable the structure to delay the flow while not producing any overflow. Furthermore, site G1 (Li et al., 2009), which is identical to G2 except it has an IWS zone, demonstrated a higher performance in terms of peak delay. The IWS zone in combination with a deep soil layer improves peak delay performance.

5.4.4.4 Overflow and perforated underdrain

There are two main benefits of implementing an elevated downstream drain (overflow): runoff can be stored at the surface and is forced to percolate through the soil undergoing superior qualitative treatment. This is not the case for the vegetated swale which ultimately slows the flow down and provides a certain infiltration. Table 5.11 summarizes and compares the benefits of each structure established by the measured data.

Table 5.11 Comparing the benefits associated with the bioretention basin and vegetated swale

Element	Vegetated Swale	Bioretention Basin
Runoff Treatment	-	+
Runoff Storage	-	+
Capture of small events	+	-
Volume Reduction for larger events[a]	+	++
Peak Reduction[b]	++	++
Peak Delay[c]	-	-
Cost	-	+

[a]Of the 10 largest events, the vegetated swale reached the 67% volume reduction target for 6 events compared to 9 for the bioretention basin.
[b]Both structures reached the 67% target peak reduction for almost all events.
[c]Both structures show a low fraction of events reaching the target R_{delay}.

Overall, the bioretention basin underperformed due to the measurement of outflow from small rainfall events and the lack of substantial delay in peak discharge. Nevertheless, the bioretention did show good retention capacity and both structures showed large reductions in peak flow values. It is possible that designing the vegetated swale with two cells in series separated by a 250 mm concrete pipe permitted a good performance. Runoff entering the upstream cell is required to traverse 50 m of sandy media (84%) with a high infiltration rate before reaching the downstream drain. Additionally, although it was not quantified, the regulator installed at the exit of the vegetated swale probably contributed highly to its performance.

Finally, the LID-BMP chosen at a specific site ultimately depends on the requirements. If water treatment is not required, the vegetated swale provides adequate quantitative control and is also less costly to construct than the bioretention basin.

5.5 Conclusion

The hydraulic performance of a bioretention basin built in low permeability soils without an IWS zone was evaluated by considering the bioretention abstraction volume, the volume discharge ratio, the peak reduction and the peak delay. This was compared to a vegetated swale built without an elevated downstream drain or perforated underdrain conduit. Both designs included vortex regulators installed on the conduit draining the outflow of the structure to the combined sewer system.

It proved questionable that a baseline BAV could be established due to the potential influence of varying rainfall characteristics and initial soil moisture conditions. Nevertheless, a field derived BAV of 23 m^3 was determined through a linear regression of outflow vs inflow volume data. This was compared to a theoretical BAV of 28.1 m^3 (22% error) calculated using initial soil moisture contents values determined in the field which was deemed more accurate than the idealized case where the RZMS reached the wilting point and the LMS reach the field capacity.

By evaluating the outflow peaks, it was determined the regulator only influenced the performance of the vegetated swale. The performance of the bioretention basin and vegetated swale resulted in a retention capacity of 72% (VS) and 84% (BB). The vegetated swale withheld runoff completely from 14% of events whereas the bioretention basin only 5%. The probability of achieving the R_{peak} target (<0.33) was 94% (VS) and 98% (BB) and the R_{delay} target (>6) was 30% (VS) and 25% (BB). With the inclusion of a vortex regulator, the vegetated swale represents a viable option for quantity control.

A focus of bioretention control is the capture of small rainfall events. However, since a sizeable portion of volume which flows into the basins stems from large events, designing structures which can manage these is important. Especially if the LID-BMP drains to a downstream treatment plant which is more concerned with combined sewer overflows than the minute amounts of volume produced by small storms.

Substantial reduction in flow can be achieved using bioretention basins constructed in low permeable soils with a conventional underdrain design. This was achieved by increasing the bioretention area to drainage area ratio which was shown to provide superior benefits in terms of global volume retention performance compared to an increase in the soil depth or implementation of an IWS zone.

Nevertheless, the basin only fully captured 2 of the 30 events with an inflow inferior to 23 m^3. Thus, should the capture of small events be necessary, an increase in the BA:IDA ratio is not enough and must be accompanied by one of the following design elements: a deepening of the soil depth, the addition of an IWS zone, an increase in the media clay content or the installation of a cap-orifice device on the underdrain exit.

It remains unclear why the structure did not fully capture small events. Further research/analysis would need to be undertaken to explain this phenomenon.

CHAPTER 6 ARTICLE 2: MODELING A BIORETENTION BASIN AND VEGETATED SWALE WITH A TRAPEZOIDAL CROSS-SECTION USING SWMM'S LID CONTROLS.

Julia Bond, M.ScA Candidate; Essoyeke Batchabani, P. Eng, Ph.D.; Musandji Fuamba, P. Eng., Ph.D., M.ASCE, David Courchesne, P. Eng., and Guy Trudel, Arch.

Journal of Water Management Modeling

Abstract

The main characteristics of Low Impact Development solutions are defined in the United States Environmental Protection Agency's Stormwater Management Model using a specific object, termed Low Impact Development control module. Data collected in 2019 from the monitoring of a pilot project in Montreal was used to verify the ability of the bio-retention control to accurately simulate outflow from structures with an atypical cross-section. Two types of basins were modelled; one with an underdrain pipe and runoff storage potential (bioretention basin) and the other without (vegetated swale). Initially, the surface area of the structures was modelled as identical to the field area. A parametric calibration required maximizing the hydraulic conductivity of the soil and minimizing the conductivity slope. It was necessary to adjust the design component of the model to improve the calibration with resulting Nash-Sutcliff Efficiency values increasing from 0.206 to 0.614 for the vegetated swale and from -0.686 to -0.348 for the bioretention basin. Thus, the module presented better predictive capabilities for a basin with a simpler overall design. A general method is suggested to model structures with trapezoidal cross-sectional areas ensuring the accurate prediction of their performance using the tools already available in the software.

6.1 Introduction

6.1.1 Background

Traditional stormwater management methods drain runoff as quickly and efficiently as possible to downstream water bodies (MDDEFP, 2014). However, concerns emerged about the influence of continual runoff and pollutant loading of downstream water bodies. It was established that one of the largest contributors to non-point source pollution of estuaries and lakes is the urban runoff generated by regularly occurring storm events which make up 90% of storms in a year (USEPA, 1983). Furthermore, with the rise in urban development and subsequent expansion of impervious areas, stormwater runoff volume has increased leading to more frequent combine sewer overflows (CSO) and conveyance system surcharge (Stovin et al., 2013). In order to address these issues, a new thinking around stormwater management evolved focused on control of runoff quantity, groundwater recharge, water quality and stream bank erosion (MDDEFP, 2014). Low Impact Development (LID) ensures a site is designed to have similar predevelopment hydrologic behavior by managing runoff at the source. Structural micro-solutions have been developed as strategies to encourage the infiltration of rainwater into the ground.

The decision to implement any LID structure must consider the particularities of the site (e.g. topography, soil characteristics, utilization of the surrounding land and scale of impervious surfaces) which influence their performance. Regional rainfall patterns also direct their effectiveness (Gallo et al., 2012). A direct consequence of the difficulty in standardizing these solutions is the resistance of professionals towards implementation without physical proof of their benefits. Therefore, local pilot projects are a necessity to encourage overall adoption (Eckart et al., 2017; Ewing et al., 2000).

Hydrologic models can be used to understand the benefits of implementing LID facilities into the landscape and predict their capabilities in handling a variety of rainfall events. Modelling LID structures accurately requires the representation of a multitude of processes from surface runoff to infiltration and soil percolation. The strength of the model depends on the detail of representation of these processes and the methods which connect them (Elliott & Trowsdale, 2007).

One popular and complex model used for a range of applications is PCSWMM (Rossman, 2015) (Personal Computer Storm Water Management System), a modelling software available through

Computational Hydraulics Inc. which uses the U.S. Environmental protection agency's (USEPA's) SWMM engine. In 2010, the SWMM5 engine (version 5.0.021) was upgraded to allow the modelling of a variety of LID structures such as a bio-retention cell, infiltration trench, permeable pavement, rain barrel, vegetative swale, rain garden, green roof and rooftop disconnection.

Bioretention basins (also called rain gardens) emulate natural watersheds by infiltrating and treating stormwater runoff (DeBusk et al., 2010; PGCo, 2007; USEPA, 1999). As a LID solution, they can be utilized for a variety of purposes, namely, to attenuate peak flow, minimize runoff volume and pollutant loading, encourage evapotranspiration, reduce stream erosion and replenish groundwater aquifers (Davis, 2008; Davis et al., 2009; Dietz, 2007; Dietz & Clausen, 2005). Their standard design includes a depression in the ground containing an engineered soil material, an assortment of vegetative species, a layer of bark mulch to prevent soil erosion, and a perforated underdrain pipe if the natural soil has a low permeability (Eckart et al., 2017).

McCutcheon and Wride (2013) compared measured outflow data with outflow simulated by the bio-retention cell module in SWMM. The structures modelled were two small rain gardens which collected water from a rooftop. The tributary area to rain garden area ratio was 5:1. The performance of the basins was assessed based on the volume of water which had overflowed from the rain gardens. Results depicted a good alignment between observed and simulated overflows for both long-term and single-event analysis (McCutcheon & Wride, 2013). A previous study completed in 2012 by the same author which also modelled bioretention basins in SWMM but was not calibrated against field data was used as comparison. It was established that the field data ensured a much better performance of the model.

Considering the continually growing interest in implementing these stormwater management practices, research is needed which aids in understanding SWMM's ability to predict their behavior and performance (Niazi et al., 2017).

One aspect of modelling LID structures in SWMM which is not discussed in the literature is the influence a change in the cross-sectional area could have on the water balance analysis. The LID control module object does not require a user input value for the slope of the sides of the layers thus assuming a rectangular cross-section. No other studies were identified which discuss the impact of this assumption nor provide solutions to properly model this type of situation.

The main objective of this paper is to evaluate the ability of the SWMM engine bioretention control module to meet the proposed efficacy targets when simulating the transformation from rainfall to runoff/outflow through two different LID structures with trapezoidal cross-sections. As required, a simple method will be developed to aid in the modelling of this specific case based on simulated results and any issues that arose during calibration.

The structures, which were built on a large boulevard in Montreal, were monitored and field tests were performed to characterize the soil type. The steps required to complete the modelling of the LID solutions in PCSWMM are:

1. Building an accurate representation of the site in the model.
2. Determining appropriate initial input parameter values.
3. Performing a Sensitivity Analysis.
4. Determining the optimal values of the influential parameters (calibration).
5. Validating the calibration with an independent dataset.
6. If necessary, re-calibrating and re-validating until the prescribed performance criteria are met.

6.2 General methodology

6.2.1 Overview of the bio-retention cell LID control module

Each LID control type has parameters defining its characteristics, which in the case of a bio-retention cell detail three distinct layers: the surface layer, the soil layer and the storage layer. It is also possible to model the cell with or without an underground perforated pipe. The movement of water between the layers over time, calculated in mm/h, is obtained by considering the water balance of each individual layer. Solving this continuum numerically at each runoff time step determines how an inflow hydrograph to the LID unit is converted into some combination of runoff, sub-surface storage, sub-surface drainage and infiltration into the surrounding native soil (Rossman & Huber, July 2016).

The Green-Ampt equation (Rossman & Huber, July 2016) is used to model infiltration and applies only when there are saturation conditions that form in the top soil layer, otherwise infiltration directly equals inflow.

Darcy's equation [Eq. (6.1)] governs the relationship between decreasing soil moisture content and hydraulic conductivity and therefore models the percolation speed of water through partially saturated soil:

$$f_2 = \frac{K_{rs}}{e^{HCO(\emptyset_2 - \theta_2)}} \tag{6.1}$$

where f_2 = percolation speed (mm/hr); HCO = conductivity slope; and $\emptyset_2 - \theta_2$ = moisture content deficit (m^3/m^3).

In SWMM, the hydraulics of the underdrain pipe are modelled as a function of the height accumulated above its base as in [Eq. (6.2)]:

$$q = C_D(h_3)^{\eta_{3D}} \tag{6.2}$$

where q = underdrain unit discharge (m^3/m^2s); h_3 = head above the base of the underdrain (m); C_D = discharge coefficient (no units); and η_{3D} = discharge exponent.

Eq. (6.3) uses the orifice equation by Torricelli, and a drainage exponent of 0.5:

$$C_D = 504{,}257 * C_{od}(\frac{\pi r^2}{A_{LID}}) \tag{6.3}$$

where A_{LID} = footprint area of the LID unit (m^2); C_{od} = orifice discharge coefficient (no units); and r = radius of drain (m).

Another parameter which affects the outflow from the underdrain is the offset height, D_{3D}, of the drain from the bottom of the storage layer, which is an element of the physical design of the basin. Outflow from the underdrain will only occur once the water level in the storage layer has reached this height.

6.3 Sensitivity analysis

The goal of the sensitivity analysis is to understand the influence of parameter uncertainty on model output. An objective function is defined as a property of the simulated response function in consideration, in this case the outflow hydrograph (James, 2005). The total output volume can be

used for long-term simulation and the peak flow can be used for single-event simulation (Peng & Stovin, 2017).

The sensitivity of parameters was quantified using Eq. (6.4) (James, 2005):

$$\text{Relative Sensitivity} = \frac{\partial COF/COF}{\partial p/p} \tag{6.4}$$

where COF = computed objective function; and p = parameter value.

The parameters were increased by 25% and 50% all the while keeping the other parameters constant as proposed by Jewell et al. (1978) and Rosa et al. (2015).

There are elements other than individual parameter values to consider in the sensitivity analysis, namely, the infiltration model used for the pervious sections of general subcatchments.

Additionally, in order to verify the model's sensitivity to evaporation rates, average monthly daily evaporation rates of 0, 4.2, 4.6 and 4.6 mm/day for April, May, June and July, respectively, were obtained directly from Environment Canada (2018) for the years 1981 to 2010. These were input instead of the measured temperature data climate file and subsequently increased by 25% and 50%.

Another aspect to consider is the spatial discretization of the model (Lee et al., 2018). Although the site modelled in this study is quite small compared to an entire watershed, there remained two surfaces to consider for spatial division: the sidewalk (1% slope) and adjacent grassy hillside (average slope of 55%). The question remained whether to model two surfaces with their own respective parameter values or one lumped surface with a slope of 1% and proportional % imperviousness.

6.4 Calibration and validation

Model calibration involves adjusting the input parameters to reduce the error between simulated and observed results until the pre-defined performance criteria are met. Only the sensitive parameters were considered thereby permitting a more efficient calibration process (Peng & Stovin, 2017).

The validation of the model involves running the simulation with a separate rainfall data set and assessing the model's performance. If the performance metrics are not met, the model requires additional calibration (USEPA, 1999).

There are multiple studies and documents that support the idea that in the case of rainfall/runoff models it is significantly more accurate to simulate over the entire period of the study, therefore, a continuous calibration was completed (James, 2005; Rosa et al., 2015; Shamsi & Koran, 2017).

The accuracy of the model was evaluated using three performance criteria. The Nash-Sutcliffe coefficient is a model efficiency parameter used to assess specifically the predictive power of hydrological models (Nash & Sutcliffe, 1970). It evaluates the closeness of the simulated data vs the observed as compared to a 1:1 line and can range from negative infinity to 1. The value of 1 represents a case of null error between the simulated and observed data. Performance required is $NSE > 0.5$ (Dongquan et al., 2009). The other performance criteria used are defined as: retention, which considers the difference in the effluent volume, and detention, which considers the start time, duration and peak of the hydrograph (Peng & Stovin, 2017). It was required that the % difference between the simulated and measured values for both the effluent volume and peak flow be less than 25% (Fuamba et al., 2019).

6.5 Application to a case study

6.5.1 Description of the LID structures

The cells (30 m long x 3.5 m wide) are located between a 10 m road span and 4 m sidewalk. The drainage area to LID facility area is approximately 4.5:1. Each individual cell has a 0.5 to 1 % longitudinal slope and collects water from a section of the street through a rectangular catch basin and a single 150 mm diameter pipe.

The site is composed of two different kinds of units: bioretention basin (BB) and vegetated swales (VS). A unit is composed of 2 to 3 individual cells in series, which are connected by a 250 mm diameter concrete pipe. Each set of cells drains to the combined sewer network (located under the sidewalk) through a drain located at the downstream end of the last cell making up the LID structure. The difference between the two types of LID structures is the flow path the collected runoff will follow. In the case of the bioretention basin, the downstream drain is elevated (500 mm) forcing the rainwater to be stored in the cell, percolate deeply into the soil and be collected by a perforated pipe installed underneath the soil structure. The vegetated swale does not store runoff since its drain is at the same elevation as the bottom of the cell and does not have an underground perforated conduit. This means that once the surface layer of the soil is saturated, the excess runoff

will flow towards the drain and empty into the combined sewer network directly without first passing through the 600 mm soil layer. This greatly reduces the water treatment capabilities of the VS. In addition, the specific basins modelled in this study include flow regulators at their exit installed on the conduit linking the overflow drain to the sewer system.

6.5.2 Additions for monitoring

Instrumentation access wells (IAW or manhole) were constructed in the sidewalk to intersect the outflow from a set of LID structures. An extra manhole was also built at one location without a LID unit to intersect runoff directly from the street and called control site or standard (STD) monitoring point. The control site (STD-M12) was added as a substitute to measuring the inflow into each cell since the design of the inflow conduits and catch basins did not facilitate installation of monitoring equipment. Although this permits the approximation of the inflow runoff per unit area of impervious surface, the fact that the real inflow volumes were not measured increases the risk of error.

6.5.3 Modelling the direct street connections in PCSWMM

The monitoring sites which collect water directly from the street were modelled as typical urban drainage systems by routing the outflow from the impervious subcatchment to a junction representing a street drain. This junction was connected to a second junction (representing the IAW) via a 200 mm-diameter conduit with a Manning coefficient of 0.013, which is typically used for aged PVC pipes (Brière, 2000).

6.5.4 Modelling the LID structures in PCSWMM

In the initial simulation, the surface area of the LID subcatchments was equated to that in the field. A comparison between the structure of the bioretention basin assumed by SWMM (rectangular cross-section) and the actual under study (trapezoidal cross-section) is presented in Figure 6.1.

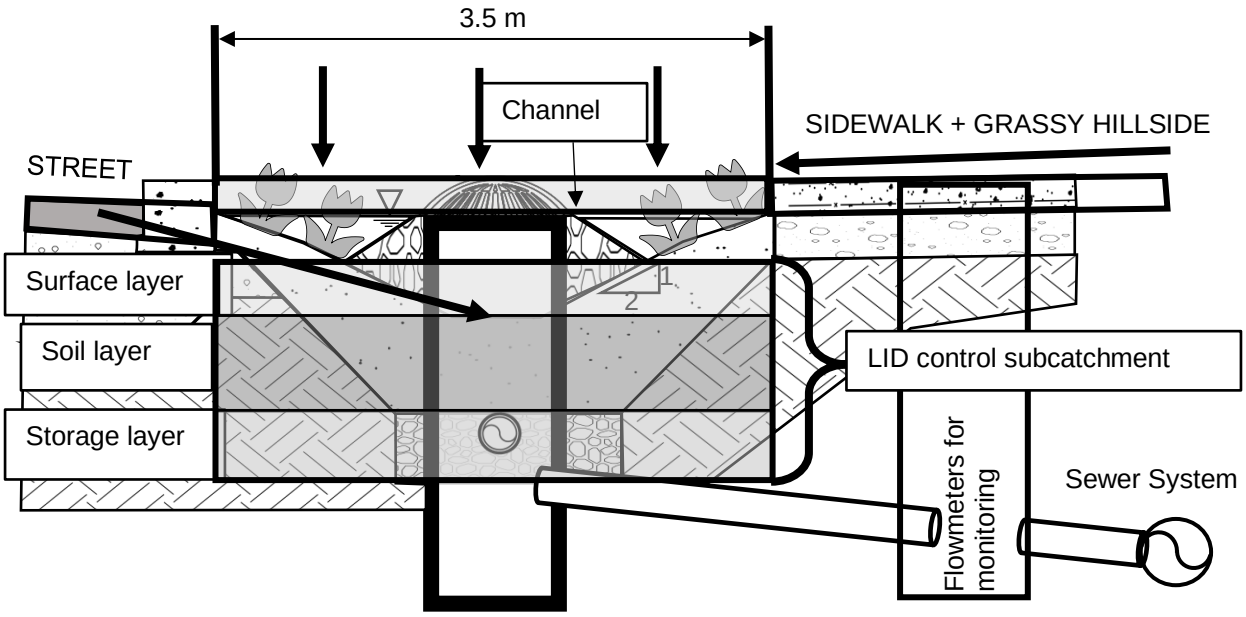

Figure 6.1 Cross-sectional view of initial model structure of the bioretention basin (Les Services EXP inc. 2018 on behalf of the City of Montreal).

The real volumes of the surface, soil and storage layers were determined to be 50.26 m^3, 127.94 m^3 and 32.80 m^3, respectively. These were compared to the volumes of the SWMM layers which have a rectangular cross-section: 101.84 m^3 for the surface (berm of 0.5 m), 122.21 m^3 for the soil (depth of 0.6 m) and 81.47 m^3 for the storage (depth of 0.4 m). It was deemed necessary to reduce the maximum attainable height (berm) of the surface layer by half to prevent an overestimation by the model of the surface storage potential (50.26 vs 101.84 m^3).

The bioretention basin cells were assigned the bio-retention cell LID control module (occupies 100% of subcatchment surface) with a berm height of 250 mm (half of the original 500 mm). The perforated underdrain coefficient of 152 was calculated using Eq. (6.3) and a C_{od} of 0.6 as suggested in section 6.5.8 of the SWMM Water Quality reference manual (Rossman & Huber, July 2016). The cells were modelled in series however in PCSWMM there is no option to route the outflow from a LID control underdrain to one in a separate subcatchment. Therefore, a rectangular channel (topmost surface in Figure 6.1) was added which connects the outflow from the upstream cell to the overflow junction at the end of the downstream cell (Figure 6.2).

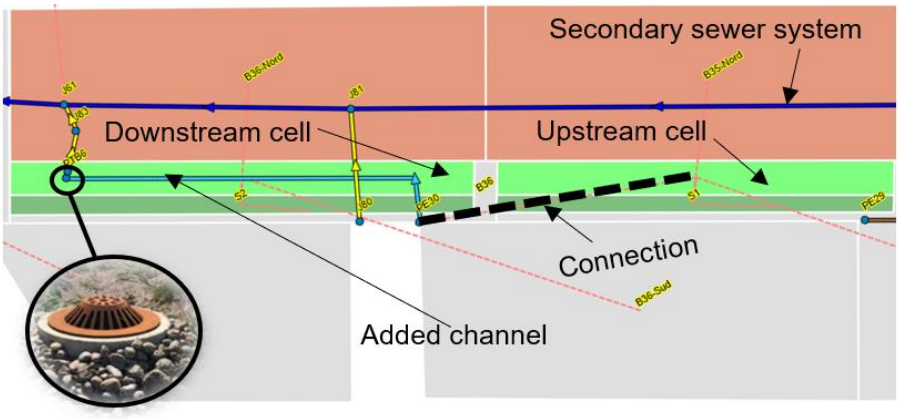

Figure 6.2 Method used to connect the underdrains of two bioretention cells in series.

Seeing as the vegetated swale was modelled as a separate sub-catchment, it was necessary for the assigned bio-retention cell LID control module to occupy 100% of subcatchment surface. A comparison between the structure of the vegetated swale assumed by SWMM (rectangular cross-section) and the actual under study (trapezoidal cross-section) is presented in Figure 6.3. The berm height and underdrain coefficient were set to zero since the VS has neither elements.

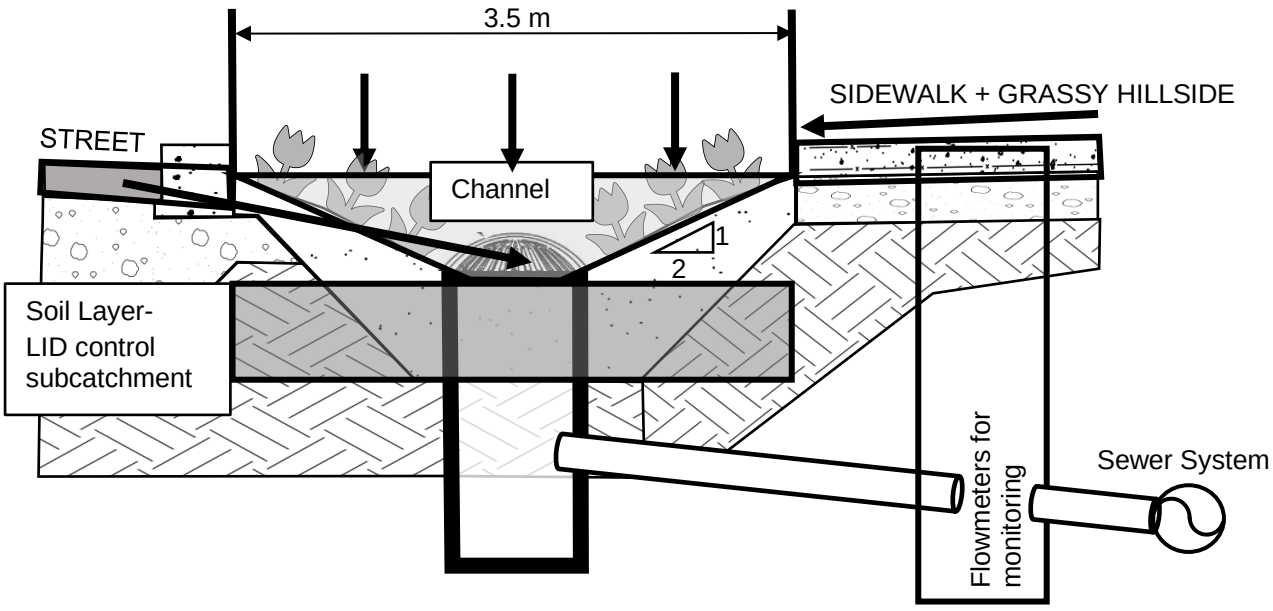

Figure 6.3 Cross-sectional view of initial model structure of the vegetated swale (Les Services EXP inc. 2018 on behalf of the City of Montreal).

Nevertheless, if a large storm occurs surcharging the exit conduit and junction, the runoff will backflow and accumulate in the basin which has a depth of 0.5 m. The likelihood of this occurring is increased by the presence of a regulator on the exit conduit. In order to ensure this backflow is collected in the basin, a trapezoidal channel (Figure 6.3) running along the LID subcatchment was connected to the junction at the exit of the basin. This channel will only collect water once the junction's capacity is breached. Figure 6.4 depicts a profile view of this design.

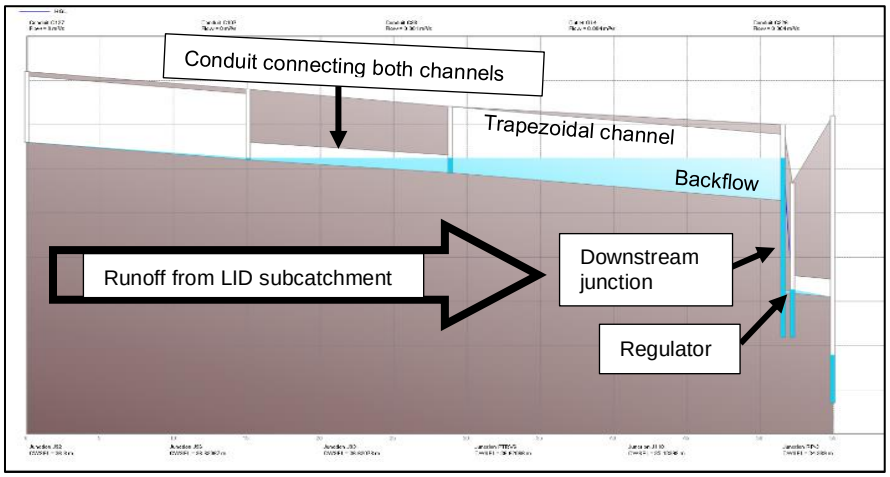

Figure 6.4 Profile view of the vegetated swale structure in PCSWMM.

During calibration, a comparison was made between measured and simulated flow hydrographs in the outflow conduit of the structures (Figure 6.5).

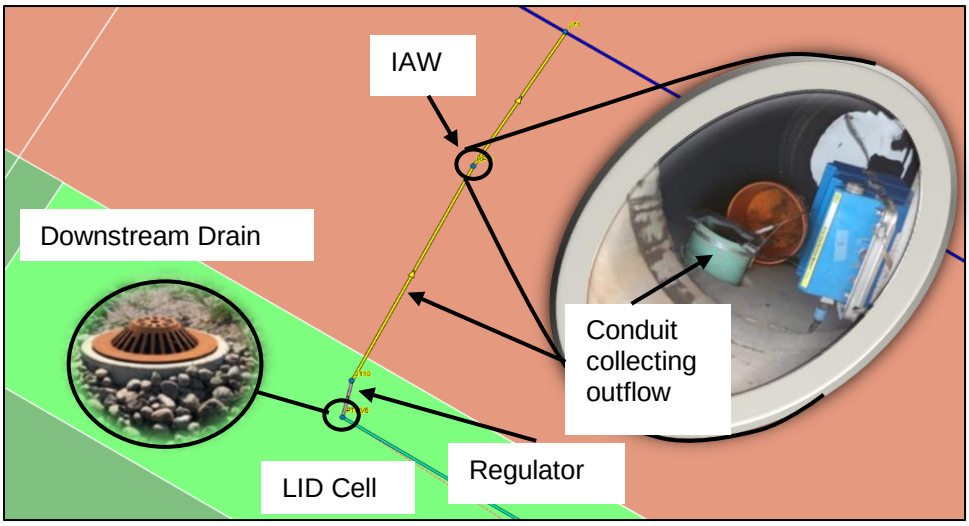

Figure 6.5 Schematic representation of the location of measured field data within the PCSWMM model.

The regulators were modelled as outlets onto which were applied a rating curve obtained from the manufacturer (a max flow of 4.5 L/s is reached when the head above the device is 1.8 m).

6.5.5 Input field data

In 2019, precipitation data for a total of 47 events was collected at a time-step of 10 minutes using a Vantage Pro Weather Station; 7 of these events had a recurrence of over 2 years (determined from local IDF curves, Mailhot and Talbot (2012)). Temperature data obtained from the same weather station was incorporated in the climatology section of the model from which SWMM calculates evaporation rates. Initial moisture contents were obtained through HOBOnet Soil Moisture Sensors installed in each basin.

A compound weir (combination of a 90° v-notch weir and a rectangular weir), fabricated in-house and calibrated in the hydraulics laboratory at Polytechnique Montréal, was installed on the conduit connecting the basin exit drain and the IAW. A Teledyne ISCO 2150 flow module, equipped with a pressure transducer, measured outflow height at a distance of $4H_{max}$ behind the weir (2-min time step). Herein, the H_{max} is the height between the notch and the bottom crest of the rectangular section (the goal is to be outside the drawdown zone as stipulated in ASTM (2013)).

Particle size analysis and permeability tests on the soils were completed to determine the soil classification. The model reporting time-step used was 1 min, the internal time-step for runoff during dry periods was 1 day and during wet periods 30 seconds.

6.5.6 Parameter estimation

The initial parameters used in the uncalibrated model were chosen based on the literature, field data or default values. The main parameters chosen are presented in Tables 6.1 and 6.2.

Table 6.1 PCSWMM parameters used in the uncalibrated model for the general sub-catchments.

Parameters	Value	Source
Manning coefficient – impervious	0.01	(James et al., 2011)
Manning coefficient – pervious	0.1	(James et al., 2011)
D store imperv (mm)	1	(James et al., 2011)
D store perv (mm)	5	(James et al., 2011)
Zero imperv (%)	25%	Default
Infiltration Model	Green-Ampt	--
Suction head (mm)	166.8	Silt loam (MDDEFP, 2014)
Conductivity (mm/hr)	6.6	
Moisture deficit	0.501	

Table 6.2 SWMM parameters used in the uncalibrated model for the LID control for both basin types.

Parameters	Value		Source
LID Control Surface Layer			
Berm height (mm)	VS	BB	Design of basins
	0	500	
Vegetation volume (fraction)	0.1		(James et al., 2011)
Surface roughness	0.3		(James et al., 2011)
LID Control Soil Layer			
Soil thickness (mm)	600		Design of basins
Soil classification	SM (Silty sand)		(García-Gaines & Frankenstein, 2015)
Hydraulic conductivity (K_s)	91		(Rossman & Huber, January 2016)
Suction head (mm)	50		(Rossman & Huber, January 2016)

Table 6.2 SWMM parameters used in the uncalibrated model for the LID control for both basin types (continued).

Parameters	Value		Source
Porosity (fraction)	VS	BB	Field Tests
	0.467	0.540	
Field capacity (FC)	0.121		(Rossman & Huber, January 2016)
Wilting point (WP)	0.057		(Rossman & Huber, January 2016)
Conductivity slope (HCO)	44		(Rossman & Huber, July 2016)
Storage Layer			
Thickness (mm)	VS	BB	Design of basins
	0	400	
Seepage rate (mm/hr)	0.875		Field Tests
Underdrain (BB)			
Underdrain coefficient	152		Calculated
Drain exponent	0.5		(Rossman & Huber, July 2016)
Offset height (mm)	200		Design of basins

The natural pervious surfaces were modelled with parameters set for a soil which is not very permeable. This was based on a geotechnical analysis of bore holes taken around the site which concluded that the natural surrounding soil was composed mainly of silt but with trace amounts of clay, sand and gravel.

6.6 Results and discussion

6.6.1 Sensitivity analysis

A separation of the sidewalk and grassy hillside surfaces did not result in any significant change in the volume or peak flow, therefore, in order to reduce the work of creating the model, a lumped subcatchment with a 1% slope and proportional % impervious was conserved.

The model was not sensitive to changes in the general subcatchment parameters (Manning N, Dstore and Zero imperv %). The infiltration model used for the general subcatchments did have large impact on the outflow volume from the basins with an increase in 14% and 17% for VS and BB respectively, when changing from Green-Ampt to Horton (the model default parameters were used).

Table 6.3 presents the relative sensitivities of the objective functions (total effluent volume and peak flow) to the incremental increase of the most pertinent bio-retention cell LID control module parameters and the constant monthly daily evaporation rates.

Table 6.3 Relative sensitivities of total effluent volume and peak flow to the bio-retention cell LID control module parameters for both basin types.

% change	**25%**				**50%**			
Basin	**VS**		**BB**		**VS**		**BB**	
Parameter	**Total Vol. (%)**	**Peak Flow (%)**	**Total Vol. (%)**	**Peak Flow (%)**	**Total Vol. (%)**	**Peak Flow (%)**	**Total Vol. (%)**	**Peak Flow (%)**
Manning coefficient	-0.8	-0.9	-0.6	-1.4	0	0	0	0
Surface slope	-1.0	-1.9	-0.4	-0.5	0	0	0	0
Porosity	-18.4	0	-28.8	0	-18.4	0	-29.0	0
Wilting point	1.8	0	0	0	1.9	0	0	0
Conductivity	-3.8	0	2.1	102.6	-19.0	0	1.7	86.5
Conduct. slope	24.7	2.8	9.9	0	22.1	1.9	9.1	0
Seepage rate	-9.4	-0.9	-8.6	0	-7.3	-0.5	-8.2	-0.6
Evaporation rates	-20.7	-0.9	-30.5	0	-20.7	-1.4	-28.4	0

Parameters for which the relative sensitivity was zero, namely, suction head, vegetation fraction, field capacity and wilting point were not included in Table 6.3. In order of largest to smallest effect on the overall effluent volume for the vegetated basin are conductivity slope, evaporation rates, porosity, seepage rate, conductivity, wilting point, surface slope and Manning coefficient. The bioretention basin was most sensitive to porosity and evaporation rates followed by conductivity slope and seepage rate. The peak flow was most influenced by conductivity for the bioretention basin. As for the vegetated basin, none of the parameters considered largely affected the peak flow.

6.6.2 Street connection results (STD monitoring site)

Figure 6.6 presents the simulated and observed effluent hydrographs for two significant events as well as the data from all simulated events for the control site STD-M12. It's possible to note a very close alignment between observed and simulated data which can provide a certain validation of the equipment used to measure the flow.

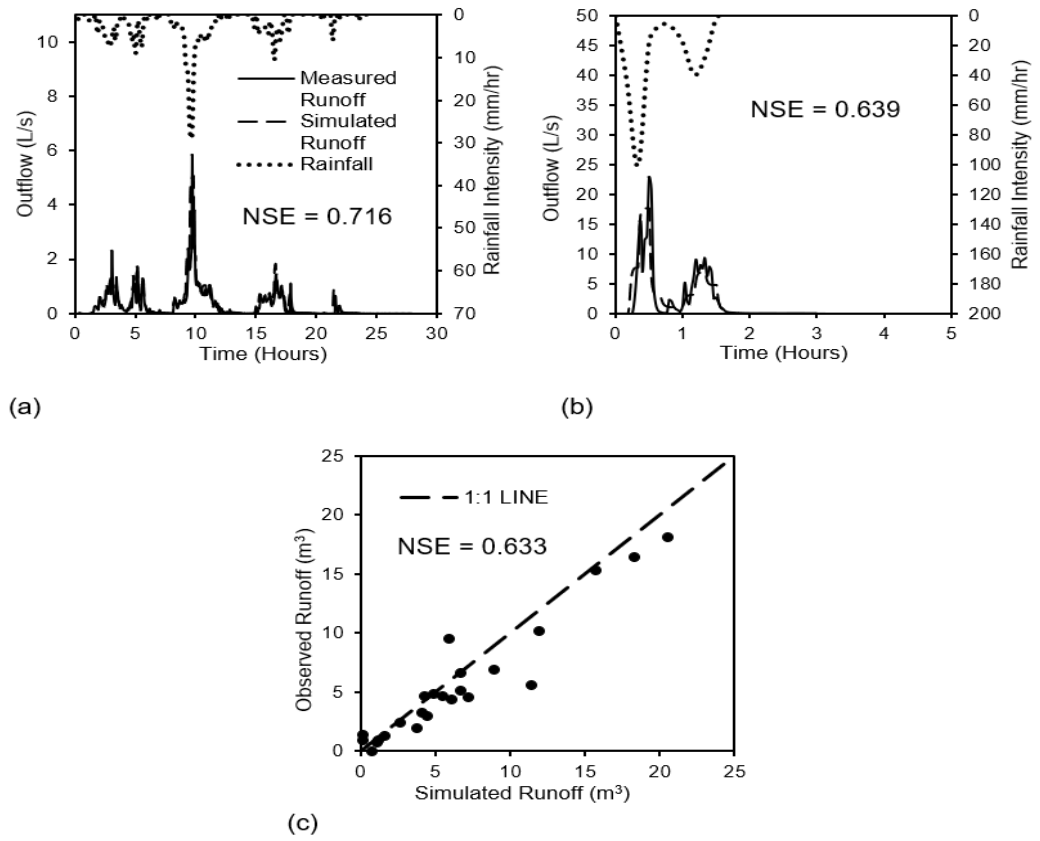

Figure 6.6 Simulated and measured effluent volume results for two major events (a & b) and long-term simulation of all rainfall events (c) from April to July 2019 for site STD-M12.

6.6.3 Parametric calibration

The period considered for calibration was selected as April 18th to July 30th (28 events for a total depth of 434 mm) while the rest of the data was used for validation.

The uncalibrated results presented the need to resolve three main issues:

- Time to start of runoff dis-alignment (detention metric).
- Peak flow overestimation (detention metrics).
- Outflow volume overestimation (retention metric).

To improve the model's predictions the sensitive parameters were optimized all the while staying within their realistic range suggested by the literature, in this case, Rossman and Huber (July 2016). A parameter was considered calibrated either once the error between the two curves was acceptable

according to the performance parameters or once the range of possible values was exhausted (Rosa et al., 2015). The calibration was done manually as it is not possible to use the automatic calibration option for LID controls in PCSWMM.

6.6.3.1 Vegetated Swale

The uncalibrated results presented an overestimation of the outflow however yielded good alignment of runoff in time. Thus, the focus of the calibration process was reducing the error between the measured and simulated outflow volume (retention metric).

The soil percolation speed, modelled by Eq. (6.1), is a function of three influential parameters: the conductivity slope (HCO), the porosity and the hydraulic conductivity (K_s). The porosity could not be altered since it was already maximized for the soil type. The final values for HCO and K_s were chosen as the respective minimum and maximum of the typical ranges suggested in Rossman and Huber (July 2016), namely, 30 and 140 mm/h. This maximizes the soil percolation speed which will ensure a larger volume of runoff infiltrates into the media prior to reaching the downstream drain, reducing the simulated outflow.

Although the model was sensitive to the seepage rate, its value was determined through field tests in contrast to the K_s which was chosen from literature values. It was deemed more prudent not to change the seepage rate since the natural soils were confirmed to have a high fines content.

As for the evaporation rates, a maximization of these values would ensure more storage was available prior to rainfall events thus reducing the outflow. A group of average monthly daily evaporation rates were calculated using the Thornthwaite equation and Environment Canada temperature data from 2018 (Environment Canada, 2018). Furthermore, the climate file data was transformed into approximate average monthly daily rates using the LID output files. Both sets of values were similar to those used in the sensitivity analysis. Therefore, an increase in the evaporation rates could not be justified.

6.6.3.2 Bioretention Basin

In the case of the bioretention basin, all three issues previously highlighted needed to be resolved: volume and peak overestimation and hydrograph timing dis-alignment. Since the design of the bioretention basin is different than the vegetated swale, the effect of parameter variation on the results will differ. The same alterations to the speed of percolation as done for the vegetated swale

will not affect the outflow volume but rather the timing of runoff. In order to better align the observed and simulated hydrographs, the same parameter alterations were made as those for the vegetated swale.

It was not possible to alter the volume of outflow from the structure since changes to the evaporation rates yield no improvement in the results and the porosity was already maximized.

6.6.4 Redesign calibration

The parametric calibration of the model resulted in complete retention of all medium to small events even if outflow was observed in the measured data for many of them.

Thus, the model predicted outflow to occur only for the largest events. Table 6.4 presents a characterization of these rainfall events based on the total precipitation depth, the duration of the event, the maximum intensity, the antecedent dry days (ADD) and the initial moisture content of the soil (measured/simulated). All are predicted to influence the performance of the LID structures. The final calibration was focused on events 1 to 5.

Table 6.4 Characteristics of the largest rainfall events that occurred between April and November 2019.

Event #	**Start Date (Y-M-D) and Time (h:min)**	**Rain Depth (mm)**	**Rainfall Duration (h:min)**	**Peak Intensity (mm/h)**	**ADD**	**Initial Volumetric Moisture Content % (VS)**		**Initial Volumetric Moisture Content % (BB)**	
						Obs.	**Sim.**	**Obs.**	**Sim.**
1	2019-04-18 17:55	48.66	39:20	16.46	3.05	NA	31.0	NA	32.2
2	2019-05-09 19:35	57.12	24:05	28.98	6.29	NA	23.3	31.7	28.5
3	2019-07-11 7:30	34.04	3:40	74.70	4.85	29.8	23.1	30.0	28.5
4	2019-07-21 5:50	29.97	1:20	97.56	2.70	30.4	24.4	32.2	28.1
5	2019-07-30 19:10	43.68	1:30	100.56	9.50	27.7	20.5	31.3	24.8
6	2019-10-01 14:45	50.13	7:35	58.11	0.53	32.5	25.6	33.6	34.6
7	2019-10-31 14:10	63.15	19 :30	19.80	0.38	33.3	34.6	34.0	34.7

[a]NA = not applicable.

Although the parametric calibration reduced the difference between the simulated and measured data for both structures, it did not yield acceptable values for the predefined performance metrics. The model was still overestimating the outflow regardless of the soil percolation speed being

maximized. Therefore, it was concluded that it would not be possible to appropriately calibrate the model by only changing the user input parameters. It was deemed necessary to test alternative methods of designing the structures in PCSWMM. It was hypothesized that it is necessary to not only consider the volume of the soil layer but also its shape. SWMM models the soil layer as a rectangle whereas the cross-section of the soil layer in the field has an irregular shape. Theoretically, the runoff from the sidewalk initially flows through the layer of soil which follows a 2:1 slope in which the vegetation is planted (topsoil) prior to percolating further down into the main 0.6 m deep soil layer. Therefore, in order to more accurately capture the shape of the soil layer, it was split into two different modelling elements as shown in Figure 6.7.

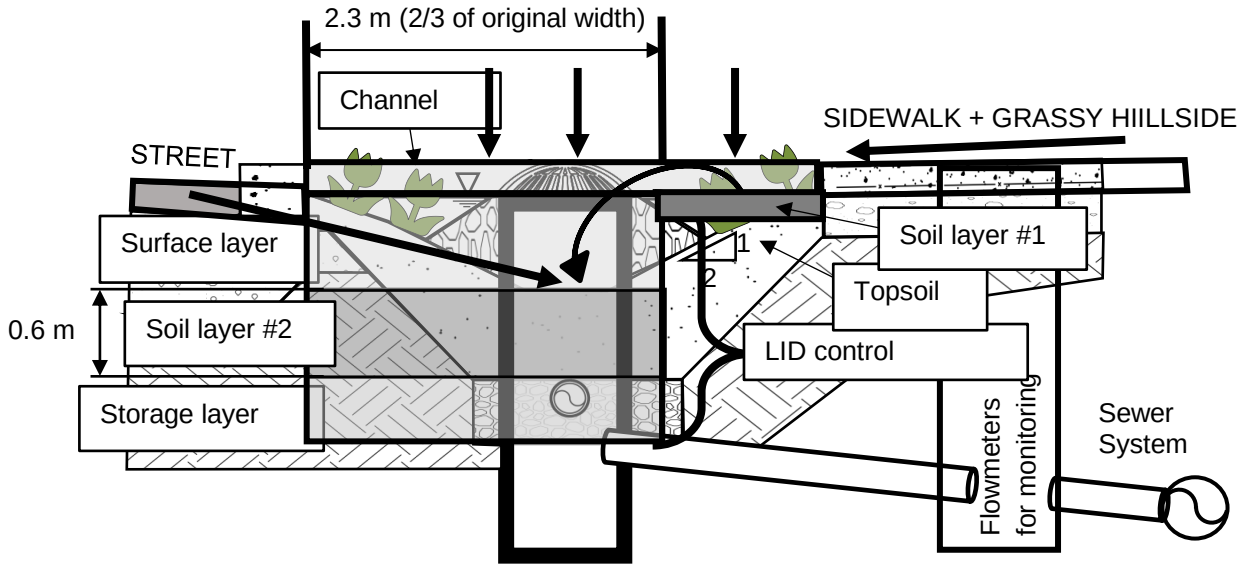

Figure 6.7 Cross-sectional view of the restructured LID solutions in the model (Les Services EXP inc. 2018 on behalf of the City of Montreal).

The bottom 0.6 m of soil is represented by the main LID subcatchment modelling element (soil layer #2 in Figure 6.7). The width of the LID subcatchment was adjusted to ensure that the modelled soil volume matched the actual (~80.4 m^3). The berm height of the surface layer was returned to its field value of 500 mm since the potential runoff volume was no longer being overestimated. As for the topsoil, two cases were considered for its representation. The first involved an additional LID subcatchment where the soil layer was applied the same parameters as that of layer #2 (no

storage or surface layers). Its thickness was chosen by equating the volumes. The second used a general subcatchment (no LID control applied) which employed the Green-Ampt infiltration method. The latter (represented in Figure 6.7) was conserved, since it yielded the best results. The general subcatchment (soil layer #1 in Figure 6.7) was modelled as zero % impervious with infiltration parameters matching those input into the main LID control soil layer (K = 140 mm/h, suction head = 50 mm and initial moisture deficit = 0.467). These alterations were made to both the vegetated swale and the bioretention basin (the swale was still applied a berm height of zero).

6.6.4.1 Long-term Continuous-based Evaluation

A comparison between the performance metrics obtained from the parametric calibration and those obtained from the redesign calibration for the entire calibration period are presented in Table 6.5.

Table 6.5 Global performance metrics of both the parametric and redesign calibration cases for the bioretention basin and vegetated swale.

Site	Total Measured Outflow Volume (m^3)	Highest Measured Peak Flow (L/s)	NSE		% error Total Outflow Volume		% error Single Peak Flow	
			Parametric Calib.	Redesign Calib.	Parametric Calib.	Redesign Calib.	Parametric Calib.	Redesign Calib.
Vegetated Swale	80.97	4.90	0.206	0.614	33.9	12.4	25.3	28
Bioretention Basin	34.13	1.93	-0.686	-0.348	96.6	81.2	25.4	0

The overall ability of the model to predict the outflow from the vegetated basin was improved by the change in structure and deemed acceptable (NSE > 0.5). As for the bioretention basin, although the alteration in the design improved the global NSE, it still presented a negative value.

6.6.4.2 Short-term Event-based Evaluation

More complete results characterizing the outflow hydrographs are presented in Tables 6.6 and 6.7. For the two events which occurred earlier in the year (#1 and #2), there was an issue with data collection in the VS for low flows which was later resolved. Therefore, it is assumed the flow volumes are underestimated and thus the error between simulated and observed data is less than

what is presented. These events were still included in the analysis since the high intensity peaks were successfully captured.

Table 6.6 Outflow volume and peak flow results for the 5 major rainfall events used in the calibration process.

Event #	Effluent Volume (Retention)						Peak Flow (Detention)					
	VS			BB			VS			BB		
	Obs. (m^3)	Sim. (m^3)	% error	Obs. (m^3)	Sim. (m^3)	% error	Obs. (L/s)	Sim. (L/s)	% error	Obs. (L/s)	Sim. (L/s)	% error
1	5.38[a]	15.42	187	3.48	16.13	364	0.68	0.84	24	0.21	0.70	233
2	7.04[a]	17.62	150	4.94	18.51	275	3.32	2.80	16	0.58	1.31	126
3	10.61	6.50	39	3.14	4.48	43	4.87	3.30	32	1.28	0.50	61
4	6.45	6.28	3	3.94	2.63	33	3.80	3.35	12	1.64	0.17	90
5	10.92	13.41	23	8.99	9.80	9	4.90	3.53	28	1.93	1.93	0

[a]Flow volume was underestimated at the start of the study period due to an error in flowmeter settings.

Table 6.7 Detention metric results for the 5 major rainfall events used in the calibration process.

Event #	Start time of Runoff (Detention)						Duration of Runoff (Detention)					
	VS			BB			VS			BB		
	Obs. (h:min)	Sim. (h:min)	Diff. (h:min)	Obs. (h:min)	Sim. (h:min)	Diff. (h:min)	Obs. (h)	Sim. (h)	% error	Obs. (h)	Sim. (h)	% error
1	20:24	20:45	0:21	20:40	22:25	1:45	8.60[a]	14.7	71	13.0	25.5	96
2	5:33	5:33	0:00	5:40	6:10	0:30	2.50[a]	14.1	464	3.0	18.7	523
3	10:42	10:43	0:01	10:43	11:33	0:50	2.30	1.70	26	2.0	4.9	145
4	6:44	6:44	0:00	6:51	8:50	1:59	1.00	1.00	0	1.2	7.0	483
5	19:15	19:23	0:08	19:29	20:30	1:01	2.50	2.50	0	2.1	5.0	138

[a]Flow duration was underestimated at the start of the study period due to an error in flowmeter settings.

A single-event analysis (Figure 6.8) presents the simulated and observed effluent hydrographs for two significant events (#2, May 9th-10th, and #5, July 30th). There were 6.29 antecedent dry days before event #2 and 9.5 ADD before event #5. The field derived initial moisture content of the soil in the vegetated swale was not available for event #2 (Table 6.4). Therefore, the initial soil moisture contents simulated by the model were used to establish any difference between the two cases. The simulated initial soil moisture contents were found to be 28.5% (#2)/24.8% (#5) for BB and 23.3%

(#2)/20.5% (#5) for VS. The observed initial moisture content in the soil for BB was 31.7% (#2) and 31.3% (#5). Hence the model predicted a lower water content in the soil prior to the more intense rainfall event (#5) whereas the observed data for BB showed no variation.

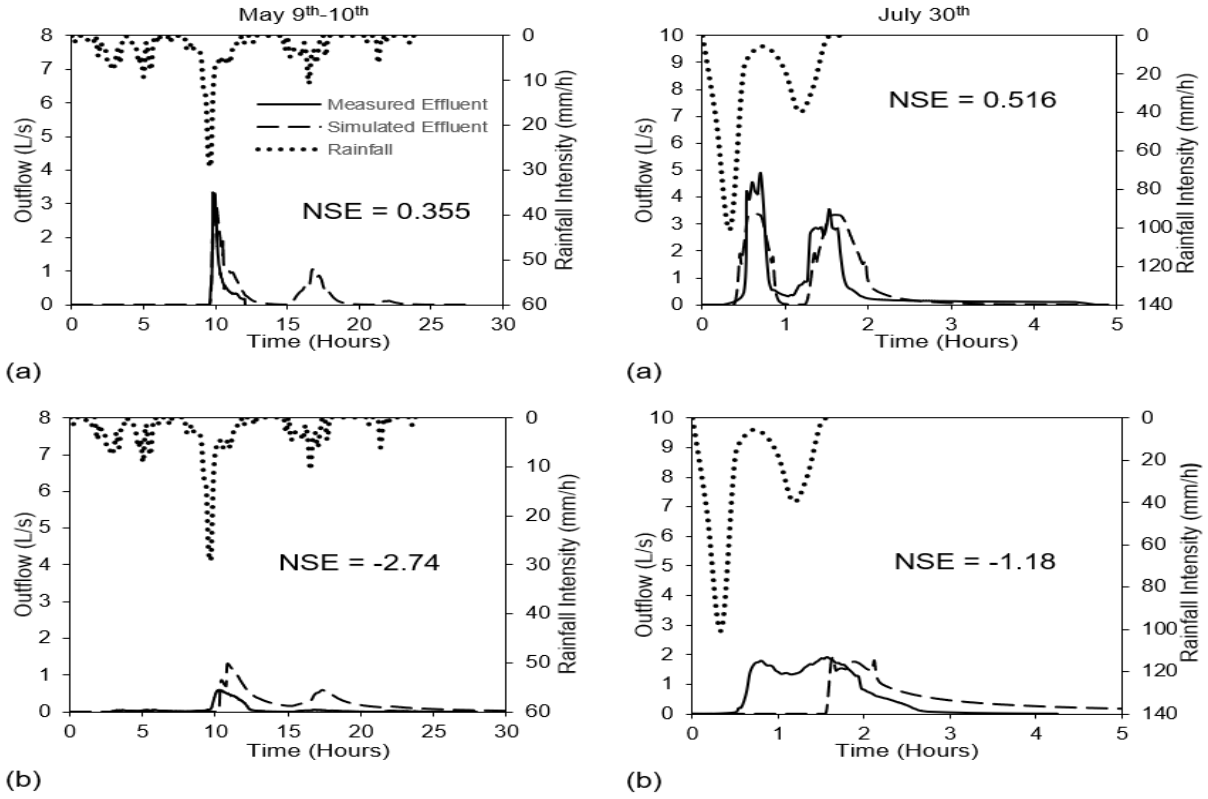

Figure 6.8 Comparison between measured and simulated effluent hydrographs for two significant rainfall events (#2 and #5): (a) vegetated swale; (b) bioretention basin.

6.6.4.3 Vegetated Swale

The positive global accuracy of the vegetated swale calibration was not seen for all rainfall events when considered separately.

The general trend in Table 6.6 indicates a better performance for events with a short duration (#3, 4, 5) for volume retention and an acceptable error for all events in terms of peak flow. Table 6.7 showed a good alignment in terms of the start of runoff between observed and simulated data except for event #3 which began 1 hour later in the model. The model predicted a much longer duration of outflow for events #1 and #2 compared to the measurements.

The unsuccessful measurement of low flow which occurred earlier in the study affected the observed data presented for event #2 in Figure 6.8 (a). This contributed to the error seen between simulated and observed data.

Nonetheless, promising results for the vegetated swale are demonstrated in Figure 6.8 (a). For the July 30th event, the curves align very well in terms of start time of runoff (8 min lag for simulated), duration (no error) and volume of runoff (23% error). However, the first peak was somewhat underestimated (28% error). As for the first peak to occur in event #2, although the curves have the same shape (less than 10% error for peak flow and runoff start time), the model predicts a larger volume (73% error).

6.6.4.4 Bioretention Basin

In the case of the bioretention basin, the volume retention trend (Table 6.6) is the same as the VS with a superior performance for events #3 to 5. This is also observed for the peak flow. However, there is no identifiable trend for the detention metrics (Table 6.7).

A major tendency noticed in the observed data for the bioretention basin is that the outflow is measured quickly after the rainfall peak. For both events, the time between the max intensity of the rainfall event and the associated discharge peak was less than 30 minutes and the discharge ended less than an hour after the end of the event.

For event #2, the simulated peak reacts similarly in time with the observed data (difference of only 20 minutes) whereas five times more volume is simulated by the model. This is compared to a large misalignment for event #5 (1 hour between peaks) which could be due to the way the bio-retention cell module is modelled in SWMM. The storage layer must fill up first before water can exit the underdrain. In this case there is a 200 mm offset between the base of the storage layer and the bottom of the drain. The reason this offset is not present in event #2 seems to be because there had already been 30 mm of rain that fell before the peak intensity occurred which filled up the storage layer. As for outflow volume in BB for July 30th, there is only a 9% difference between the two curves.

Considering all 5 events, three different issue categories were identified: a flow overestimation, a difference in the shape of the hydrographs or a misalignment in time. Thus, the issue creating the error between the simulated and observed data was not consistent. When calibrating, alterations

made in either the input parameters or the structure's design might reduce the error for some events but worsen it for others, consistently culminating in a negative global NSE. It is therefore necessary, in the case of the bioretention basin, to have multiple calibration parameter sets for specific categories of rainfall events.

6.6.4.5 Influence of Rainfall Characteristics

Event #2 produced 30% more rain than #5 but was less intense (peak intensity of 28.98 vs 100.56 mm/h for event #5) due to its long duration. Thus, 36% less outflow (7.04 m^3 vs 10.92 m^3 for #5) was measured at the exit of the VS. This difference is assumed to be smaller than what is being reported because of formerly mentioned reasons.

Nonetheless, the observed data show a proportional relationship between outflow volume and the average intensity of an event. The same tendency is seen in the BB with the longer event producing 45% less outflow (4.94 vs 8.99 m^3 for #5). This can be described alternatively as the outflow volume and duration of an event being inversely proportional.

Conversely, the simulated data show the opposite: a proportional relationship between outflow volume and event duration. This contradiction between observed and simulated outflow volume results is the cause of the larger % error for event #2.

Events #1 and 3 have comparable heights (48.66 mm for #1 vs 34.04 mm for #3) but very different durations (39.3h for #1 vs 3.7h for #5). The simulated initial soil moisture contents were found to be 32.2% (#1)/28.5% (#3) for BB and 31.0% (#1)/23.1% (#3) for VS. Hence the soil was predicted to contain less water prior to the more intense rainfall event (#3).

Considering volume retention, the same opposing tendency between measured and simulated results is observed for both structures. Regardless of its lower depth, the 3.7-hour long event produced twice as much outflow (observed at VS) compared to the 39.3-hour long event. The simulated results present an opposing tendency with 58% less outflow volume for the shorter event. In this case the lower initial moisture content influenced the results.

Regarding outflow hydrograph peak flow and duration, when comparing events #1 and #3, both observed and simulated results for the VS show the same trend: a larger peak flow and smaller duration of flow for event #3 (the shorter and more intense rainfall). The bioretention basin also

presents this tendency except for the peak flow of the simulation results which show a smaller value for event #3.

Other influential rainfall characteristics can be identified which essentially describe the detailed form of the event (pattern). More specifically, the location of the peak intensity, the number of peaks to occur and the time between them, etc. However, the capacity to evaluate the influence of individual parameters is compromised as their number rises due to the small dataset of events which generated a reaction from the model. Therefore, a larger set of data would be required in order to produce multiple calibration sets based on a detailed categorization of the precipitation events.

6.6.5 Validation

Once the accuracy of the calibration was deemed acceptable, a validation of the model was performed using the data collected from August 1st to November 5th, 2019 (19 events for a total of 464.6 mm and 4 significant rainfall events). The validation was only completed for the vegetated swale since the bioretention basin was not successfully calibrated.

The assessment of the validation results is that it was successful with a global NSE of 0.555 and an outflow volume and peak flow % error of 11.9 and 33.4, respectively. Specific results for two rainfall events are presented in Table 6.8.

Table 6.8 Performance results for two events considered in the validation of the vegetated swale calibration.

Descriptive Metric	**Events October 1st (Table 6.4)**	**Event October 31st (Table 6.4)**
NSE	0.51	0.818
Measured outflow volume (m^3)	20.43	27.76
Simulated outflow volume (m^3)	19.38	33.53
% error outflow volume	5.1	20.8
Measured peak flow (L/s)	4.94	3.80
Simulated peak flow (L/s)	3.29	2.86
% error peak flow	33.4	24.7

6.7 Conclusion

LID micro-structures represent viable solutions to aid in lessening the impacts of urban development through the infiltration of stormwater runoff into the ground. Hydrologic models can be used to aid in the implementation of such systems in the urban landscape. It is necessary to ensure the steps undergone to model specific projects are representative of reality and completed as accurately as possible.

Calibrating a bioretention basin (BB) and vegetated swale (VS) in PCSWMM resulted in very different outcomes. It was determined that the modelled representation of a LID solution must be carefully considered especially when the structure's cross-sectional shape does not follow the assumptions made in SWMM's calculations.

The magnitude of model sensitivity to the user input parameters was quantified by increasing the initial parameter value by 25 and 50% and calculating a relative sensitivity. The parameters affecting the speed of percolation were identified as most influential: conductivity slope (HCO), hydraulic conductivity (K_s) and porosity (ϕ_2). A 50% increase in the parameter value resulted in relative sensitivities (global outflow volume) of 22.1% (HCO), -19% (K_s) and 18.4% (ϕ_2) for the VS. The bioretention presented relative sensitivities of 9.1% (HCO), 1.7% (K_s) and -29% (ϕ_2). The peak flow of the BB was highly influenced by the K_s (86.5%). The hydrologic model was also influenced by evaporation rates [-20.7% (VS), -28.4% (BB)].

The parameter optimization process resulted in a maximization (based on acceptable ranges) of the K_s (140 mm/h) and minimization of the HCO (30). However, this parametric calibration did not meet the predefined performance metrics for both structures.

The soil layer of the constructed cells has a trapezoidal cross-section in contrast with the rectangular cross-section assumed by SWMM. In the final calibration, the soil section was split in two with the topsoil filling the sides of the trapezoid represented by a general subcatchment (Green-Ampt infiltration model as in the LID control module). The runoff from the adjacent sidewalk was routed onto this topsoil layer which was then routed to the main LID structure. This alteration proved very beneficial for the calibration of the vegetated swale (NSE from 0.206 to 0.614) albeit still not adequate for the bioretention basin (NSE from -0.686 to -0.348).

Although the vegetated swale calibration did produce globally positive results (NSE > 0.5), an event-based analysis showed that this acceptability was not consistent for all events. Of the 47 successfully measured events, 35 produced measured outflows but only 12 were simulated by the model. The latter included the largest events to occur during the study. Of these significant events, 6 had an NSE > 0.5. The observed data presented an inversely proportional relationship between outflow volume and event duration. In contrast, the model predicted a proportional relationship. Therefore, when comparing two events with similar depths, less outflow was measured for the longer event whereas the model simulated a large increase in outflow. This contradicting tendency was the largest source of error in the vegetated swale calibration. In summary, the model optimization presented herein was deemed most accurate for large events with a short duration.

Further investigation is needed to identify the true source of the misalignment between the observed and simulated outflow hydrographs. Nevertheless, it was found that the bioretention basin model was more sensitive to changes in the pattern of a rainfall event than the VS. Seeing as precipitation events can be characterized using a variety of attributes, a larger dataset would be required to develop multiple parameter optimization sets specific to different categories of events.

CHAPTER 7 GENERAL DISCUSSION

7.1 Threshold value for hydrograph determination

When generating the flow hydrographs at each measurement location, a threshold height value was subtracted from each total height value measured by the probe. This is necessary since the calibration curves define the relationship between flow and the water level above the crest of the weir. Theoretically, this value should remain constant over the entire period of study since it represents the physical distance between the bottom of the conduit and bottom of the v-notch of the weir. However, using the initial threshold value produced unrealistic results for certain events. This is clear when analyzing the inflow data collected at the control site STD-M12. Figure 7.1 presents the measured inflow with respect to inflow calculated using the rational method (section 3.1.4.3) assuming 10% losses. It is apparent that for most events, the measured is the same as the calculated, confirming the average runoff coefficient of 0.9 for this site. There is a slight tendency for smaller events to have less measured flow since a larger portion of the flow is lost on the surface.

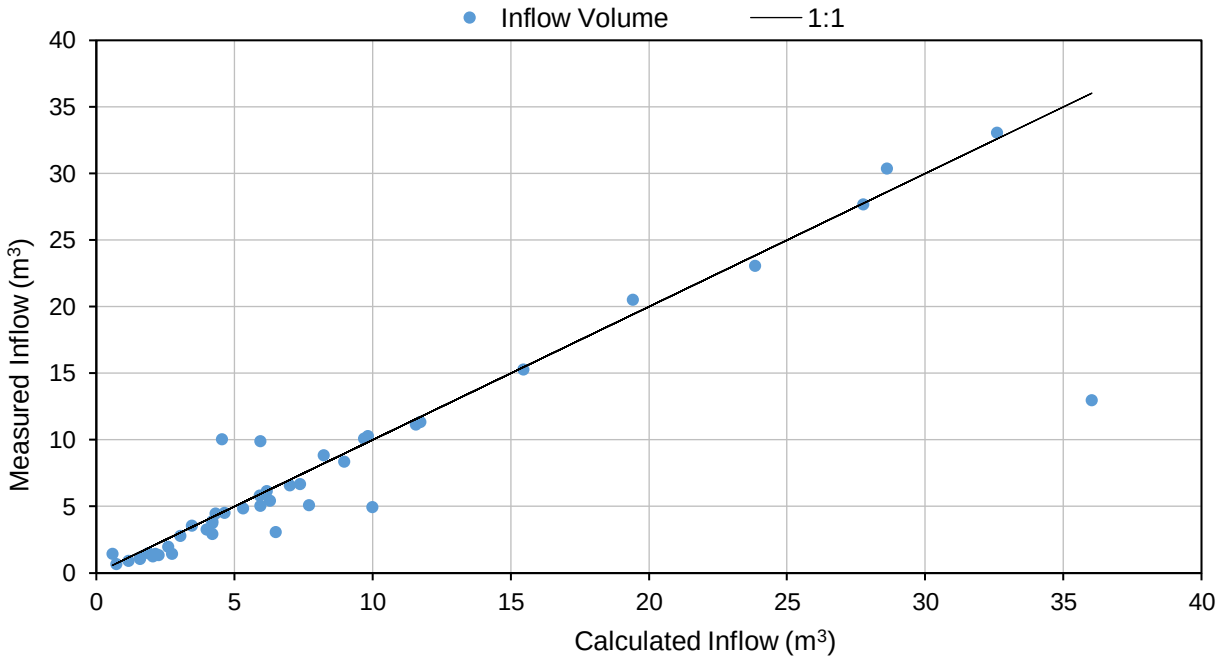

Figure 7.1 Total measured inflow volume vs volume of inflow calculated using the rational method

The outlier point occurring for the calculated flow of 36 m^3 is for the event occurring from October 31st at 14:10 to November 1st at 9:40 (63.15 mm of rain). The original threshold value of 39 mm (for site STD- M12) was subtracted from the measured heights. However, this resulted in a very small measured volume of 13 m^3. At the end of the next day the total height read by the probe was 20 mm and was still descending (no stabilization), although, prior to this event, the weir was verified for leaks. The conclusion is that for certain events, using the value determined in the field for the threshold did not culminate in a realistic value for measured inflow volume.

A possible source of error could stem from a de-calibrated probe. An easy way to correct this would be to see at what point the data stabilized after the rainfall and use this as the threshold. However, as explained previously, the height value read by the probe continued to decline and did not stabilize before the subsequent event. Therefore, for such cases, the runoff coefficient for the site STD-M12 was determined from events with similar characteristics which did not present this issue.

One additional possibility to explain the small measured volume is that a large portion of the flow never entered the street catch basin and was routed elsewhere due to the size of the event, but this is difficult to determine.

For events where the height measured inside the conduit was larger than its diameter, indicating hydraulic surcharge, the inflow was calculated using the rational method with the coefficient of 0.9 (impervious surface).

7.2 Measurement uncertainty

The calculation of the error presented in Appendix G is focused on the propagation of the height measurement uncertainty. As per the instrument's user manual, this error was presented as very small: 0.008 mm/mm. The methodology presented in Appendix G was applied to the outflow hydrograph for the bioretention basin (May 23rd rainfall event) and culminated in an error of only 0.96 L on a total of 584 L. This would characterize the data as highly precise. However, there are many sources of error which are not easily quantifiable which can contribute to error being larger than this. Developing a method to appropriately quantify the error surrounding the monitoring of LID structures was not the focus of this memoire. However, it is an important aspect which must be quantified to understand the limitations of the established performance results. A future project focused solely on this would be beneficial to the research community.

CHAPTER 8 CONCLUSION AND RECOMMENDATIONS

8.1 Summary of research findings

This research project evaluated the hydraulic performance of a vegetated swale (VS) and bioretention basin (BB) built on a large boulevard in Montreal. Of the events successfully measured, 78% (VS) and 91% (BB) achieved the targeted 67% volume retention. The empirical probability of reaching 67% in peak flow reduction was measured as 94% for VS and 98% for BB. The structures were not as successful in reducing the slopes of the entrance hydrographs since only 30% (VS) and 25% (BB) of events attained the target of 6 for delay ratio, R_{delay}. This means that the time elapsed between the beginning of the entrance runoff and the peak of the effluent flow was less than 6 times the time elapsed between the beginning of the entrance flow and the peak of the entrance flow for most events. Interestingly, the two structures showed similar abilities of peak flow detention.

An unexpected result was the inability of the bioretention basin to completely capture the outflow from small rainfall events that occur frequently while simultaneously showing a large retention for events with a return period above 2 years. When determining the Bioretention Abstraction Volume (BAV), a suggested primary design parameter, it was assumed that although outflow was measured for small events, the volume was negligible (< 2.5 m^3). Thus, a linear regression was only completed on events which produced more than 2.5 m^3 of outflow. The field derived BAV determined was 23 ± 10.9 m^3 [95% confidence interval (CI)].

It was established that the theoretical equations presented in the literature to calculate a low, average and high BAV represented an idealized case. By evaluating the field derived initial moisture contents of the media, it was determined that the soil never reached the minimal values used in the theoretical calculations (wilting point and field capacity). Therefore, theoretical BAV values of 18.8 m^3 (low), 28.1 m^3 (average) and 82.1 m^3 (high) were calculated using the measured initial moisture contents. The theoretical average BAV determined this way was much closer to the field derived value (22% difference but within the 95% CI) than the idealized theoretical average BAV (59.1 m^3).

A slope of 0.41 defined the linear relationship between outflow and inflow volume for the bioretention basins which was constructed in low permeable soils with a conventional underdrain

design. This indicates an average retention of 59% of the inflow volume by the structure. Increasing the BA:IDA ratio (24% vs a typical 5-10%) was shown to provide superior benefits in terms of global volume retention performance compared to an increase in the soil depth or implementation of an IWS zone. Nevertheless, should the capture of small events be necessary, an increase in the BA:IDA ratio is not enough and must be accompanied by an increase in the soil depth, implementation of an IWS zone, increase in the clay content of the soil or installation of a cap-orifice regulator.

A more in-depth understanding of the influence of these design parameters can be gained by building a hydrologic model of the structures. This was completed using the USEPA's SWMM engine implemented in PCSWMM. The field data collected to evaluate the hydraulic performance of the LID solutions was subsequently used to calibrate and validate the model thereby improving the behavior predictions.

A gap in the literature was identified for cases where a LID structure modelled using the bio-retention cell control module had an atypical cross-section (differing from the assumed rectangle). Thus, it was deemed important to understand the influence of this assumption on the model's simulation of the outflow.

The LID subcatchments in the model were initially designed with the same surface area as those in the field. A sensitivity analysis of this un-calibrated model identified the most influential parameters as those affecting the percolation speed through the media: hydraulic conductivity (K_s), conductivity slope (HCO) and porosity (ϕ_2). Increasing the parameter values by 50% yielded relative sensitivities on the global outflow volume of 22.1% (HCO), -19% (K_s) and -18.4% (ϕ_2) for the vegetated swale. The values for the bioretention basin were 9.1% (HCO), 1.7% (K_s) and -29% (ϕ_2). The hydraulic conductivity had a larger impact (86.5%) on the peak flow than on the volume exiting the bioretention basin. The model was also sensitive to the evaporation rates [-20.7% (VS), -28.4% (BB)].

Optimal values for the HCO and hydraulic conductivity were identified as 30 and 140 mm/h, respectively. Although increasing the porosity and the evaporation rates would improve the calibration, these parameters were not changed as they were already set to the higher limit of their logical range in the initial un-calibrated simulation. Although this parameter optimization did improve the alignment between measured and simulated results, it did not satisfy the prescribed

performance metric targets. So, it was necessary to alter the design of the structures in the model. Due to the irregular cross-section of the soil layer, it was deemed more accurate to divide it into two units: one representing the bottom 600 mm main section and one representing the topsoil. The width of the main LID subcatchment was reduced to equate the simulated and actual volumes of the bottom soil layer. The topsoil was represented by a completely pervious general subcatchment. The infiltration in the latter was modelled using Green-Ampt method with parameters equal to those applied to the main layer LID subcatchment. Finally, this change markedly improved the calibration of the vegetated swale (NSE from 0.206 to 0.614) but was still not adequate for the bioretention basin (NSE from -0.686 to -0.348). The modelled bioretention basin was more sensitive to the pattern of the rainfall events. Thus, it would be beneficial to develop separate parameter optimizations for different categories of events. Since the model only simulated outflow for the largest events, the resulting dataset (5 events) was small making it difficult to calibrate for different categories. In the end, based on an event-based analysis, the calibration put forth was shown to be most accurate for large rainfall events with a short duration.

Finally, the hydraulic performance of the vegetated swale was comparable to the bioretention basin since both presented high overall retention capacities with 72% for VS and 84% for BB. Both structures were able to greatly reduce the peak flows and showed a limited capacity in detaining the runoff. Additionally, the VS retained a larger number of the small rainfall events compared to BB. The behavior of this structure is also simpler to model and predict accurately. Thus, this makes the vegetated swale a viable option for hydraulic control at a smaller cost than the bioretention basin. Nevertheless, the bioretention basin did retain more volume during the largest events and 12% more volume overall. Due to its ability to both control stormwater quantitatively and qualitatively, it remains a promising LID solution. With an increase in the soil depth and better understanding of the details behind the modelling of these more complex designs, they can be optimized to provide a performance that outweighs their higher cost.

8.2 Recommendations and future improvements

8.2.1 Direct measurement of inflow

Assumptions were made in order to permit an indirect measurement of the inflow. The nature of the surface at the STD measurement point was assumed similar to the impervious surfaces of the LID facilities. Additionally, it was assumed that the inflow was directly proportional to the drainage surface. This means the entire street and sidewalk sections contributed to the runoff entering the basins. It is possible at times that the capacity of the street catch basins was breached and thus a part of the runoff rooted elsewhere. It would be beneficial to find a method which would permit the installation of a flowmeter at the entrance of at least one basin to verify the accuracy of the indirectly measured and calculated inflow volumes.

8.2.2 Deepening of LID-BMP media layer

As presented in a variety of other research studies, a larger media depth is beneficial towards the hydraulic performance of bioretention basins. Therefore, in terms of alterations to the design of the structures, an increase in the media depth is suggested. This is since the current layer has a minimum depth as compared to typical values. This change in the design will require additional costs however the benefits it could provide are shown to be significant.

8.2.3 Installation of a cap-orifice on the underdrain conduit

Seeing as the project presented herein is a pilot, it can be used as a real sized prototype. Thus, some alterations in its design post construction can be completed. It would be interesting to determine if the bioretention basin could perform adequately without the underdrain in the spring and summer. This would require the addition of a cap-orifice (initially completely closed) on the downstream end of the underdrain. Thus, the entire bowl of the structure would be used for the largest storms and an understanding of the natural exfiltration rates would be gained. The idea is to see if the characterization of the permeability of the natural soils is homogenous and representative.

8.2.4 Development of multiple calibration sets

As established, the calibration of the bioretention basin was not completed during this project. Further investigation would be required to understand the true source of the lack of alignment

between measured and simulated data. A more in depth understanding of the calculations behind the modelling of a bioretention basin and studying of the LID control output files would shed light on the issue. Furthermore, a larger dataset would ensure the rainfall events could be divided into categories which could be each used for a separate parameter optimization.

8.2.5 Calibration process

A beneficial addition to the SWMM model would be the ability to automatically calibrate the LID control. Developing this option could be the basis for a research project. This would ensure that the parameter values chosen are optimal and would reduce the time required for calibration.

8.2.6 Study of structures during winter months

The study of these structures during the winter climate was not explored. However due to the location of the LID structures, understanding their benefits during winter is important. Thus, a suggested avenue for future research is to attempt to do the same analysis but for the months of November to March. This would involve developing a winter monitoring methodology and evaluating the change brought to the water balance across the structures.

8.2.7 Variographic analysis of flow data

Variography provides a means to characterize the structure of variations in data sets. The typical application for time-series variograms deals with sampling of chemical variations process flows. However, it is a useful tool which can be used for data analysis in other disciplines.

A variogram, as presented in Figure 8.1, consists of a graphic representation of variance classed by interval length, in our case time interval between flow measurements. Many references exist which explain the calculations behind it (Gy, 1992; Matheron, 1963; Matheron, 1965; Minnitt & Pitard, 2008; Pitard, 1993; Thisteda & Esbensenb, 2017).

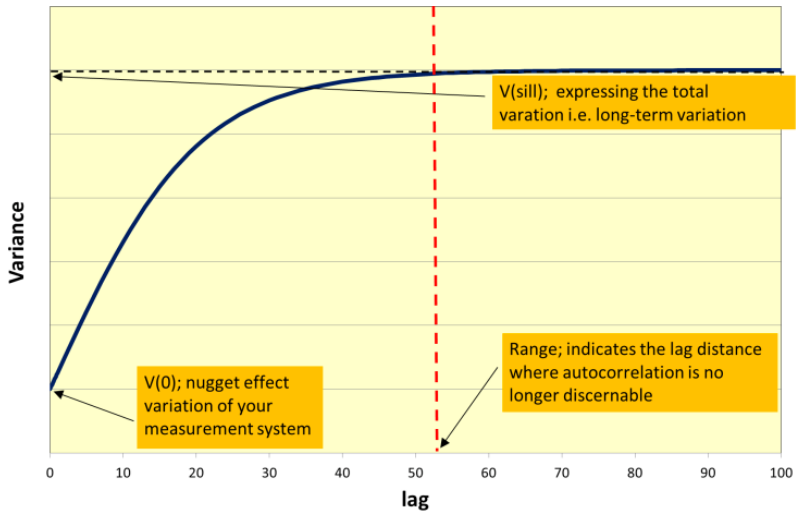

Figure 8.1 Example of variogram and explanation of its components (used with permission from Thisteda and Esbensenb (2017))

The data in this project consists of a time series at each flow measuring point. Variograms could be calculated for selected measurement points (STD-M12, BB-M10, VS-M3) flow data and volume data, using 2-minute intervals. The sequential water flow from M12 to M3 and M12 to M10 means that the data sets are in a sense representing progressive steps in a process flow. Comparing the variability signal at each process step can yield insight on the nature of the variability transformation at each step.

The variogram can provide an empirical statement on important aspects of the studied data set. These would include:

- Vj0 the random measurement error (true nugget effect)
- Vj1 the random measurement error plus high-frequency variation that occurs between measurements, thus representing the practical error on data
- The range, meaning the time required to reach the sill (Figure 8.1), gives an estimate of the time attenuation of a structure versus the input flows
- The maximum variance on the inlet versus the outlet flows
- The evolution of the variogram from the inlet M12 to bioretention M10 versus swale M3 would give a quantitative description of system dynamics

8.2.8 Perspectives

One aspect not focused on in this study was the influence of rainfall characteristics on the performance of the structures. This was only briefly explored in the discussion of the second article. It was established however, that simply categorizing events based on global attributes (depth, duration, peak flow) was not enough. It would be more beneficial to examine the pattern of the events: number, magnitude and timing of peak flows. Thus, a larger set of data which would permit a categorization of this nature would aid in exploring the relationship between the nature of the rainfall and the performance of the bioretention basin both in the field and in the model. Developing this dataset would require monitoring during a span of multiple years. The same long-term monitoring is required to understand the qualitative performance of the basins as well as the change in performance of the soil due to clogging. The conclusion is that the inconsistent nature of rainfall requires long-term study and does not permit sound conclusions to be drawn with merely a few months of data. This is especially true for the bioretention basin which represents a more complex design and is influenced by a larger number of processes. In order to establish clearer trends in relation to the influence of rainfall event types on bioretention basin performance, it is suggested to change the timeline of the project towards one which involves monitoring the structures for multiple years. This would permit a better statistical analysis and understanding of the long-term performance of the structures.

REFERENCES

Aceves, M. C., & Fuamba, M. (2016). Methodology for selecting best management practices integrating multiple stakeholders and criteria. Part 2: case study. *Water, 8*(2), 56.

Ahiablame, L. M., Engel, B. A., & Chaubey, I. (2012). Effectiveness of low impact development practices: literature review and suggestions for future research. *Water, Air, Soil Pollution 223*(7), 4253-4273.

ASTM. (1995). Standard Guide for Selection of Weirs and Flumes for Open-Channel Flow Measurement of Water. In (Vol. D5640). West Conshohocken, PA.

ASTM. (2013). Standard Test Method for Open-Channel Flow Measurement of Water with Thin-Plate Weirs. In (Vol. ASTM D5242-92). West Conshohocken, PA.

BMP Database. (2009). Urban Stormwater BMP Performance Monitoring Manual. In: Geosyntec Consultants and Wright Water Engineers, Inc., .

Booth, D. B., & Jackson, C. R. (1997). Urbanization of aquatic systems: degredation thresholds, stormwater detection, and the limits of mitigation. *Journal of the American Water Resources Association, 33*(5), 1077-1090.

Brière, G. F. (2000). *Water distribution and collection* (2nd ed.): Polytechnique International Press.

Brown, R., & Hunt, W. (2011). Underdrain configuration to enhance bioretention exfiltration to reduce pollutant loads. *Journal of Environmental Engineering, 137*(11), 1082-1091.

Brown, R. A., & Hunt III, W. F. (2011). Impacts of media depth on effluent water quality and hydrologic performance of undersized bioretention cells. *Journal of Irrigation and Drainage Engineering, 137*(3), 132-143.

Burszta-Adamiak, E., & Mrowiec, M. (2013). Modelling of green roofs' hydrologic performance using EPA's SWMM. *68*(1), 36-42.

Chapman, C., & Horner, R. R. (2010). Performance assessment of a street-drainage bioretention system. *Water Environment Research, 82*(2), 109-119.

Cunnane, C. (1978). Unbiased plotting positions—a review. *Journal of Hydrology, 37*(3-4), 205-222.

Davis, A. P. (2008). Field performance of bioretention: Hydrology impacts. *Journal of Hydrologic Engineering, 13*(2), 90-95.

Davis, A. P., Hunt, W. F., Traver, R. G., & Clar, M. (2009). Bioretention technology: Overview of current practice and future needs. *Journal of Environmental Engineering, 135*(3), 109-117.

Davis, A. P., Traver, R. G., Hunt, W. F., Lee, R., Brown, R. A., & Olszewski, J. M. (2012). Hydrologic performance of bioretention storm-water control measures. *Journal of Hydrologic Engineering, 17*(5), 604-614.

DeBusk, K., & Wynn, T. (2011). Storm-water bioretention for runoff quality and quantity mitigation. *Journal of Environmental Engineering, 137*(9), 800-808.

DeBusk, K. M., Hunt, W. F., & Line, D. E. (2010). Bioretention outflow: Does it mimic nonurban watershed shallow interflow? *Journal of Hydrologic Engineering, 16*(3), 274-279.

Dietz, M. E. (2007). Low impact development practices: A review of current research and recommendations for future directions. *Water, air, soil pollution 186*(1-4), 351-363.

Dietz, M. E., & Clausen, J. C. (2005). A field evaluation of rain garden flow and pollutant treatment. *Water, Air, Soil Pollution 167*(1-4), 123-138.

Dietz, M. E., & Clausen, J. C. (2006). Saturation to improve pollutant retention in a rain garden. *Environmental science & technology*, *40*(4), 1335-1340.

Dongquan, Z., Jining, C., Haozheng, W., Qingyuan, T., Shangbing, C., & Zheng, S. (2009). GIS-based urban rainfall-runoff modeling using an automatic catchment-discretization approach: a case study in Macau. *Environmental Earth Sciences, 59*(2), 465.

Eckart, K., McPhee, Z., & Bolisetti, T. (2017). Performance and implementation of low impact development–A review. *Science of the Total Environment, 607*, 413-432.

Elliott, A., & Trowsdale, S. A. (2007). A review of models for low impact urban stormwater drainage. *Environmental modelling software*, *22*(3), 394-405.

Energy Independence and Security Act (EISA), Pub. L. No. 110-140 (2007). https://www.epa.gov/laws-regulations/summary-energy-independence-and-security-act

Environment Canada. (2018). Données des stations pour le calcul des normales climatiques au Canada de 1981 à 2010 - Montréal/Pierre Elliott Trudeau Intl A - Évaporation. from Environment Canada https://climat.meteo.gc.ca/climate_normals/results_1981_2010_f.html?searchType=stnName&txtStationName=Montr%C3%A9al&searchMethod=contains&txtCentralLatMin=0&txtCentralLatSec=0&txtCentralLongMin=0&txtCentralLongSec=0&stnID=5415&dispBack=0

Environment Canada, F. (2018). Données des stations pour le calcul des normales climatiques au Canada de 1981 à 2010 - Montréal/Pierre Elliott Trudeau Intl A - Précipitation. from Environment Canada https://climat.meteo.gc.ca/climate_normals/results_1981_2010_f.html?searchType=stnName&txtStationName=Montr%C3%A9al&searchMethod=contains&txtCentralLatMin=0&txtCentralLatSec=0&txtCentralLongMin=0&txtCentralLongSec=0&stnID=5415&dispBack=0

Ewing, S. A., Grayson, R. B., & Argent, R. M. (2000). Science, citizens, and catchments: Decision support for catchment planning in Australia. *Society Natural Resources 13*(5), 443-459.

Flint, K. R., & Davis, A. P. (2007). Pollutant mass flushing characterization of highway stormwater runoff from an ultra-urban area. *Journal of Environmental Engineering, 133*(6), 616-626.

Fuamba, M., Branger, F., Braud, I., Batchabani, E., Sanzana, P., Sarrazin, B., & Jankowfsky, S. (2019). Value of distributed water level and soil moisture data in the evaluation of a distributed hydrological model: Application to the PUMMA model in the Mercier catchment (6.6 km2) in France. *Journal of Hydrology, 569*, 753-770.

Gallo, C., Moore, A., & Wywrot, J. (2012). Comparing the adaptability of infiltration based BMPs to various US regions. *Landscape urban planning, 106*(4), 326-335.

García-Gaines, R., & Frankenstein, S. (2015). USCS and the USDA Soil Classification System: Development of a Mapping Scheme.

Géhéniau, N., Fuamba, M., Mahaut, V., Gendron, M. R., & Dugué, M. (2014). Monitoring of a rain garden in cold climate: case study of a parking lot near Montreal. *Journal of Irrigation Drainage Engineering 141*(6), 04014073.

Grant, D. M., & Dawson, B. D. (1997). ISCO Open Channel Flow Measurement Handbook. In. Lincoln, NE: ISCO Environmental Division.

Guo, J. C., & Luu, T. M. (2015). Operation of cap orifice in a rain garden. *Journal of Hydrologic Engineering*, *20*(10), 06015002.

Gy, P. M. (1992). *Sampling of heterogeneous and dynamic material systems: theories of heterogeneity, sampling and homogenizing*: Elsevier.

Harbor, J. M. (1994). A practical method for estimating the impact of land-use change on surface runoff, groundwater recharge and wetland hydrology. *Journal of the American Planning Association, 60*(1), 95-108.

Herrera, J., Bonilla, C. A., Castro, L., Vera, S., Reyes, R., & Gironás, J. (2017). A model for simulating the performance and irrigation of green stormwater facilities at residential scales in semiarid and Mediterranean regions. *Environmental Modelling and Software, 95*, 246-257.

Holman-Dodds, J. K., Bradley, A. A., & Potter, K. W. (2003). Evaluation of Hydrologic Benefits Of Infiltration Based Urban Storm Water Management 1. *JAWRA Journal of the American Water Resources Association, 39*(1), 205-215.

Hunt, W., Jarrett, A., Smith, J., & Sharkey, L. (2006). Evaluating bioretention hydrology and nutrient removal at three field sites in North Carolina. *Journal of Irrigation and Drainage Engineering, 132*(6), 600-608.

Hunt, W., Smith, J., Jadlocki, S., Hathaway, J., & Eubanks, P. (2008). Pollutant removal and peak flow mitigation by a bioretention cell in urban Charlotte, NC. *Journal of Environmental Engineering, 134*(5), 403-408.

James, W. (2005). Rules for responsible modelling. In (4th ed.). Guelph: CHI.

James, W., Rossman, E. L., & James, C. R. W. (2011). *User's Guide to SWMM* In (pp. 905).

JCGM. (2008). Evaluation of measurement data — Guide to the expression of uncertainty in measurement. In.

Jennings, A. A., Adeel, A. A., Hopkins, A., Litofsky, A. L., & Wellstead, S. W. (2012). Rain barrel–urban garden stormwater management performance. *Journal of Environmental Engineering, 139*(5), 757-765.

Jewell, T. K., Adrian, D. D., & Nunno, T. J. (1978). Methodology for calibrating stormwater models. *Journal of the Environmental Engineering Division, 104*(3), 485-501.

Joo, J., Lee, J., Kim, J., Jun, H., & Jo, D. (2014). Inter-event time definition setting procedure for urban drainage systems. *Water Environment Journal, 6*(1), 45-58.

Khan, U. T., Valeo, C., Chu, A. V., & Van Duin, B. (2012). Bioretention cell efficacy in cold climates: Part 1—hydrologic performance. *Canadian Journal of Civil Engineering, 39*(11), 1210-1221.

Konrad, C. P., Booth, D. B., & Burges, S. J. (2005). Effects of urban development in the Puget Lowland, Washington, on interannual streamflow patterns: Consequences for channel form and streambed disturbance. *Water Resources Research, 41*(7).

Kuichling, E. H., Rudolph (1889). *The relation between the rainfall and the discharge of sewers in populous districts* (Vol. 20). New York: American Society of Civil Engineers.

Lee, J. G., Nietch, C. T., & Panguluri, S. (2018). Drainage area characterization for evaluating green infrastructure using the Storm Water Management Model. *Hydrology Earth System Sciences, 22*(5), 2615-2635.

Leon Harter, H. (1984). Another look at plotting positions. *Communications in Statistics-Theory and Methods, 13*(13), 1613-1633.

Les Services EXP inc. (2019). *Rapport d'analyse hydraulique - Aménagement complet*. (MTR-00015664-A5-on behalf of the City of Montreal).

Li, H., Sharkey, L. J., Hunt, W. F., & Davis, A. P. (2009). Mitigation of impervious surface hydrology using bioretention in North Carolina and Maryland. *Journal of Hydrologic Engineering, 14*(4), 407-415.

Mahmoud, A., Alam, T., Rahman, M. Y. A., Sanchez, A., Guerrero, J., & Jones, K. D. (2019). Evaluation of field-scale stormwater bioretention structure flow and pollutant load reductions in a semi-arid coastal climate. *Ecological Engineering, 1*, 100007.

Mailhot, A., & Talbot, G. (2012). Courbe IDF - Montreal-Pierre Elliot Trudeau Intl A. from Atlas agroclimatique du Quebec http://www.agrometeo.org/atlas/idf_station/MONTREAL-PIERRE_ELLIOTT_TRUDEAU_INTL_A/Montr%C3%A9al-Pierre%20Elliot%20Trudeau%20Intl%20A/7025250/false

Marsalek, J., Rochfort, Q., Brownlee, B., Mayer, T., & Servos, M. (1999). An exploratory study of urban runoff toxicity. *Water science technology, 39*(12), 33-39.

Matheron, G. (1963). Principles of geostatistics. *Economic geology, 58*(8), 1246-1266.

Matheron, G. (1965). Les variables régionalisées et leur estimation [Regionalized variables and their estimation]. *Paris: Editions Masson*.

McCutcheon, M., & Wride, D. (2013). Shades of Green: Using SWMM LID controls to simulate green infrastructure. *Water Manag. Model, 21*, 289-301.

MDDEFP. (2014). *Stormwater Management Guide*. QC, Canada Retrieved from http://www.environnement.gouv.qc.ca/eau/pluviales/guide.htm

Minnitt, R., & Pitard, F. (2008). Application of variography to the control of species in material process streams:% Fe in an iron ore product. *Journal of the Southern African Institute of Mining and Metallurgy, 108*(2), 109-122.

Moscrip, A. L., & Montgomery, D. R. (1997). Urbanization, flood frequency, and salmon abundance in Puget lowland streams. *JAWRA Journal of the American Water Resources Association, 33*(6), 1289-1297.

Nash, J., & Sutcliffe, J. (1970). River forcasting using conceptual models, 1. A discussion of principles. *J. Hydrol, 10*, 280-290.

National Research Council. (2008). *Urban stormwater management in the United States*. Retrieved from Washington, DC:

Niazi, M., Nietch, C., Maghrebi, M., Jackson, N., Bennett, B. R., Tryby, M., & Massoudieh, A. (2017). Storm water management model: Performance review and gap analysis. *Journal of Sustainable Water in the Built Environment, 3*(2), 04017002.

Passeport, E., Hunt, W. F., Line, D. E., Smith, R. A., & Brown, R. A. (2009). Field study of the ability of two grassed bioretention cells to reduce storm-water runoff pollution. *Journal of Irrigation and Drainage Engineering, 135*(4), 505-510.

Passeport, E., Vidon, P., Forshay, K. J., Harris, L., Kaushal, S. S., Kellogg, D. Q., . . . Stander, E. K. (2013). Ecological engineering practices for the reduction of excess nitrogen in human-influenced landscapes: A guide for watershed managers. *Environmental management, 51*(2), 392-413.

Peng, Z., & Stovin, V. (2017). Independent validation of the SWMM green roof module. *Journal of Hydrologic Engineering, 22*(9), 04017037.

PGCo, P. G. s. C. (2007). *Bioretention Manual* Prince George's County, Maryland

Pitard, F. F. (1993). *Pierre Gy's sampling theory and sampling practice: heterogeneity, sampling correctness, and statistical process control*: CRC press.

Qin, H.-p., Li, Z.-x., & Fu, G. (2013). The effects of low impact development on urban flooding under different rainfall characteristics. *Journal of environmental management, 129*, 577-585.

Rosa, D. J., Clausen, J. C., & Dietz, M. E. (2015). Calibration and verification of SWMM for low impact development. *JAWRA Journal of the American Water Resources Association, 51*(3), 746-757.

Rossman, L., & Huber, W. (January 2016). *Storm Water Management Model Reference Manual Volume I, Hydrology*. (EPA/600/R-15/162A). Washington, DC

Rossman, L., & Huber, W. (July 2016). *Storm Water Management Model Reference Manual Volume III – Water Quality*. (EPA/600/R-16/093). Washington, DC

Rossman, L. A. (2015). *Storm water management model user's manual version 5.1*. (EPA/600/R-14/413b). Cincinnati

Schwab, G. O., Fangmeier, D. D., Elliot, W. J., & Frevert, R. K. (1993). *Soil and water conservation engineering* (4 ed.). New York: Wiley.

Shamsi, U. M. S., & Koran, J. (2017). Continuous Calibration. *Journal of Water Management Modeling*.

Spitzer, D. W. (1996). *Flow Measurement Practical Guides for Measurement and Control*. NC: Instrument Society of America.

Stovin, V. R., Moore, S. L., Wall, M., & Ashley, R. M. (2013). The potential to retrofit sustainable drainage systems to address combined sewer overflow discharges in the T hames T ideway catchment. *Water Environment Journal 27*(2), 216-228.

Teledyne ISCO. (2016). 2150 Area Velocity Flow Module and Sensor, Installation and Operation Guide.

Thisteda, E., & Esbensenb, K. H. (2017). *Improvement practices in process industry—the link between process control, variography and measurement system analysis.* Paper presented at the TOS forum.

USBR. (2001). *Water Measurement Manual*. Retrieved from https://www.usbr.gov/tsc/techreferences/mands/wmm/index.htm

USEPA. (1983). *Final Report of the Nationwide Urban Runoff Program (NURP)* (NTIS PB84-185552). Retrieved from Washington, DC.:

USEPA. (1999). *Combined Sewer Overflows Guidance For Monitoring and Modeling*. (Report No 832-B-99-002). Washington, DC

USEPA. (1999). *Storm Water Technology Fact Sheet-Bioretention*. (Washington Dc, US Environmental Protection Agency, Office of Water).

USGS. (1999). The Quality of Our Nation's Waters: Nutrients and Pesticides. In: US Geological Survey Circular 1225.

Walsh, C. J., Roy, A. H., Feminella, J. W., Cottingham, P. D., Groffman, P. M., & Morgan, R. P. (2005). The urban stream syndrome: current knowledge and the search for a cure. *Journal of the North American Benthological Society, 24*(3), 706-723.

WCI Physics. The Burns Guide to Uncertainties and Error Propagation. Retrieved from http://www.mjburns.net/SPH4U/Burns%20Error%20Analysis%20techniques.pdf

Williams, E. S., & Wise, W. R. (2006). Hydrologic impact of alternative approaches to storm water management and land development. *JAWRA Journal of the American Water Resources Association, 42*(2), 443-455.

Winston, R. J., Dorsey, J. D., & Hunt, W. F. (2016). Quantifying volume reduction and peak flow mitigation for three bioretention cells in clay soils in northeast Ohio. *Science of the Total Environment, 553*, 83-95.

Zahmatkesh, Z., Burian, S. J., Karamouz, M., Tavakol-Davani, H., & Goharian, E. (2014). Low-impact development practices to mitigate climate change effects on urban stormwater runoff: Case study of New York City. *Journal of Irrigation Drainage Engineering 141*(1), 04014043.

APPENDICES

APPENDIX A ADDITIONAL MONITORING SITE DETAILS

Table A.1 Surface areas used to calculate the inflow volume of runoff

Monitoring Site	LID-BMP Surface (m^2)	Impervious Surface (m^2)	Tributary area: LID-BMP ratio
VB-M-3	167.42	854.58	5.0:1
BB-M-10	203.68	858.82	4.2:1
STD-M-12	NA	634.00	NA

Table A.2 Slopes of the conduits at the exit of the sites monitored

Monitoring site	Slope (°)
RV-10-11-M-3	0.9
B-29-30-M-10	0.4
STD-M-12	0.4

APPENDIX B DETAILS OF THE WEIR CALIBRATION PROCESS

Laboratory calibration process

1. The weirs were constructed as a combination of a 90° triangular v-notch and a rectangular weir with dimensions presented in Figure B.1. These dimensions were chosen to ensure that the conduit capacity would not be compromised. The ASTM Standard "Open-Channel Flow Measurement of Water with Thin-Plate Weirs" (2013), was consulted and the following aspects were considered:
    a. The weir is symmetrically designed
    b. The thickness of the section follows the rule shown in Figure B.2

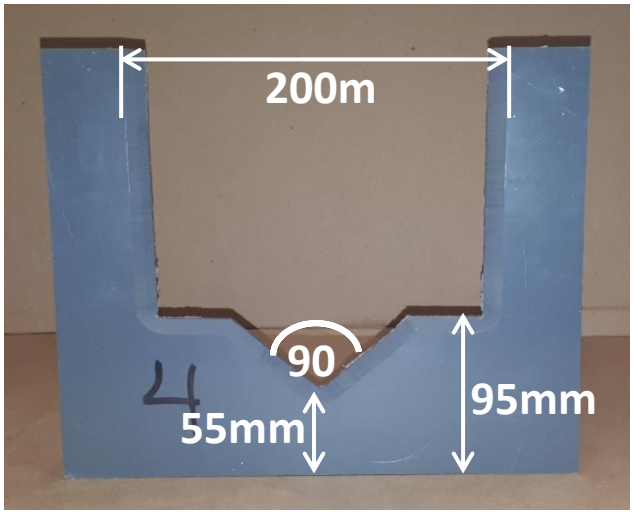

Figure B.1 Compound weir fabricated in the Polytechnique Montréal hydraulics laboratory

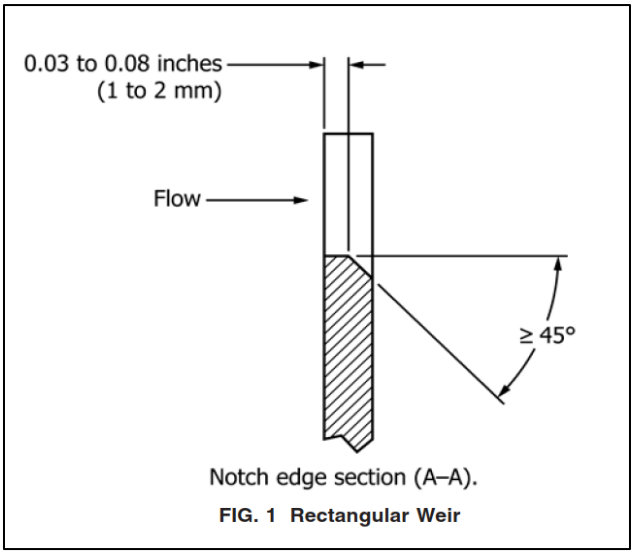

Figure B.2 Standard for the thickness of the section (ASTM, 2013)

2. A conduit section with the same cross-sectional diameter and shape as the one in the field was installed inside the rectangular laboratory testing channel as shown in Figure B.3. The laboratory conduit section was lined with a rehabilitation envelope whereas in the field the conduits were made of PVC, therefore, the manning coefficients of the two were slightly different.

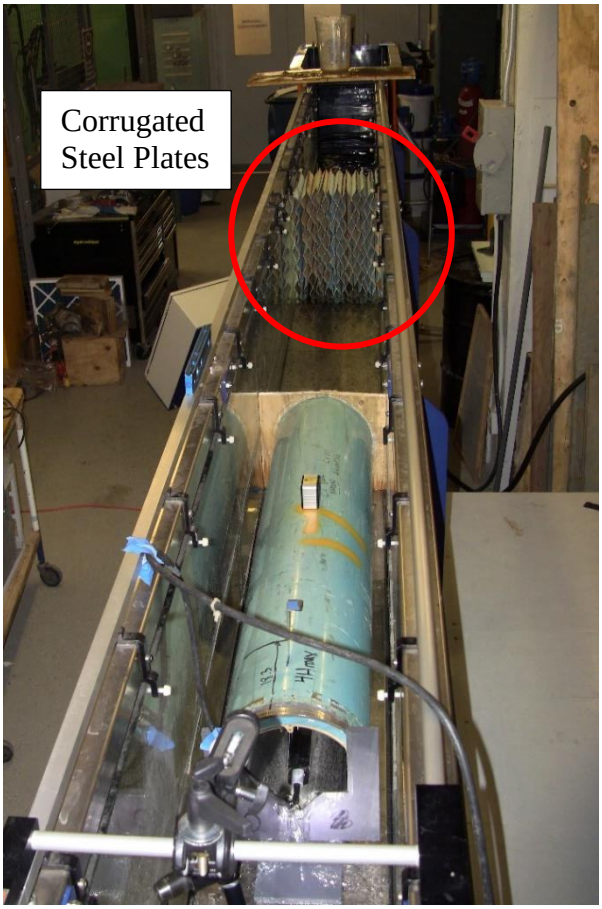

Figure B.3 Installation of conduit section inside testing channel

3. Wooden slabs were used to block off the area around the circular conduit and ensure the flow would only enter the conduit. The flow would pass through the channel continuously forming a loop.
4. The weir was installed on the front end of the conduit using a stainless-steel adjustable pipe clamp.
5. The slope of the testing channel was set to the slope of the conduit in the field (see Table A.2 for exact values for each site).
6. The diameter and shape of the conduit was specified inside the settings of the flowmeter module and the probe water depth measurement was zeroed (calibrated).
7. The probe was firmly attached to a metal mounting ring which was installed inside the conduit section (Figure B.4) at a distance D equal to four times the maximum head ($4H_{max}$)

over the vertex of the v-notch (ASTM, 2013). This criterion ensures the sensor is measuring the water height in a laminar area and eliminates the height reduction effect from the drawdown of flow over the crest of the weir. The total H_{max} was not considered since the conduit section was not long enough to place the probe so far back. The height measurement was verified at a location after the $4H_{max}$ spot used and it was shown that it did not change therefore the measurement was deemed outside the drawdown effect zone.

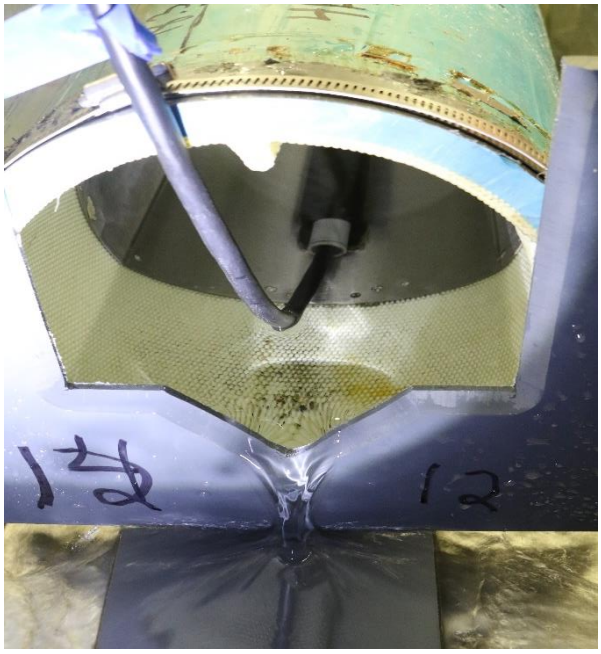

Figure B.4 Installation of the probe inside the conduit using the mounting ring

8. Corrugated steel plates were installed at the entrance of the canal to produce a laminar flow, ensuring optimal measurement accuracy (Figure B.3). A closer view is presented in Figure B.5.

Figure B.5 Closer view of corrugated steel plate

9. The channel pump was turned on and a consistent flow was established. A butterfly valve was adjusted manually to control the flow.
10. To establish the rating curve, 19 measurement points were taken. The minimum flow the channel could provide with the pump was 0.5 L/s which represented the highest flow in the v-notch section. Therefore, in order to generate a rating curve for the v-notch section, it was necessary to find another way to produce flow in the channel.
11. Flow rates below 0.5 L/s were generated using a hose placed at the beginning of the channel and were measured using a bucket and stopwatch.
12. The two calibration curves, one for the v-notch section and one for the rectangular section, were produced by changing the flow incrementally and measuring the associated depth of flow using the probe.
13. Each height reading was taken 3 times and the average was retained to reduce random error.
14. For the first readings, the height values measured with the probe we're verified using physical measurement made using a ruler. If the values did not match, the probe would have to be re-calibrated. Once the probe was deemed well-calibrated, the physical verifications were done less frequently to save time.

15. The distance between the bottom of the weir and the vertex of the v-notch, as shown in Figure B.6, is the threshold of the crest. When the water level in the pipe is lower than this value, there is no flow. Thus, to generate the rating curves, each reading of the water height by the sensor must be corrected by subtracting the height of the threshold. The corrected heights were then plotted with their associated flow values.

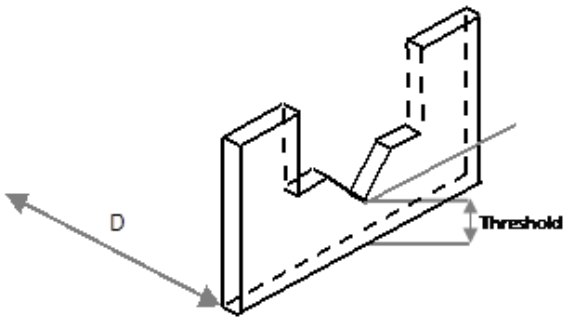

Figure B.6 Important dimensions to consider during installation

16. The power-type trend curve and the polynomial-type trend curve were chosen for the largest flows and the smallest flow rates, respectively. The correlation coefficient was the criterion in order to choose the type of trend curve.

Field calibration process

1. Install the inlet hose of the pump inside the monitoring manhole located downstream of the weir (Figure B.7). The hose will suction the stagnant water located in the bottom of the monitoring manhole.

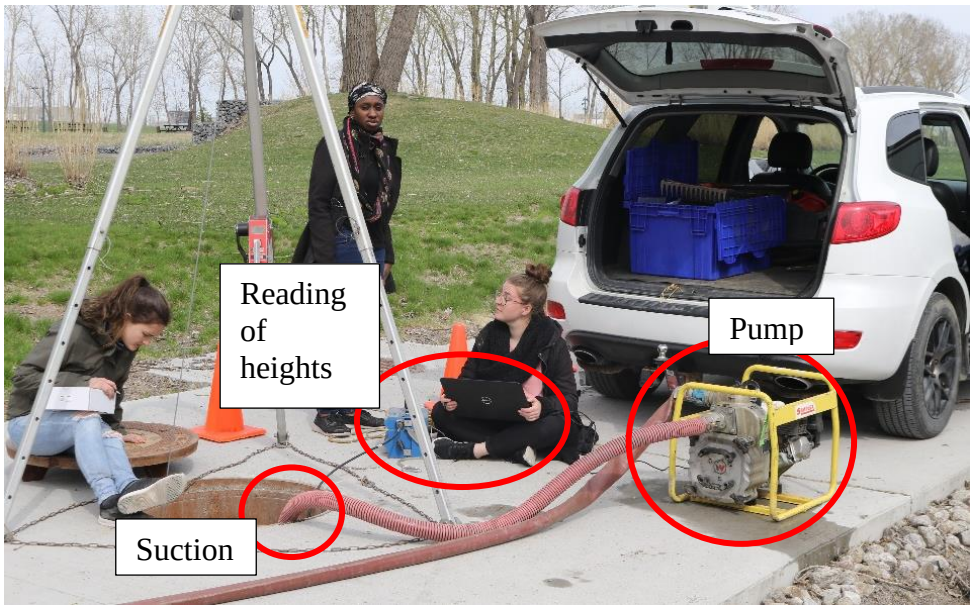

Figure B.7 Connecting the pump to the water supply inside the monitoring manhole (downstream of weir)

2. Install the outlet hose of the pump inside the drain of the LID facility which is located upstream of the weir (Figure B.8). This will complete the circuit and permit the suctioned water to flow through the conduit on which is installed the weir (closed system).

Figure B.8 Connecting the pump to the outflow point: the drain of the vegetated swale which is upstream of the weir

3. The technician is to descend into the monitoring manhole where a bucket is installed underneath the conduit and weir. The bucket must be labelled to identify incremental volumes (Figure B.9).

Figure B.9 Volume increments identified in a bucket used to established flow rates

4. Connect the computer to the flowmeter module to take live readings of the height of water measured by the probe (Figure B.7).

5. Prepare a timer to measure the flow passing through the conduit (Figure B.10).

Figure B.10 A view of the set up inside the monitoring manhole

6. Once all researchers stationed, turn on the pump to a consistent flow: begin at the lowest possible flow through the system which generates runoff above the weir notch.
7. For each volume level reached in the bucket, note the height of flow and the time on the stopwatch (Figure B.11).

Figure B.11 Stages of one flow measurement point (4 measurements to determine an average)

8. Incrementally increase the flow provided by the pump and repeat step 7 for each flow point. Ensure that a flow point is measured only when the nappe above the weir has stabilized and the flow is as laminar and uniform as possible.

Calibration curves

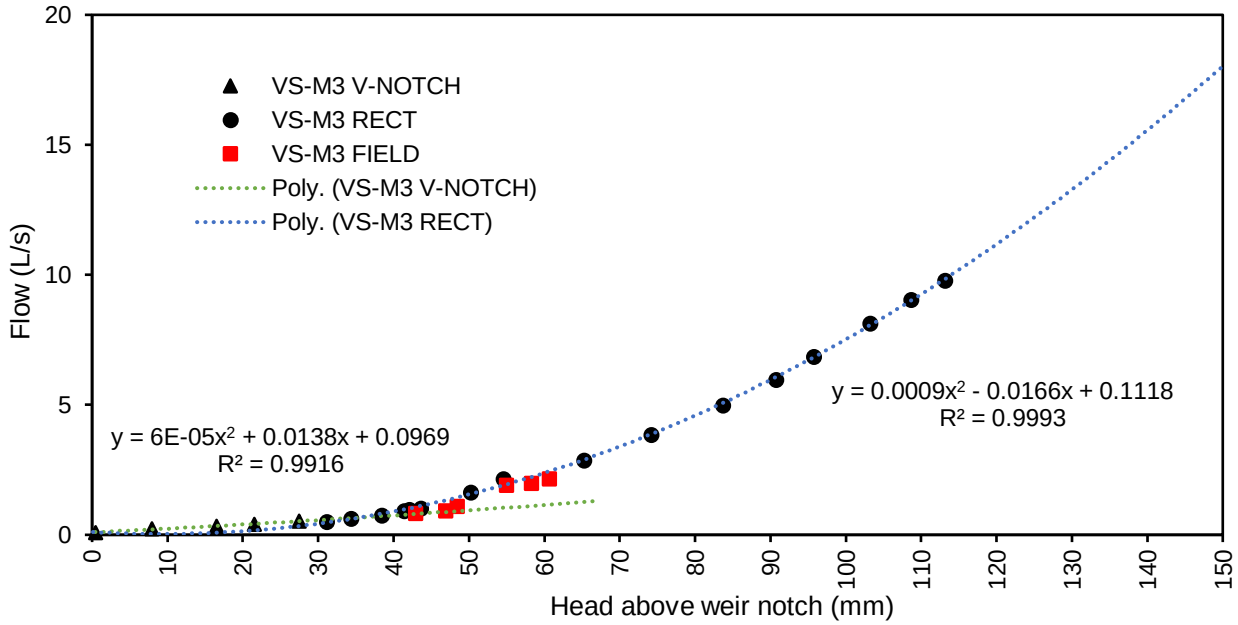

Figure B.12 Rating curve developed in the laboratory and in the field for monitoring site VS-M3

Note: A power trendline for the lower part of the v-notch was not necessary for the vegetated swale since the minimum of the quadratic occurs at -115 mm.

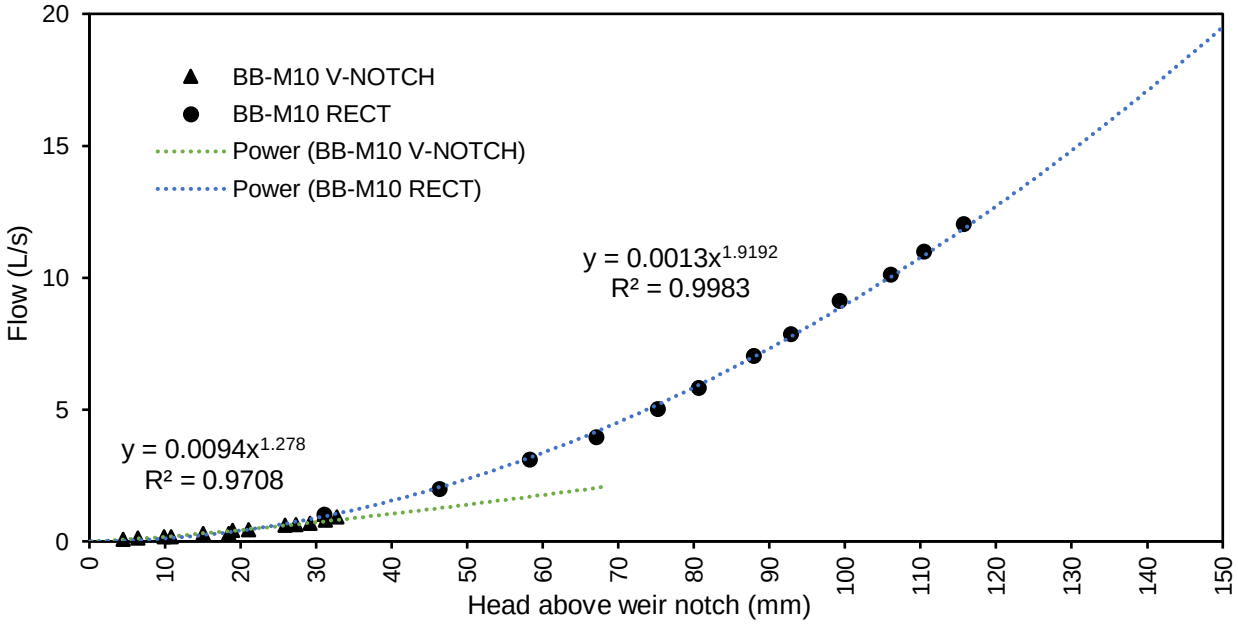

Figure B.13 Rating curves developed in the laboratory for monitoring site BB-M10

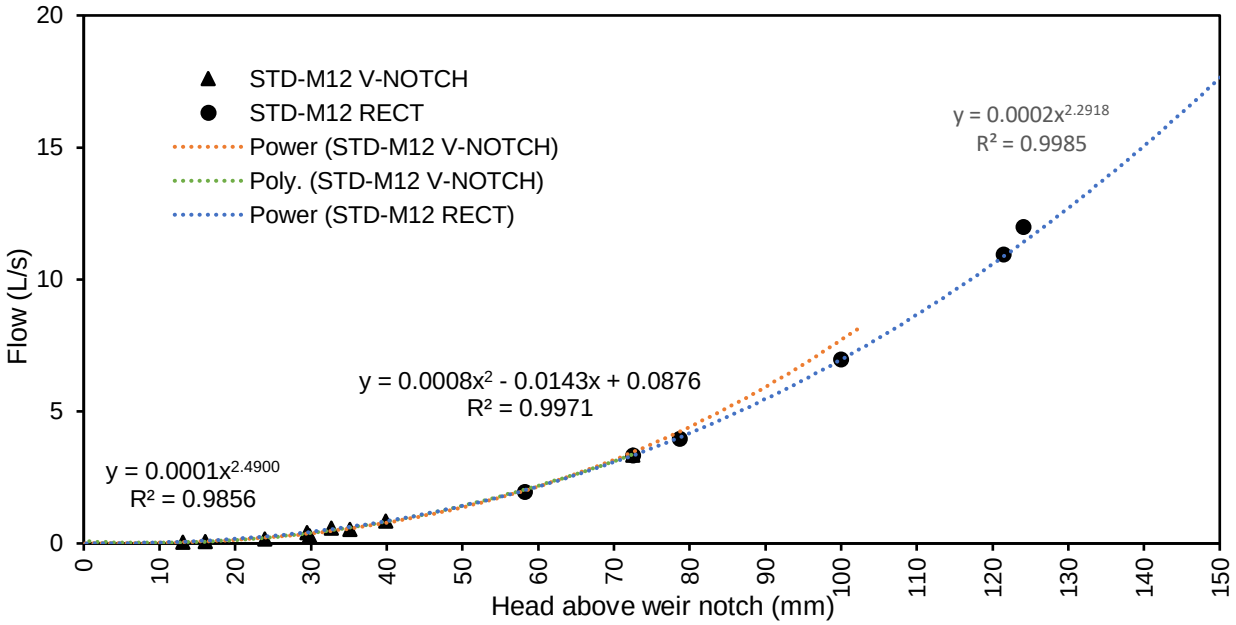

Figure B.14 Rating curves developed in the laboratory for monitoring site STD-M12

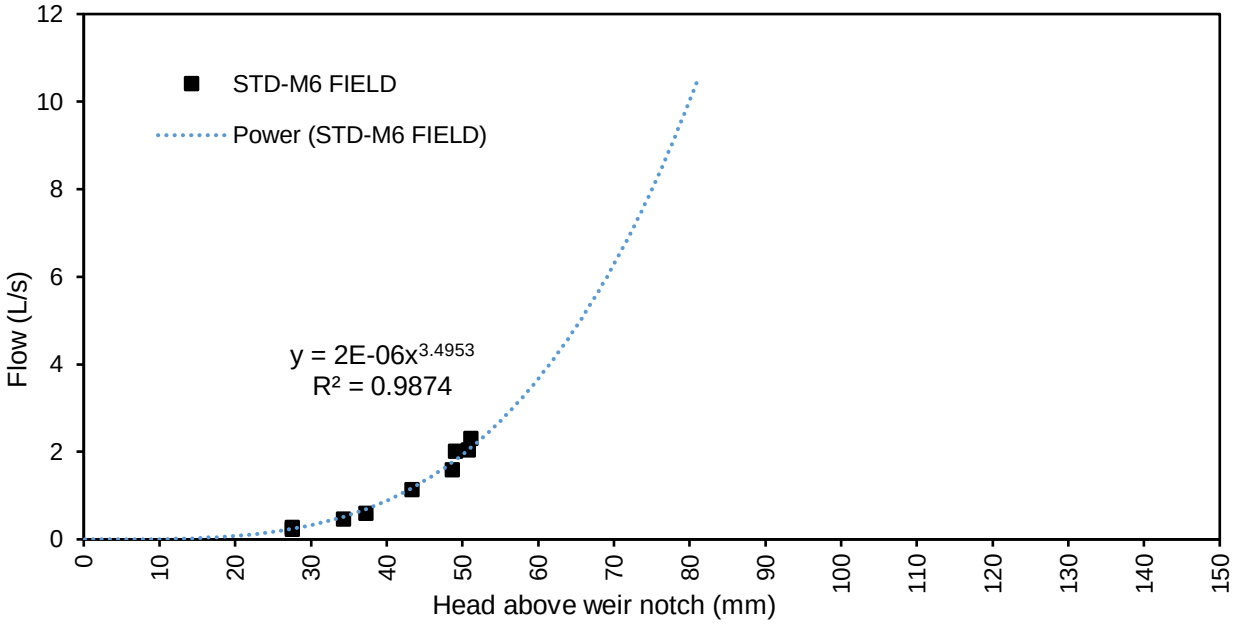

Figure B.15 Rating curve developed in the field for monitoring site STD-M6 not used in the analysis

APPENDIX C CHARACTERISTICS OF RAINFALL EVENTS - 2019

Table C.1 Attributes of all rainfall events measured using a rain gauge with a time-step of 5 min

# of Rainfall Event	Start Date and Time (Y-M-D and HH:MM)	End Date and Time (Y-M-D and HH:MM)	Duration (HH:MM)	Average Intensity (I_{avg}) (mm/hr)	Maximum Intensity (I_{max}) (mm/hr)	Total Depth (mm)	Antecedent Dry Days (ADD)
18	2019-04-18 17:55	2019-04-20 9:15	39:20	1.24	16.5	48.7	3.05
19	2019-04-23 22:15	2019-04-24 12:10	13:55	0.67	4.80	9.30	3.54
20	2019-04-26 9:40	2019-04-27 12:30	26:50	1.01	4.80	27.1	1.90
21	2019-05-01 16:20	2019-05-02 3:35	11:15	0.98	6.00	11.0	4.16
22	2019-05-03 8:45	2019-05-03 12:35	3:50	0.94	3.00	3.59	1.22

Table C.2 Attributes of all rainfall events measured using a weather station and a time-step of 10 min.

# of Rainfall Event	Start Date and Time (Y-M-D and HH:MM)	End Date and Time (Y-M-D and HH:MM)	Duration (HH:MM)	Average Intensity (I_{avg}) (mm/hr)	Maximum Intensity (I_{max}) (mm/hr)	Total Depth (mm)	Antecedent Dry Days (ADD)
23	2019-05-09 19:35	2019-05-10 19:40	24:05	2.37	28.98	57.12	6.29
24	2019-05-13 23:10	2019-05-14 15:40	16:30	0.82	3.06	13.50	3.15
25	2019-05-19 6:10	2019-05-19 8:40	2:30	2.12	4.56	5.31	4.60
26	2019-05-19 18:40	2019-05-19 19:10	0:30	4.06	6.12	2.03	0.42
27	2019-05-20 0:20	2019-05-20 1:00	0:40	10.50	15.24	7.00	0.75
28	2019-05-23 16:40	2019-05-24 3:45	11:05	1.86	22.86	20.57	3.65
29	2019-06-02 6:20	2019-06-02 7:20	1:00	1.26	3.06	1.26	9.11
30	2019-06-02 10:30	2019-06-02 13:20	2:50	2.68	6.12	7.58	0.13
31	2019-06-10 23:50	2019-06-11 6:40	6:50	2.96	15.24	20.25	8.44
32	2019-06-14 5:50	2019-06-14 8:30	2:40	2.76	13.74	7.35	2.97
33	2019-06-15 14:30	2019-06-15 21:20	6:50	1.52	7.62	10.39	1.25
34	2019-06-20 12:55	2019-06-20 19:40	6:45	0.58	3.00	3.94	4.65
35	2019-06-25 7:35	2019-06-25 14:30	6:55	1.77	14.23	12.27	9.15
36	2019-06-29 16:25	2019-06-29 20:30	4:05	3.54	44.07	14.44	4.08
37	2019-06-30 7:50	2019-06-30 9:35	1:45	4.55	8.06	7.96	0.47
38	2019-07-05 9:30	2019-07-05 9:50	0:20	3.03	4.56	1.01	5.00
39	2019-07-06 9:50	2019-07-06 11:10	1:20	7.81	27.42	10.41	1.38
40	2019-07-11 7:30	2019-07-11 11:10	3:40	9.28	74.70	34.04	4.85
41	2019-07-11 18:20	2019-07-11 21:30	3:10	4.08	30.48	12.92	0.30
42	2019-07-13 20:50	2019-07-13 22:20	1:30	5.41	39.60	8.12	1.97
43	2019-07-19 6:10	2019-07-19 7:00	0:50	3.35	12.80	2.79	5.33
44	2019-07-21 5:50	2019-07-21 7:10	1:20	22.48	97.56	29.97	2.70
45	2019-07-30 19:10	2019-07-30 20:40	1:30	29.12	100.56	43.68	9.50
46	2019-08-09 21:00	2019-08-09 23:20	2:20	3.15	15.24	7.35	10.01
47	2019-08-28 11:00	2019-08-28 20:20	9:20	1.68	7.62	15.71	18.49
48	2019-08-30 6:40	2019-08-30 8:30	1:50	9.27	42.66	16.99	1.43
49	2019-09-02 0:20	2019-09-02 7:50	7:30	2.30	6.12	17.22	2.66
50	2019-09-04 2:40	2019-09-04 13:10	10:30	1.67	21.36	17.51	1.78
51	2019-09-07 16:10	2019-09-07 20:40	4:30	1.64	9.12	7.36	3.13
52	2019-09-11 4:10	2019-09-11 6:50	2:40	1.23	10.68	3.29	3.31

Table C.2 Attributes of all rainfall events measured using a weather station and a time-step of 10 min (continued).

# of Rainfall Event	Start Date and Time (Y-M-D and HH:MM)	End Date and Time (Y-M-D and HH:MM)	Duration (HH:MM)	Average Intensity (I_{avg}) (mm/hr)	Maximum Intensity (I_{max}) (mm/hr)	Total Depth (mm)	Antecedent Dry Days (ADD)
53	2019-09-14 1:20	2019-09-14 8:10	6:50	0.89	7.62	6.05	2.77
54	2019-09-26 10:10	2019-09-26 20:40	10:30	1.08	12.18	11.37	12.08
55	2019-09-28 10:00	2019-09-28 15:30	5:30	0.83	4.56	4.56	1.56
56	2019-09-30 23:30	2019-10-01 2:00	2:30	1.92	4.56	4.79	4.12
57	2019-10-01 14:45	2019-10-01 22:20	7:35	6.61	58.11	50.13	0.53
58	2019-10-03 22:50	2019-10-04 1:50	3:00	0.92	3.06	2.76	2.06
59	2019-10-07 3:50	2019-10-07 8:40	4:50	2.15	6.12	10.37	3.08
60	2019-10-16 19:40	2019-10-17 21:25	25:45	2.90	12.00	74.55	9.47
61	2019-10-27 6:40	2019-10-27 21:50	15:10	2.76	10.68	41.79	9.92
62	2019-10-31 1:30	2019-10-31 5:10	3:40	1.03	3.06	3.76	3.15
63	2019-10-31 14:10	2019-11-01 9:40	19:30	3.24	19.80	63.15	0.38
64	2019-11-05 7:10	2019-11-05 18:10	11:00	0.98	9.12	10.83	3.90

APPENDIX D CATEGORIZATION OF RAINFALL EVENTS

Table D.1 Category number assigned to each rain characteristic for each measured event.

# of event	# Duration	# I_{avg}	# I_{max}	# Rainfall Depth	# ADD
18	5	2	3	5	3
19	4	1	1	2	3
20	5	2	1	5	1
21	4	1	2	3	4
22	2	1	1	1	1
23	5	3	4	5	5
24	5	1	1	3	3
25	2	3	1	2	4
26	1	4	2	1	1
27	1	5	3	2	1
28	4	2	4	4	3
29	1	2	1	1	5
30	2	3	2	2	1
31	3	3	3	4	5
32	2	3	3	2	2
33	3	2	2	3	1
34	3	1	1	1	4
35	3	2	3	3	5
36	3	4	5	3	4
37	1	4	2	2	1
38	1	4	1	1	4
39	1	5	4	3	1
40	2	5	5	5	4
41	2	4	4	3	1
42	1	4	4	2	1
43	1	4	3	1	4
44	1	5	5	5	2
45	1	5	5	5	5
46	2	4	3	2	5
47	4	2	2	4	5
48	1	5	5	4	1

Table D.1 Category number assigned to each rain characteristic for each measured event (continued).

# of event	# Duration	# I_{avg}	# I_{max}	# Rainfall Depth	# ADD
49	4	3	2	4	2
50	4	2	4	4	1
51	3	2	2	2	3
52	2	2	3	1	3
53	3	1	2	2	2
54	4	2	3	3	5
55	3	1	1	1	1
56	2	2	1	1	4
57	4	4	5	5	1
58	2	1	1	1	2
59	3	3	2	3	3
60	3	5	3	5	5
61	5	3	3	5	5
62	2	2	1	1	3
63	5	4	3	5	1
64	4	1	2	3	3

APPENDIX E ISSUES WHICH AROSE DURING THE PROJECT

Monitoring methodology

Issue #1 - Laboratory calibration

Initially, the flow passing through the conduit was not completely laminar nor uniform. To correct this, corrugated steel plates (Figure B.5) were installed in the open channel upstream of the conduit ensuring measurement accuracy (Figure B.3).

Issue #2 - Field calibration of vegetated swale

As shown in Figure B.12, the field calibration of the vegetated swale resulted in the measurement of flow points in a limited range along the curve. The pump was unable to provide accurate smaller flows. Additionally, it was not possible to attain the head required to generate the maximum design flow of the regulator (4.5 L/s). Therefore, only a section of the laboratory curve was validated.

Issue #3 - Field calibration of a control site

Figure B.15 presents the field calibration of a monitoring site which was not used for analysis. The conduit connecting the street catch basin to the monitoring manhole was composed of two sections connected by a 45° elbow which had very different slopes. Thus, it was not possible to re-create the field conditions in the laboratory. The same issue (#2) previously discussed arose and only a section of the curve was measured in the field. Since the trendline is a power function, the small flows are underestimated, and the largest flows are overestimated. This led to illogical values when calculating the runoff volumes measured at the site.

Issue #4 – Weather station – high intensity rainfall event

For the event of October 17th, strong winds overturned the weather station and thus data was lost. The necessary data was instead retrieved from the 3 city gauges which were typically used for validation. This was also the case for a few events which had a rainfall intensity much higher than the maximum capacity of the rain gauge inside the weather station.

Issue #5 – Timestep and threshold value chosen for data collection

It is possible in the Teledyne ISCO 2150 module to select two different timesteps with respect to the water level being measured. The threshold value selected dictates which timestep is used. This can improve battery lifespan and prevent data storage overload. At the beginning of the study,

theoretically highly efficient values were selected. The vegetated swale, for example, had an initial threshold value of 30 mm (height above which water begins to flow over the weir). An initial timestep of 4 hours was chosen for heights below this value. Once the level reached 30 mm, the timestep was set to change to 2 minutes. This would permit the collection of a detailed hydrograph while not draining the battery. However, it was concluded that the timestep of 4 hours was not adequate since it provided too long a period without any information on the behavior of the flow. Additionally, it was not possible to determine a variation in the threshold with these settings and low flow data was lost for a few events. The final parameters chosen were 15 minutes timestep for heights below the threshold and 2 minutes for heights above. The threshold was also measured multiple times throughout the study period to ensure the value inserted into the instrument settings were correct. In summary, it is necessary to choose settings which ensure the necessary amount of data is collected for analysis while not reducing the functionality of the instrument.

Data processing and calculations

Issue #1 – Uncertainty in peak inflow magnitude

The peak flow entering a LID structure was derived from the peak measured at the control site STD-M12 by proportioning the impervious drainage areas of both sites. Thus, it is assumed the total area (sidewalk + street) draining into both LID cells contributes towards a single peak inflow. However, if it were possible directly measure the inflow peak, two values smaller than the calculated peak would be obtained since each cell collects runoff from a separate section of the street. It is unclear which peak inflow should be compared to the outflow peak. The worst-case scenario was considered which assumes, if the site were constructed without the LID facility, that the inflow from the impervious area would drain to a single point. It is possible that using this larger peak creates a bias in the peak reduction results towards high performance, for both structures.

APPENDIX F MODEL CALIBRATION STEPS

Parametric calibration

1. From an analysis of the initial uncalibrated simulation, it was determined that an outflow volume reduction was needed for both structures as well as a re-alignment of the hydrographs for the bioretention basin.
2. The sensitivity analysis demonstrated that a maximization of the percolation speed would be beneficial. Initial values were chosen to maximize the hydraulic conductivity (140 mm/h) and minimize the conductivity slope (30). These were based on the logical range of each provided by Rossman and Huber (July 2016).
3. An overestimation of the outflow by the model remained although it was reduced. However, there remained no other influential parameters to alter since an increase in the evaporation rates and the soil porosities was not justified.
4. It was concluded that, in order to decrease the outflow, it would be necessary to decrease the inflow into the structure since there remained no options for adjusting the LID control parameters. Additionally, adjusting the parameters chosen for the adjacent general subcatchments (no LID control) did not provided enough volume reduction (if any) to improve the calibration. The remaining option was redesigning the structures in the model.

Redesign Calibration

1. The shape of the soil layer section modelled in SWMM was compared to the actual cross-section shape. This permitted a better understanding of the inaccuracies which remained in the flow path of the runoff and the connection between the soil layer and the drainage surfaces. The runoff from the sidewalk was not flowing directly to the main LID subcatchment. This section of the soil layer required a separate representation in the model.
2. Two methods were tested: one which represents the topsoil using another LID control (no surface or storage layer) and one which uses a general subcatchment (no LID control). To maintain accuracy, the parameters were chosen to match the values in the main soil layer.
3. The second option using the general subcatchment presented superior results. This greatly improved the calibration which, in the case of the vegetated swale, met the performance

targets. No further alterations were made. As for the bioretention basin, the redesign improved the NSE however it remained negative. Due to time constraints and the complexity the bioretention basin calibration presents, no further alterations were made as part of this project.

APPENDIX G EXAMPLE OF UNCERTAINTY QUANTIFICATION

Propagation of height measurement uncertainty

An example of a rating curve generated for the control site STD-M12 is presented in Figure B.14.

The two types of equations used for the height and flow relationship are power and a 2nd degree polynomial. The error is propagated differently for the two cases.

First, the quantification of the uncertainty from the height measurement will be determined through the error propagation equations (section 3.2.3.2.1).

The calibration equations for the control site STD-M12 are presented in Table G.1.

Table G.1 Calibration equations developed for control site STD-M12

Height range (mm)	Calibration equation (Q in L/s)
H > 72	$Q = 0.0002*H^{2.2918}$
H ≤ 72	$Q = 0.0008*H^2 – 0.0117*H + 0.0368$

The random error on the height measurement is 0.008 mm/mm (Teledyne ISCO, 2016).

For example, H = 166 mm (H > 72);

Step 1: $Z_1 = {X_1}^{2.2918}$ where X_1 = H; from Eq. (3.11)

$$\Delta z_1 = |2.2918| \frac{0.008 * 166}{|166|} |166^{2.2918}|$$

$$\Delta z_1 = 2245.50$$

Step 2: $Z_2 = 0.0002*X_2$ where $X_2 = H^{2.2918}$; from Eq. (3.10)

$$\Delta z_{final} = 0.0002 * 2245.50 = 0.4491$$

The uncertainty of H propagates to be an uncertainty of 0.4491 L/s on Q where H = 166 mm and Q = 24.5 L/s

Now for H < 72, H = 65.97 mm;

Step 1: $Z_3 = 0.0008*{X_3}^2$ where X_3 = H; from Eq. (3.10) and (3.11)

$$\Delta z_3 = 0.0008 * |2| \frac{0.008 * 65.97}{|65.97|} |65.97^2|$$

$$\Delta z_3 = 0.0557$$

Step 2: Z_4 = 0.0117*X_4 where X_4 = H; from Eq. (3.10)

$$\Delta z_4 = 0.0117 * 0.008 * 65.97 = 0.00617$$

Now the uncertainty on Q is, for a summation;

Where $Z_5 = Z_3 + Z_4 + 0.0368$; from Eq. (3.12)

$$\Delta z_{final} = \sqrt{(0.0557)^2 + (0.00617)^2 + (0)^2}$$

$$\Delta z_{final} = 0.0561\ L/s$$

The uncertainty of H propagates to be an uncertainty of 0.0561 on Q where H = 65.97 and Q = 2.62 L/s

However, it is also necessary to add the uncertainty associated with the trendline generated by Excel in each case. It is possible to find the standard error on the y value of the trendline (in this case the flow) using the built-in equation LINEST which can be used for both power and 2nd degree polynomials.

The standard errors are:

For the power: 0.01464 L/s

For the 2nd degree polynomial: 0.06065 L/s

The 3rd error to consider is the one associated with the reading of the pump value. However, this value is not known. The total error will therefore be calculated without this source using Eq. (3.13).

For case 1, H = 166 mm:

$$Qe_t = \sqrt{(0.4491)^2 + (0.01464)^2} = 0.4493\ L/s$$

For case 2, H = 65.97 mm

$$Qe_t = \sqrt{(0.0561)^2 + (0.06065)^2} = 0.0826\ L/s$$

Uncertainty of volume

To calculate the error on each incremental volume measurement, where $V_i = Q_i * (t_i - t_{i-1})$, it is necessary to know the error associated with the Q at that time-step. If we assume that the error

associated with time is 0, then we are multiplying the error of Q by a constant and can use Eq. (3.10) to obtain the error:

$$\Delta V = 120 * 0.4493 = 53.92\ L\ for\ case\ 1, H = 166\ mm$$

$$\Delta V = 120 * 0.0826 = 9.91\ L\ for\ case\ 2, H = 65.97\ mm$$

The relative errors are 1.83% and 3.15% for case 1 and 2 respectively.

To calculate the random error of the entire volume, ΔV_T (obtained by numerical integration of the flow hydrograph), the following equation is used:

$$\Delta V_T = \frac{\sqrt{(\Delta V_1)^2 + (\Delta V_2)^2 + \cdots}}{n}$$

Where $V_T = V_1 + V_2 + \ldots$ and n = the number of sample points.